Karlsruher Institut für Technologie

Institut für Theoretische Teilchenphysik

QCD Corrections to Heavy Sterile Neutrino Decays

Zur Erlangung des akademischen Grades eines

DOKTORS DER NATURWISSENSCHAFTEN (Dr. rer. nat.)

von der KIT-Fakultät für Physik des
Karlsruher Instituts für Technologie (KIT) genehmigte

DISSERTATION

von

M.Sc. Tim Robin Kretz
geboren in Karlsruhe

Referent: Prof. Ulrich Nierste
Koreferent: Prof. Thomas Schwetz-Mangold

Tag der mündlichen Prüfung: 31. Juli 2026

Für meine Familie

Disclaimer:

Artificial Intelligence (AI) has been used during the making of this thesis to support the grammar and style of the text. ChatGPT[1] has been used throughout the thesis to assist with spelling and grammar, as well as to paraphrase selected sentences for improved clarity and conciseness. All suggested changes were carefully reviewed before incorporation.

Furthermore, ChatGPT has been used in Mathematica code generation to help in plotting results. All proposed changes were checked and tested to ensure factual correctness. No generative AI tools have been used to derive or evaluate any of the results presented in this thesis.

[1]Conversational AI model of OpenAi, `https://chatgpt.com` (Access: 24. June 2026)

Erklärung:

Ich versichere wahrheitsgemäß, die Arbeit selbstständig verfasst, alle benutzten Hilfsmittel vollständig und genau angegeben und alles kenntlich gemacht zu haben, was aus Arbeiten anderer unverändert oder mit Abänderungen entnommen wurde sowie die Satzung des KIT zur Sicherung guter wissenschaftlicher Praxis in der Fassung vom 30. September 2021 beachtet zu haben.

Karlsruhe, den 24. Juni 2026

. . . .

(Tim Robin Kretz)

Abstract

Sterile neutrinos N are a compelling extension of the Standard Model and are realised for example, by appending right-handed neutrino fields to the Standard Model; introducing them in this way is referred to as the seesaw mechanism of type I, if a (lepton-number violating) Majorana mass term much larger than the electroweak scale is added to the lagrangian. The interactions of Standard Model particles with (sterile) neutrinos are then governed by a sterile-active mixing matrix element (often simplified to a single mixing angle) $V_{N\ell}$. Standard Model neutrino interactions generally scale with $1 - |V_{N\ell}|^2$ while sterile neutrino interactions come with the factor $|V_{N\ell}|^2$. The mixing angles are experimentally constrained to be very small. In this work we consider the effects of hadronic decay modes of sterile neutrinos in the mass range $1\,\mathrm{GeV} \lesssim m_N \lesssim 6\,\mathrm{GeV}$. To that end we calculate the fully inclusive hadronic sterile neutrino decay rate using the known Standard Model gauge boson correlators. We calculate both the charged-current and the neutral-current decay rate using the correlator up to $\mathcal{O}(\alpha_s^4)$ in the chiral limit as well as their quark mass corrections up to $\mathcal{O}(\alpha_s^3)$ in the charged-current case and $\mathcal{O}(\alpha_s^2)$ in the neutral-current case. We present analytical expressions for the inclusive decay rate up to $\mathcal{O}(\alpha_s^3)$ in the massless case and utilise a series representation of the Källén function at $\mathcal{O}(\alpha_s^4)$. Similarly we find analytical expressions for the massive corrections up to $\mathcal{O}(\alpha_s^2)$ and in terms of this series representation at $\mathcal{O}(\alpha_s^3)$. The inclusion of the higher-order QCD corrections allows us to find the sterile neutrino mass range in which a perturbative description of hadronic sterile neutrino decays is possible. Thus for the hadronic decays $N \to \ell X$ and $N \to \nu X$, where X is the hadronic system in the final state, the calculation of branching fractions is possible for sterile neutrino masses $1.5\,\mathrm{GeV} \lesssim m_N < m_{D^+} + m_\ell$, $3.5\,\mathrm{GeV} \lesssim m_N < 2m_{D^0}$, and $4.6\,\mathrm{GeV} \lesssim m_N \lesssim 5.0\,\mathrm{GeV}$ for $\ell = e, \mu$ as well as for $1.5\,\mathrm{GeV} \lesssim m_N < m_\tau$, $3.0\,\mathrm{GeV} \lesssim m_N < m_{D^+} + m_\tau$, and $4.6\,\mathrm{GeV} \lesssim m_N \lesssim 6.5\,\mathrm{GeV}$ for $\ell = \tau$. Within these windows we make predictions for the proper decay length of the sterile neutrino.

For our calculation of the charged-current inclusive decay rate we have also accounted for the mass of the final state charged lepton. We can use these results to constrain the mixing angle for tau lepton decays into sterile neutrinos $\tau \to NX$. From the τ lifetime we find the mixing angle to be constrained to $|V_{N\tau}| = |\sin\theta| \lesssim 0.2$ for $m_N = 600\,\mathrm{MeV}$. In the case $m_N > m_\tau$ we find $|\sin\theta| \leq 11.8 \cdot 10^{-2}$ at the 1σ level. Furthermore we study the impact of sterile neutrinos on τ branching fractions. While the leptonic τ decays prefer unphysical values of the mixing angle $\cos\theta > 1$ the semi-hadronic decays $\tau \to \nu_\tau \pi$ and $\tau \to \nu_\tau K$ together permit a non-zero mixing angle at the 1σ level of $|\sin\theta| = (9.1^{+3.7}_{-7.8}) \cdot 10^{-2}$.

Zusammenfassung

Sterile Neutrinos N sind eine attraktive Erweiterung des Standard Modells (SM) und werden zum Beispiel durch die Erweiterung des SM um rechtshändige Neutrinofelder realisiert; diese Art der Erweiterung des SM ist bekannt als Seesaw-Mechanismus vom Typ I (zu dt. Wippenmechanismus), sofern ein (leptonzahlverletzender) Majorana-Massenterm, deutlich größer als die elektroschwache Skala, in den Lagrangian eingeführt wird. Wechselwirkungen von (sterilen) Neutrinos mit anderen SM Teilchen sind dann vollständig durch das Mischungsmatrixelement (oft zu einem einzelnen Mischungswinkel vereinfacht) $V_{N\ell}$ fixiert. Die Stärke von SM Neutrino Wechselwirkungen skaliert dann mit dem Faktor $1 - |V_{N\ell}|^2$, wohingegen die der sterilen Neutrinos mit $|V_{N\ell}|^2$ skaliert. Die Mischungswinkel sind experimentell zu sehr kleinen Werten eingeschränkt. In dieser Arbeit untersuchen wir den Effekt von hadronischen Zerfallsmodi steriler Neutrinos im Massenbereich $1\,\text{GeV} \lesssim m_N \lesssim 6\,\text{GeV}$. Unter Verwendung der bekannten Eichbosonkorrelatoren berechnen wir die volle inklusive hadronische sterile Neutrino Zerfallsrate. Wir berechnen sowohl die Zerfallsrate mithilfe des Korrelators des geladenen und des ungeladenen Stromes bis zur Ordnung $\mathcal{O}(\alpha_s^4)$ im chiralen Grenzfall als auch die Quarkmassenkorrekturen bis zur Ordnung $\mathcal{O}(\alpha_s^3)$ für den geladenen Strom und bis zur Ordnung $\mathcal{O}(\alpha_s^2)$ für den ungeladenen Strom. Wir präsentieren analytische Ausdrücke für die inklusive Zerfallsrate bis zur Ordnung $\mathcal{O}(\alpha_s^3)$ im masselosen Fall und verwenden eine Reihendarstellung der Källén Funktion für die Beiträge zur Ordnung $\mathcal{O}(\alpha_s^4)$. Ebenso finden wir analytische Ausdrücke für die massiven Beiträge bis zur Ordnung $\mathcal{O}(\alpha_s^2)$ und berechnen die Beiträge zur Ordnung $\mathcal{O}(\alpha_s^3)$ unter Verwendung der Reihendarstellung. Die QCD Korrekturen höherer Ordnung ermöglichen es den Massenbereich steriler Neutrinos zu finden, der es erlaubt die hadronische Zerfallsrate mithilfe von störungstheoretischen Mitteln zu berechnen. Es ist möglich für die hadronischen Zerfälle $N \to \ell X$ und $N \to \nu X$, wobei X das hadronische System im Endzustand ist, Verzweigunsverhältnisse in den Massenfenstern $1.5\,\text{GeV} \lesssim m_N < m_{D^+} + m_\ell$, $3.5\,\text{GeV} \lesssim m_N < 2m_{D^0}$ und $4.6\,\text{GeV} \lesssim m_N \lesssim 5.0\,\text{GeV}$ für den Fall $\ell = e, \mu$ sowie für $1.5\,\text{GeV} \lesssim m_N < m_\tau$, $3.0\,\text{GeV} \lesssim m_N < m_{D^+} + m_\tau$ und $4.6\,\text{GeV} \lesssim m_N \lesssim 6.5\,\text{GeV}$ für den Fall $\ell = \tau$ zu berechnen und Vorhersagen über die Zerfallslänge des sterilen Neutrinos zu machen. Für die Berechnung der inklusiven Zerfallsrate des geladenen Stromes ist es notwendig den Effekt des massiven Leptons im Endzustand zu berücksichtigen. Daher können wir unsere Ergebnisse ebenso verwenden, um den Mischungswinkel mithilfe von Tau Lepton Zerfällen in sterile Neutrinos $\tau \to NX$ einzuschränken. Die τ Lebensdauer beschränkt den Mischungsinkel für $m_N = 600\,\text{MeV}$ auf den Wert $|V_{N\tau}| = |\sin\theta| \lesssim 0.2$ und im Fall $m_N > m_\tau$ auf den Wert $|\sin\theta| \leq 11.8 \cdot 10^{-2}$ auf dem 1σ Niveau. Darüber hinaus untersuchen wir den Einfluss von sterilen Neutrinos auf die τ Verzweigungsverhältnisse. Wohingegen leptonische τ Zerfälle die unphysikalischen Werte des Mischungswinkels $\cos\theta > 1$ bevorzugen, erlauben die semi-hadronischen Zerfälle einen von Null verschiedenen Mischungswinkel auf dem 1σ Niveau von $|\sin\theta| = (9.1^{+3.7}_{-7.8}) \cdot 10^{-2}$.

List of Publications

Parts of this thesis are based on published work.

Parts of the thesis are based on the publication:

[1] Tim Kretz and Ulrich Nierste. "QCD corrections to charged-current decays with Heavy Sterile Neutrinos in initial or final state and their impact on τ decays". In: *JHEP* 06 (2026), p. 146. DOI: 10.1007/JHEP06(2026)146. arXiv: 2512.00476 [hep-ph].

Publications and preprints not discussed in this thesis:

[1] Florian U. Bernlochner et al. "Model independent bounds on heavy sterile neutrinos from the angular distribution of $B \to D^* \ell \nu$ decays". In: *JHEP* 01 (2025), p. 040. DOI: 10.1007/JHEP01(2025)040. arXiv: 2410.11945 [hep-ph].

[2] Motoi Endo et al. "$b \to c$ semileptonic sum rule: extension to angular observables". In: *Eur. Phys. J. C* 85.9 (2025). [Erratum: Eur.Phys.J.C 85, 1050 (2025)], p. 961. DOI: 10.1140/epjc/s10052-025-14598-9. arXiv: 2506.16027 [hep-ph].

[3] Motoi Endo et al. "$b \to c$ semileptonic sum rule: exploring a sterile neutrino loophole". In: (Mar. 2026). arXiv: 2603.15029 [hep-ph].

Contents

List of Figures

List of Tables

1. Introduction

The beauty of particle physics is the incredible energy range over many orders of magnitude at which we can study the features of elementary particles. We can measure elementary particles at tiny spatial separations in particle colliders while at the same time we can obtain bounds on the very same particles probed in colliders from the structure formation in the early universe. Over the course of the last few decades many elementary particles have been discovered with the last particle predicted by the Standard Model (SM) of particle physics being discovered in 2012: the Higgs boson [1, 2]. The Higgs boson is closely tied to the generation of mass of all observed particles. However, there is one particle in the SM that may well obtain its mass through a different mechanism and which interacts so weakly that it can escape from exploding stars yet still interacts strongly enough with matter such that it is not elusive to our earth-bound detectors. The particle in question is the neutrino. It has been hypothesised to exist by Wolfgang Pauli in 1930 to explain the continuous energy spectrum of the electron in β decays [3]. Later on, Enrico Fermi proposed a theoretical description of β decay which is referred to today as the Fermi theory and paved the way for a modern understanding of effective field theories [4]. Subsequently the neutrino has been discovered in 1956 by Cowan and Reines [5] and even neutrinos originating from the supernova 1987A have been detected in the water Cherenkov detector Kamiokande-II [6]. Neutrinos are quite peculiar particles; within the quantum field theoretical framework of the SM they are expected to be massless. Contrary to this expectation we observe that they oscillate meaning the flavour state in which a given neutrino is produced does not necessarily coincide with the flavour state measured in the experiment detecting it. This can only happen if at least two of the three neutrinos are not massless. Currently the KATRIN experiment yields the tightest direct laboratory bound on the squared effective electron antineutrino mass $m_\nu < 0.45\,\mathrm{eV}$ [7]. In addition, there are various constraints on the sum of the neutrino masses coming from cosmology; the mass of the neutrino can influence the cosmic microwave background, the abundance of light elements, and the large-scale structure formation in the universe. Bounds obtained from these observables can be significantly tighter than the KATRIN bound, albeit they are also significantly more model-dependent (see e.g. Ref. [8] for an overview).

All of these effects impressively demonstrate that neutrinos possess a non-zero mass. Consequently, this mass must be generated through some mechanism for which the SM is currently not equipped. Even more so, any compelling mass generation mechanism should explain why the neutrino mass is so small that to this day we have only observed that the neutrino masses are orders of magnitude smaller than the masses of all other SM particles. A promising mechanism in this regard is the seesaw mechanism, in particular the seesaw mechanism of type I [9–13]. In the SM neutrino masses are absent because it foresees no right-handed neutrino fields and hence no Dirac type mass term can be generated. The seesaw mechanism of type I appends a right-handed neutrino field to the SM. Therefore, a Dirac type mass for the neutrino can be generated. However, since the right-handed neutrino field does not carry any quantum numbers i.e. it is uncharged with respect to the SM gauge group it also permits Majorana type masses. To this day it is not clear whether the SM neutrinos are of Dirac or of Majorana type i.e. whether the SM neutrino is its own anti particle. One way this can be probed is through neutrinoless double β decays ($0\nu\beta\beta$). In the $0\nu\beta\beta$ the energy spectrum of the two emerging electrons is measured. For neutrinos of Majorana type there is a decay mode in which no neutrinos are produced in the final state and the measured sum of the electrons' energy corresponds to the energy freed in the nuclear decay. There are currently several experiments studying $0\nu\beta\beta$, no signal has yet been observed (see Ref. [14] for an overview).

The addition of the right-handed neutrino field doubles the number of physical neutrino mass eigenstates. Limiting the discussion to a single active neutrino flavour ν_ℓ mixing with a sterile neutrino N, the admixtures of the two chiral fields are governed by the mixing matrix element $V_{N\ell}$.[1] One mass eigenstate corresponds to the observed active neutrino close to the SM neutrino and is predominantly composed of the left-handed component of the neutrino field (and conversely only a small component of the right-handed field); the other mass eigenstate corresponds to the mostly sterile neutrino and is predominantly composed of the right-handed component of the neutrino field. In the seesaw mechanism of type I the SM neutrino mass is small because it is suppressed by the inverse heavy sterile neutrino mass. The mechanism thus naturally explains why the SM neutrino mass is small at the cost of introducing a new particle in the form of the sterile neutrino with a mass larger than the SM neutrino. Sterile neutrinos introduced through the seesaw mechanism of type I interact in exactly the same way as SM neutrinos do with the only difference being that their couplings to all other SM particles are suppressed by the mixing angle.

In general, direct detection of active neutrinos is difficult. Since neutrinos are interacting very weakly, large detector volumes are required to measure them directly. Sterile neutrinos interact even more weakly than SM neutrinos and are thus even more difficult to detect directly. In any collider experiment the signature of neutrinos is always missing energy. This means that to some extent interactions with SM neutrinos are already not fully explored; in fact, if there are additional particles that interact similarly to SM neutrinos then they would likely not be detected as they would remain hidden behind the background of SM neutrino effects. This makes sterile neutrinos interesting, as their effects could very well be hidden in existing data! The study of sterile neutrinos is thus popular and their effects on many different pressing questions of physics have been studied extensively e.g. in the context of Dark Matter [15, 16] or leptogenesis [17, 18] to just name a few. In these contexts sterile neutrinos with masses between a few eV and several GeV have been considered and there are many ongoing and proposed future experiments searching for sterile neutrinos at all of these mass scales (see Ref. [19]). Since the heavier, mostly sterile neutrino interacts similarly to the SM neutrino this means in

[1] Often the mixing matrix elements are written in terms of sines and cosines of a mixing angle $\theta_{N\ell}$. Throughout this work we will use the terms mixing matrix element and mixing angle synonymously.

particular that it also participates in the weak interaction mediated by the W and the Z bosons. This offers the possibility that a sufficiently heavy neutrino with a mass in the range $1\,\text{GeV} \lesssim m_N \lesssim 6\,\text{GeV}$ can decay hadronically. We call such neutrinos in this mass range heavy sterile neutrinos (HSN) throughout this work. The decay rate of an HSN is proportional to the HSN mass and the mixing angle of the HSN with the respective SM neutrino: $\Gamma_N \propto |V_{N\ell}|^2 m_N^5$. Depending on the mass and the value of the mixing angle the HSN can thus have proper decay lengths between a few millimetres and several kilometres. As such the observable signatures at particle colliders drastically change from being almost indistinguishable from background events to escaping the detector without interacting at all. Through the interaction with the weak gauge bosons the HSN can decay into quarks and thus hadrons in the final state. If the HSN is sufficiently heavy, decays into several mesons could be possible. A simple tree-level estimation of the decay rate into quarks alone could underestimate the size of the inclusive hadronic decay rate. In this work we study the influence of the addition of the inclusive hadronic decay modes of the HSN on the HSN lifetime.

To achieve our goal of predicting the lifetime of a sterile neutrino we need several different ingredients. We introduce them in Chapter 2 where we give a brief overview of the Standard Model and illustrate some important aspects of renormalisation. Then we present the known gauge boson correlator, which plays a crucial role in our calculation and conclude the chapter by giving a more detailed overview of sterile neutrinos. The main part of the decay rate calculation is constituted in Chapter 3. We present the calculation of the inclusive hadronic sterile neutrino decay rate for both the charged and the neutral current cases separately. For both the charged and the neutral current contributions we include quark mass corrections. In Chapter 4 we assess the stability of the perturbative results with respect to the renormalisation scale. We find a mass window for sterile neutrinos coupling either to tau leptons or muons that permits a perturbative description. In the window where both the charged- and the neutral-current contribution are well behaved we calculate the total sterile neutrino decay rate and give some branching ratios into certain final states. Furthermore we apply the calculation of the charged-current decay of sterile neutrinos to tau lepton decays into a sterile neutrino and a hadronic final state. From the tau lepton lifetime and its branching fractions into leptonic and semi-hadronic final states we find constraints on the mixing angle. We discuss the implications of our work for current and future colliders and give an overview over current experimental bounds. Finally, we conclude this thesis in Chapter 5.

2. Theoretical Foundations

2.1. The Standard Model

The Standard Model comprises 17 types of elementary particles and describes the weak, the strong, and the electromagnetic force. It has been experimentally verified up to impressive levels of precision [20]. Here we give an overview of the SM closely following Ref. [21].

The 17 types of elementary particles are divided into six quarks (u, d, c, s, t, b) and six leptons ($\nu_e, e, \nu_\mu, \mu, \nu_\tau, \tau$); three electroweak gauge bosons: the $W^\pm$, the Z, and the photon γ; one strong force gauge boson: the gluon G; and finally the Higgs boson H responsible for the mass generation of all particles (see Tab. 2.1). The SM is both a gauged and a chiral theory, the former meaning all particles carry some charge with respect to the SM gauge group $\mathrm{SU}(3)_C \times \mathrm{SU}(2)_L \times \mathrm{U}(1)_Y$ and the latter meaning left- and right-handed components of the SM fermion fields carry different charges with respect to the $\mathrm{SU}(2)_L \times \mathrm{U}(1)_Y$ gauge group. The group $\mathrm{SU}(3)_C$ is associated with the strong interaction and is mediated by eight gluons, the respective charge is colour. $\mathrm{SU}(2)_L$ is the group of the weak isospin $\vec{T}$ mediated by three weak isospin bosons W^i and $\mathrm{U}(1)_Y$ is the hypercharge Y mediated by the B boson. We can describe the interactions of all known particles by simply writing down all terms in a Lagrangian that respect the gauge symmetry. The full SM Lagrangian is given by

$$\mathcal{L}_{\mathrm{SM}} = \mathcal{L}_{\mathrm{Fermion}} + \mathcal{L}_{\mathrm{Gauge}} + \mathcal{L}_{\Phi} + \mathcal{L}_{\mathrm{Y}}, \tag{2.1}$$

Table 2.1.: Overview of the structure and content of the Standard Model particles.

Quarks			Bosons	Higgs
$\begin{pmatrix} u \\ d \end{pmatrix}$	$\begin{pmatrix} c \\ s \end{pmatrix}$	$\begin{pmatrix} t \\ b \end{pmatrix}$	W	H
			Z	
Leptons			γ	
$\begin{pmatrix} \nu_e \\ e \end{pmatrix}$	$\begin{pmatrix} \nu_\mu \\ \mu \end{pmatrix}$	$\begin{pmatrix} \nu_\tau \\ \tau \end{pmatrix}$	G	

with each individual term being

$$\mathcal{L}_{\text{Fermion}} = \sum_{j=1}^{3} i\overline{L}_L^j \not{D} L_L^j + i\overline{Q}_L^j \not{D} Q_L^j + i\overline{\ell}_R^j \not{D} \ell_R^j + i\overline{u}_R^j \not{D} u_R^j + i\overline{d}_R^j \not{D} d_R^j, \tag{2.2}$$

$$\mathcal{L}_{\text{Gauge}} = -\frac{1}{4} G^a_{\mu\nu} G^{a,\mu\nu} - \frac{1}{4} W^a_{\mu\nu} W^{a,\mu\nu} - \frac{1}{4} B_{\mu\nu} B^{\mu\nu} + \mathcal{L}_{\text{fix}}, \tag{2.3}$$

$$\mathcal{L}_{\Phi} = (D_\mu \Phi)^\dagger (D^\mu \Phi) - V(\Phi), \tag{2.4}$$

$$\mathcal{L}_{\text{Y}} = -\overline{Q}_L \Phi Y^d d_R - \overline{Q}_L \widetilde{\Phi} Y^u u_R - \overline{L}_L \Phi Y^\ell \ell_R + \text{h.c.} \tag{2.5}$$

Here the $L_L^i = (\nu_L^i, \ell_L^i)^T$ and $Q_L^i = (u_L^i, d_L^i)^T$ are the left-handed doublets of leptons and quarks respectively; ℓ_R^i, u_R^i, and d_R^i are the right-handed singlets of the leptons and quarks ($\psi_{L/R} = P_{L/R}\psi$ where $P_{L/R} = (1 \mp \gamma_5)/2$). The D_μ are the covariant derivatives

$$D_\mu = \partial_\mu - ig_1 Y B_\mu - ig_2 \tau^a W^a_\mu - ig_s \frac{\lambda^a}{2} G^a_\mu, \tag{2.6}$$

with g_1 being the $\mathrm{U}(1)_Y$ coupling constant, Y being the hypercharge operator, g_2 being the $\mathrm{SU}(2)_L$ coupling constant, $\tau^a = \sigma^a/2$ is the weak isospin operator and σ^a are the Pauli matrices, and finally g_s is the $\mathrm{SU}(3)_C$ strong coupling constant with the $\mathrm{SU}(3)_C$ operator $\lambda^a/2$ where λ^a are the Gell-Mann matrices. The $G^a_{\mu\nu}$, $W^a_{\mu\nu}$, and $B_{\mu\nu}$ are the $\mathrm{SU}(3)_C$, $\mathrm{SU}(2)_L$, and $\mathrm{U}(1)_Y$ gauge boson field strength tensors respectively. The field strength tensors are given by $X^{\mu\nu} = \partial^\mu X^\nu_a - \partial^\nu X^\mu_a + g f^{abc} X^\mu_b X^\nu_c$ where g is the respective coupling constant of the gauge boson field X and f^{abc} is the structure constant of the respective group of the gauge boson e.g. $f^{abc} = \epsilon^{abc}$ for $\mathrm{SU}(2)_L$. The $\mathcal{L}_{\text{fix}}$ term fixes the gauge of the gluons to allow for a physical gluon propagator. The $\Phi = (\phi^+, \phi^0)^T$ is the Higgs doublet and

$$V(\Phi) = -\mu^2 \Phi^\dagger \Phi + \lambda (\Phi^\dagger \Phi)^2, \qquad \mu, \lambda > 0, \tag{2.7}$$

is the Higgs potential. Finally, there is the Yukawa term with $\widetilde{\Phi} = i\sigma_2 \Phi^*$ and the three Yukawa matrices $Y^{u,d,\ell}$. In Tab. 2.2 we present the transformation properties of all SM fields under the different gauge groups.

In Nature we do not directly observe the $\mathrm{SU}(2)_L \times \mathrm{U}(1)_Y$ structure of the SM as it is spontaneously broken by the Higgs field acquiring a non-zero vacuum expectation value (vev) $v \approx 246\,\text{GeV}$ [8]. This spontaneous symmetry breaking (SSB) breaks $\mathrm{SU}(2)_L \times \mathrm{U}(1)_Y \to \mathrm{U}(1)_{EM}$ to the QED gauge group. This SSB has far-reaching consequences: The gauge bosons before SSB are not the ones observed in nature, instead the linear combinations

$$W^\pm_\mu = \frac{1}{\sqrt{2}}(W^1_\mu \mp iW^2_\mu), \qquad \begin{pmatrix} A_\mu \\ Z_\mu \end{pmatrix} = \begin{pmatrix} \cos\theta_w & \sin\theta_w \\ -\sin\theta_w & \cos\theta_w \end{pmatrix} \begin{pmatrix} B_\mu \\ W^3_\mu \end{pmatrix}, \tag{2.8}$$

are observed; here θ_w is the Weinberg angle and is given by $\sin^2\theta_w = s_w^2 = 0.23122(6)$ [8]. These states are the mass eigenstates which obtained their mass through the Higgs mechanism [22–27]

$$\mathcal{L}_{\text{SM}} \supset \mathcal{L}_{\text{Gauge, mass}} = M_W^2 W^+_\mu W^{-,\mu} + \frac{1}{2} M_Z^2 Z_\mu Z^\mu + \frac{1}{2} M_\gamma^2 A_\mu A^\mu, \tag{2.9}$$

with

$$M_W = \frac{g_2 v}{2}, \quad M_Z = \frac{g_2 v}{2\cos\theta_w}, \quad M_\gamma = 0. \tag{2.10}$$

Furthermore the non-zero vev of the Higgs field directly leads to quark masses through the Yukawa terms. After SSB the Yukawa terms read

$$\mathcal{L}_Y^m = -\frac{v}{\sqrt{2}}\overline{d}^i_L Y^d_{ij} d^j_R - \frac{v}{\sqrt{2}}\overline{u}^i_L Y^u_{ij} u^j_R - \frac{v}{\sqrt{2}}\overline{\ell}^i_L Y^\ell_{ij} \ell^j_R + \text{h.c.} \tag{2.11}$$

The Yukawa matrices $Y^{u,d,\ell}$ are not diagonal in general. We observe that the kinetic terms in the fermion Lagrangian in Eq. (2.2) each possess a U(3) symmetry. We can use this $[\mathrm{U}(3)]^5$ symmetry of the fermion sector, which transforms each field as $Q_L \to V^u_L Q_L$, $u_R \to V^u_R u_R$, $d_R \to V^d_R d_R$, $L_L \to V^\ell_L L_L$, and $\ell_R \to V^\ell_R \ell_R$, to diagonalise both the lepton Yukawa matrix and one of the two quark Yukawa matrices with biunitary transformations [21]. However, since the left-handed up- and down-type quarks transform equally it is not possible to diagonalise both Yukawa matrices Y^u and Y^d simultaneously. The solution to this is to introduce a fourth transformation matrix V^d_L, different from V^u_L, such that indeed $(V^d_L)^\dagger Y^d V^d_R = \hat{Y}^d = \mathrm{diag}(y_d, y_s, y_b)$ and similarly $(V^u_L)^\dagger Y^u V^u_R = \hat{Y}^u = \mathrm{diag}(y_u, y_c, y_t)$ and $(V^\ell_L)^\dagger Y^\ell V^\ell_R = \hat{Y}^\ell = \mathrm{diag}(y_e, y_\mu, y_\tau)$, leading to

$$\mathcal{L}_Y^m = -\frac{v}{\sqrt{2}}\overline{d}'^i_L [(V^u_L)^\dagger V^d_L]_{ij} \hat{Y}^d_{jk} d^k_R - \frac{v}{\sqrt{2}}\overline{u}^i_L \hat{Y}^u_{ij} u^j_R - \frac{v}{\sqrt{2}}\overline{\ell}^i_L \hat{Y}^\ell_{ij} \ell^j_R + \text{h.c.}, \tag{2.12}$$

Table 2.2.: The transformation properties of all the Standard Model fields, written as $(\mathrm{SU}(3)_C, \mathrm{SU}(2)_L, \mathrm{U}(1)_Y)$ i.e. a field with the transformation properties $(\mathbf{3}, \mathbf{2}, 1/6)$ transforms as a triplet under $\mathrm{SU}(3)_C$, a doublet under $\mathrm{SU}(2)_L$, and with hypercharge $Y = 1/6$ (table adapted from Ref. [21]).

	Quarks		
$Q^1_L = (u_L, d_L)^T$	$Q^2_L = (c_L, s_L)^T$	$Q^3_L = (t_L, b_L)^T$	$(\mathbf{3}, \mathbf{2}, \frac{1}{6})$
u_R	c_R	t_R	$(\mathbf{3}, \mathbf{1}, \frac{2}{3})$
d_R	s_R	b_R	$(\mathbf{3}, \mathbf{1}, -\frac{1}{3})$
	Leptons		
$L^1_L = (\nu_e, e_L)^T$	$L^2_L = (\nu_\mu, \mu_L)^T$	$L^3_L = (\nu_\tau, \tau_L)^T$	$(\mathbf{1}, \mathbf{2}, -\frac{1}{2})$
e_R	μ_R	τ_R	$(\mathbf{1}, \mathbf{1}, -1)$
	Bosons		
	W^a_μ	$a = 1, 2, 3$	$(\mathbf{1}, \mathbf{3}, 0)$
	B_μ		$(\mathbf{1}, \mathbf{1}, 0)$
	G^a_μ	$a = 1, \ldots, 8$	$(\mathbf{8}, \mathbf{1}, 0)$
	Higgs		
	$\Phi = (\phi^+, \phi^0)^T$		$(\mathbf{1}, \mathbf{2}, \frac{1}{2})$

where we write $d_L'^i$ to point out that the down-type quarks are still in the flavour basis. Here we can identify

$$V_{\mathrm{CKM}} = (V_L^u)^\dagger V_L^d, \tag{2.13}$$

as the Cabibbo-Kobayashi-Maskawa matrix [28, 29]. It relates the interaction flavour basis to the mass basis. The Yukawa mass term becomes diagonal by rotating into the mass basis d_L

$$d_L' = V_{\mathrm{CKM}} d_L \quad \Leftrightarrow \quad \begin{pmatrix} d_L' \\ s_L' \\ b_L' \end{pmatrix} = \begin{pmatrix} V_{ud} & V_{us} & V_{ub} \\ V_{cd} & V_{cs} & V_{cb} \\ V_{td} & V_{ts} & V_{tb} \end{pmatrix} \begin{pmatrix} d_L \\ s_L \\ b_L \end{pmatrix}, \tag{2.14}$$

leading to the fermion mass term in the Lagrangian

$$\mathcal{L}_{\mathrm{SM}} \supset \mathcal{L}_Y^m = -\sum_{i=u,d,c,s,t,b} m_i \bar{q}_L^i q_R^i - \sum_{i=e,\mu,\tau} m_i \bar{\ell}_L^i \ell_R^i + \text{h.c.}, \tag{2.15}$$

where $m_i = v y_i/\sqrt{2}$. We quote the values of the elements of the CKM matrix relevant for our work

$$\begin{aligned}
|V_{ud}| &= 0.97367 \pm 0.00032 \qquad [8], \\
|V_{us}| &= 0.22431 \pm 0.00085 \qquad [8], \\
|V_{cd}| &= 0.221 \pm 0.004 \qquad [8], \\
|V_{cs}| &= 0.975 \pm 0.006 \qquad [8].
\end{aligned}$$

The price of a diagonal quark mass matrix is a non-diagonal interaction sector. There are neutral-current and charged-current interactions:

$$\mathcal{L}_{\mathrm{SM}} \supset \mathcal{L}_{\mathrm{NC}} + \mathcal{L}_{\mathrm{CC}}, \tag{2.16}$$

with

$$\mathcal{L}_{\mathrm{NC}} = \frac{g_2}{\cos\theta_w}\left[(T_3 - Q_f \sin^2\theta_w)\bar{f}\gamma^\mu P_L f - Q_f \sin^2\theta_w \bar{f}\gamma^\mu P_R f\right] Z_\mu, \tag{2.17}$$

$$\begin{aligned}
\mathcal{L}_{\mathrm{CC}} &= \frac{g_2}{\sqrt{2}}\left(\bar{u}_i \gamma^\mu P_L d_i' W_\mu^+ + \bar{\nu}_i \gamma^\mu P_L \ell_i W_\mu^+\right) + \text{h.c.} \\
&= \frac{g_2}{\sqrt{2}}\left(V_{ij}^{\mathrm{CKM}} \bar{u}_i \gamma^\mu P_L d_j W_\mu^+ + \bar{\nu}_i \gamma^\mu P_L \ell_i W_\mu^+\right) + \text{h.c.}
\end{aligned} \tag{2.18}$$

Here T_3 denotes the third component of the isospin and Q_f the electric charge of the particle f. The left-handed fields carry isospin with $T_3 = \pm 1/2$ if they are an up- or down-type particle, the right-handed fields are uncharged under isospin T_3. The electric charge follows from the third component of the isospin and the hypercharge as $Q_f = T_3 + Y$, which is known as the Gell-Mann-Nishijima formula. Both the neutral-current and charged-current Lagrangian are invariant under the U(3) flavour symmetry but the diagonalisation in the quark mass sector introduces the CKM matrix in the charged-current interactions. This leads to flavour-changing charged currents whereas flavour-changing neutral currents are forbidden at tree-level in the SM.

Despite the success of the SM in describing the elementary interactions of particles there are several shortcomings. One of these shortcomings is the absence of neutrino masses in the SM. This is a major flaw as multiple experiments show that neutrinos possess a non-zero mass. We will elaborate this issue in more detail in the last section of this chapter.

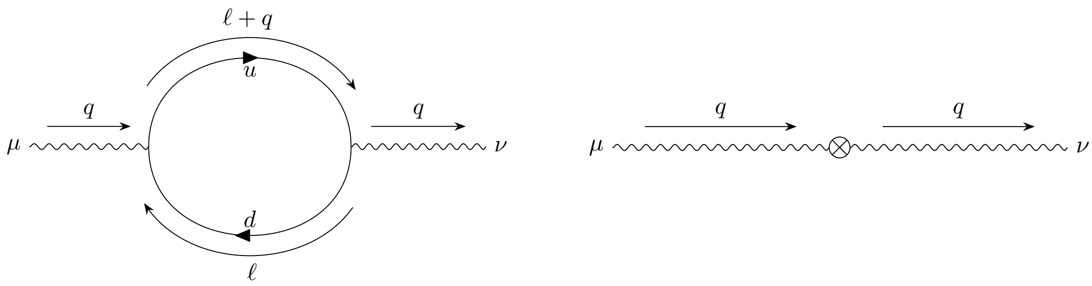

(a) One-loop gauge boson self-energy diagram

(b) Counter term

Figure 2.1.: One-loop gauge boson self-energy diagram. This constitutes the leading-order contribution to the gauge boson correlator. All diagrams in this thesis are drawn using TikZ-Feynman [33]

2.2. Renormalisation and QCD

We will utilise several properties of renormalisation and Quantum Chromo Dynamics (QCD). To that end we give a brief overview of the process of renormalising a theory and the intricacies this brings along. This is frequently discussed in textbooks and we refer to a selection here on which this section is based [21, 30–32].

In this work we will use gauge boson correlators which follow from the calculation of the gauge boson self-energy. To this end we look at a W boson self-energy, in particular the vectorial part where we set the up-type quark mass to zero (see Fig. 2.1(a)). The amplitude of this diagram reads

$$\mathcal{A}^{\mu\nu} = -N_c \frac{g_2^2 |V_{ud}|^2}{8} \int \frac{\mathrm{d}^4 \ell}{(2\pi)^4} \frac{\mathrm{Tr}[\gamma^\nu (\not\ell + \not q) \gamma^\mu (\not\ell + m_d)]}{((\ell + q)^2 + i\delta)(\ell^2 - m_d^2 + i\delta)}, \tag{2.19}$$

here the γ_μ are the Dirac γ matrices which satisfy the Clifford algebra $\{\gamma^\mu, \gamma^\nu\} = 2g^{\mu\nu}$. We can check the naive degree of divergence of the loop integral: $\mathcal{A}_{\mu\nu} \sim \int_0^\Lambda \mathrm{d}\ell \ell = \Lambda^2/2$. In the loop integral we have to integrate over all possible momenta which includes infinitely large momenta. This amounts to taking the ultraviolet cutoff $\Lambda \to \infty$ and we see the integral diverges. These divergences are artefacts of the theoretical description. Since measurable observables are finite it is necessary to regulate the divergence in this integral and subsequently renormalise the quantities in our Lagrangian that lead to this divergence in a way that a finite observable is restored. The most prominent regularisation method is dimensional regularisation which amounts to calculating the above integral in $D = 4 - 2\epsilon$ dimensions. In particular this means that all Dirac matrices have to be promoted to D dimensional objects. While this is straight forward for the Dirac matrices itself a D-dimensional version of $\gamma_5 = i\gamma_0\gamma_1\gamma_2\gamma_3$ is not well defined. Provided one encounters loop diagrams involving γ_5 special care has to be taken on how to treat it. We refer to Refs. [34–36] to name only a few. Furthermore, promoting all objects in Eq. (2.19) to D dimensions means that also all fermion and boson fields have to be promoted to D dimensions. This changes the energy dimension of the fields to $[\psi] = (D-1)/2$ and $[W_\mu^+] = (D-2)/2$. The energy dimension of the Lagrangian is fixed by the requirement that the action is dimensionless. In D dimensions this means the Lagrangian has to have dimension D. Inspecting the Lagrangian of the charged current in Eq. (2.18) we see this is only possible if in addition to the fields changing dimension the coupling constant is also promoted to $g_2 \longrightarrow g_2\mu^\epsilon$ where μ is an arbitrary parameter of dimension $[\mu] = 1$ and is called the renormalisation scale. In D dimensions the loop integral becomes

$$\mathcal{A}^{\mu\nu} = -N_c \frac{g_2^2|V_{ud}|^2}{8}\mu^{2\epsilon}\int \frac{\mathrm{d}^D\ell}{(2\pi)^D}\frac{\mathrm{Tr}[\gamma^\nu(\not{\ell}+\not{q})\gamma^\mu(\not{\ell}+m_d)]}{((\ell+q)^2+i\delta)(\ell^2-m_d^2+i\delta)}. \tag{2.20}$$

This amplitude is connected to the vectorial gauge boson correlator, which we will introduce in detail in the next section, through

$$\mathcal{A}^{\mu\nu} = i\frac{g_2^2|V_{ud}|^2}{8}\Pi^{\mu\nu}_{ud,V}. \tag{2.21}$$

The loop integral may be evaluated using e.g. Ref. [37]

$$\begin{aligned}\mathcal{A}^{\mu\nu} = {} & iN_c\frac{g_2^2|V_{ud}|^2}{8} \\ & \times\left[(-q^2g^{\mu\nu}+q^\mu q^\nu)\frac{1}{2\pi^2}\int_0^1 \mathrm{d}x(1-x)\left(x-\frac{m_d^2}{2q^2+i\delta}\right)\left(\frac{1}{\epsilon}-\ln\left(\frac{(1-x)(-xq^2+m_d^2)}{\mu^2}\right)\right)\right] \\ & + q^\mu q^\nu\frac{m_d^2}{2q^2+i\delta}\frac{1}{2\pi^2}\int_0^1 \mathrm{d}x(1-x)\left(\frac{1}{\epsilon}-\ln\left(\frac{(1-x)(-xq^2+m_d^2)}{\mu^2}\right)\right)\Bigg].\end{aligned} \tag{2.22}$$

In this way the divergences are now regularised and appear as poles $1/\epsilon$; taking $\epsilon \to 0$ reproduces the divergence. Here we used the $\overline{\mathrm{MS}}$ scheme and absorbed a term $-\gamma_E+\ln(4\pi)$, where γ_E is the Euler-Mascheroni constant, into the renormalisation scale μ [38]. In general, to get rid of these UV divergences the quantum field theory has to be renormalised. However, in the case of the correlator this UV pole only contributes to the real part of $\Pi^{\mu\nu}_{ud,V}$ and as such no electroweak renormalisation is required for a finite imaginary part (this always holds for the correlator even if gluon corrections are included, which require a QCD renormalisation for a finite imaginary part). Nevertheless, we will explain key concepts of renormalisation using this one-loop example and point out that in general electroweak renormalisations are very difficult. The idea of renormalisation is that the above calculation was performed for the bare Lagrangian i.e. the unrenormalised Lagrangian in which we denote the unrenormalised quantities by a superscript zero e.g. $W_\mu^{0,+}$. We then write the bare quantities in terms of the renormalised quantities e.g.

$$W_\mu^{0,+} = \sqrt{Z_W}W_\mu^{R,+}, \tag{2.23}$$

where the superscript R denotes it is now a renormalised quantity. A renormalisation constant Z_i has the general form

$$Z_i = 1 + g_k^2\frac{a_{1,i}}{\epsilon} + O\left(\frac{1}{\epsilon^2}\right), \tag{2.24}$$

where g_k is a gauge coupling and $a_{1,i}$ is a renormalisation scale independent constant; in our case here $g_k = g_2$. At the one-loop level only $1/\epsilon$ UV poles will be encountered whereas at the n-loop level there will be up to $1/\epsilon^n$ UV poles. In this way every quantity in the Lagrangian should be renormalised. Coming back to our one-loop example we will set the quark mass $m_d = 0$ for simplicity. It is sufficient to only renormalise the W boson field. This means we write

$$\begin{aligned}\mathcal{L}_{\rm SM} \supset -\frac{1}{2}\hat{W}^{0,+}_{\mu\nu}\hat{W}^{0,\mu\nu,-} &= -\frac{1}{2}Z_W\hat{W}^{R,+}_{\mu\nu}\hat{W}^{R,\mu\nu,-}\\ &= -\frac{1}{2}\hat{W}^{R,+}_{\mu\nu}\hat{W}^{R,\mu\nu,-} - \frac{1}{2}(Z_W-1)\hat{W}^{R,+}_{\mu\nu}\hat{W}^{R,\mu\nu,-},\end{aligned} \tag{2.25}$$

where we use the shorthand notation $\hat{X}^{\mu\nu} = \partial^\mu X^\nu - \partial^\nu W^\mu$. The first term in the last line above is the same Lagrangian as for the unrenormalised fields and will also give rise to divergences. However, now there is an additional term coming with the factor $Z_W - 1$ which is referred to as a counter term. It gives rise to the diagram in Fig. 2.1(b) which reads

$$\mathcal{A}^{\rm CT}_{\mu\nu} = -i(Z_W-1)(q^2 g_{\mu\nu} - q_\mu q_\nu). \tag{2.26}$$

This term has to cancel the $1/\epsilon$ divergence which means we can read it off of Eq. (2.22) to be

$$Z_W - 1 = -N_c\frac{g_2^2|V_{ud}|^2}{8}\frac{1}{2\pi^2}\int_0^1 \mathrm{d}x(1-x)x\frac{1}{\epsilon}. \tag{2.27}$$

Adding together the amplitudes associated with the diagram in Fig. 2.1(a) and 2.1(b) the resulting amplitude is finite

$$\begin{aligned}\mathcal{A}^R_{\mu\nu} &= \mathcal{A}_{\mu\nu} + \mathcal{A}^{\rm CT}_{\mu\nu}\\ &= iN_c\frac{g_2^2|V_{ud}|^2}{8}(-q^2 g_{\mu\nu} + q_\mu q_\nu)\frac{-1}{2\pi^2}\int_0^1 \mathrm{d}x(1-x)x\ln\left(\frac{-(1-x)xq^2}{\mu^2}\right).\end{aligned} \tag{2.28}$$

There is a certain amount of freedom in the choice of the renormalisation constants Z_i. For example one can freely add or subtract arbitrary constants. This means that constant terms cannot contribute to an observable and must cancel out in the observable. Furthermore, two independent calculations of the same loop contribution may be different up to this choice of constants which is called the renormalisation scheme dependence. If we take only the finite parts of Eq. (2.22) keeping the quark mass non-zero we obtain

$$\begin{aligned}&\left(i\frac{g_2^2|V_{ud}|^2}{8}\right)^{-1}\mathcal{A}^{\rm finite}_{\mu\nu} =\\ &\Pi^{\mu\nu}_{ud,V} = \Bigg((-q^2 g_{\mu\nu} + q_\mu q_\nu)\Bigg[-\frac{N_c}{12\pi^2}\left(\ln\left(\frac{-q^2}{\mu^2}\right) - \frac{5}{3}\right)\\ &\qquad + \frac{m_d^2}{-q^2 - i\delta}\frac{N_c}{16\pi^2}\left(-2\ln\left(\frac{-q^2}{\mu^2}\right)\right)\Bigg]\\ &\qquad + q_\mu q_\nu\left[\frac{m_d^2}{-q^2 - i\delta}\frac{N_c}{16\pi^2}\left(-4 + 2\ln\left(\frac{-q^2}{\mu^2}\right)\right)\right]\Bigg)\end{aligned} \tag{2.29}$$

where we now see that we actually obtain a constant term in the first line. A different choice of the counter term could subtract this constant part away. Furthermore, it turns out that the physical quantities calculated in this thesis only depend on the imaginary part of $\Pi^{\mu\nu}_{ud,V}$ and hence only the logarithmic term with its branch cut will contribute to an observable while the constant term drops out (for the massless parts). In contrast, the terms scaling with the quark mass m_d^2 contain constant terms as well which are individually physical. Next, we can add QCD corrections to the self-energy by adding gluons in the loop in Fig. 2.1(a). As we have sketched above, corrections including gluons will require a renormalisation of the quark fields and masses as well as the strong coupling constant g_s

$$g_s^0 = Z_s g_s^R \mu^\epsilon. \tag{2.30}$$

The renormalisation scale μ is arbitrary and thus observables should not depend on it. Furthermore, the bare quantity does not depend on the renormalisation scale. This gives rise to the differential equation

$$0 = \mu^2 \frac{\mathrm{d}}{\mathrm{d}\mu^2} g_s^0 \quad \Leftrightarrow \quad \mu^2 \frac{\mathrm{d}}{\mathrm{d}\mu^2} a_\mu = \beta(a_\mu) - \epsilon a_\mu, \tag{2.31}$$

where we defined the strong coupling constant $\alpha_s(\mu) = (g_s^R)^2/(4\pi)$, $a_\mu = \alpha_s/\pi$, and the QCD β-function. When working with fully renormalised quantities one may set $\epsilon = 0$ and obtain the renormalisation group equation (RGE) of the strong coupling constant

$$\frac{\mathrm{d}a_\mu}{\mathrm{d}\ln\mu^2} = \beta(a_\mu) = -a_\mu^2\Big[\beta_0 + \beta_1 a_\mu + \beta_2 a_\mu^2 + \ldots\Big], \tag{2.32}$$

with the coefficients β_i relevant to this work being [39–44]:

$$\beta_0 = \frac{1}{4}\left(11 - \frac{2}{3}n_f\right), \tag{2.33}$$

$$\beta_1 = \frac{1}{16}\left(102 - \frac{38}{3}n_f\right), \tag{2.34}$$

$$\beta_2 = \frac{1}{64}\left(\frac{2857}{2} - \frac{5033}{18}n_f + \frac{325}{54}n_f^2\right). \tag{2.35}$$

This allows us to relate the strong coupling constant at two different scales to each other through

$$\begin{aligned} a(\mu) =& a(\mu_0) - a(\mu_0)^2\beta_0\ell_{\mu\mu_0} + a(\mu_0)^3\Big[-\beta_1\ell_{\mu\mu_0} + \beta_0^2\ell_{\mu\mu_0}^2\Big] \\ &+ a(\mu_0)^4\Big[-\beta_2\ell_{\mu\mu_0} + \frac{5}{2}\beta_0\beta_1\ell_{\mu\mu_0}^2 - \beta_0^3\ell_{\mu\mu_0}^3\Big] + O(a(\mu_0)^5), \end{aligned} \tag{2.36}$$

where $\ell_{\mu\mu_0} = \ln(\mu^2/\mu_0^2)$. A similar equation may be found for the quark masses $m = m(\mu)$ which also depend on the renormalisation scale μ through the quark mass renormalisation

$$\frac{\mathrm{d}m}{\mathrm{d}\ln\mu^2} = -\gamma(a_\mu)m(\mu) = -m(\mu)\Big[\gamma_0 a_\mu + \gamma_1 a_\mu^2 + \gamma_2 a_\mu^3 + \ldots\Big], \tag{2.37}$$

with the relevant coefficients being [45, 46]

$$\gamma_0 = 1, \tag{2.38}$$

$$\gamma_1 = \frac{1}{16}\left(\frac{202}{3} - \frac{20}{9}n_f\right), \tag{2.39}$$

$$\gamma_2 = \frac{1}{64}\left(1249 - \left[\frac{2216}{27} + \frac{160}{3}\zeta_3\right]n_f - \frac{140}{81}n_f^2\right). \tag{2.40}$$

The solution expanded in a_μ is

$$\begin{aligned} m(\mu) =& m(\mu_0)\Bigg[1 - a(\mu_0)\gamma_0\ell_{\mu\mu_0} + a(\mu_0)^2\left(-\gamma_1\ell_{\mu\mu_0} + \frac{1}{2}\gamma_0(\beta_0+\gamma_0)\ell_{\mu\mu_0}^2\right) \\ &+ a(\mu_0)^3\Bigg(-\gamma_2\ell_{\mu\mu_0} + \frac{1}{2}(\beta_1\gamma_0 + 2(\beta_0+\gamma_0)\gamma_1)\ell_{\mu\mu_0}^2 \\ &- \frac{1}{6}\gamma_0(2\beta_0^2 + 3\beta_0\gamma_0 + \gamma_0^2)\ell_{\mu\mu_0}^3\Bigg)\Bigg]. \end{aligned} \tag{2.41}$$

We close this section by briefly commenting on effective field theories (EFT). In nature there is often a large difference in energy scales between the different particles in a given process. For example a charm quark decays via a charged current $c \to s\bar{d}u$. Notice that the W boson is far heavier than all the other particles in the process m_c, m_s, m_d, $m_u \ll M_W$. Calculating this process the resulting amplitude will involve the W boson propagator which is proportional to $1/(q^2 - M_W^2)$. Since the charm quark is much lighter than the W boson the transferred momentum q^2 is small against M_W^2 and the propagator may be Taylor expanded to $1/(q^2 - M_W^2) = -1/M_W^2 + O(q^2/M_W^2)$. In doing so the W boson disappears from the theory as a dynamical degree of freedom, it is integrated out, and we can describe the decay of a charm quark as an effective interaction between two fermionic currents

$$\mathcal{H} = \frac{\hat{C}}{M_W^2}Q, \qquad Q = (\bar{s}\gamma_\mu(1-\gamma_5)c)\,(\bar{u}\gamma^\mu(1-\gamma_5)d). \tag{2.42}$$

The operator Q is a dimension 6 operator. The Hamiltonian, however, still has dimension 4 since now there is a dimensionful coefficient $\hat{C}/M_W^2$ in which the W mass suppresses the interaction strength. The coefficient $\hat{C}$ is called the Wilson coefficient. It is common to write the Hamiltonian like

$$\mathcal{H} = \frac{G_F}{\sqrt{2}}V_{cs}^* V_{ud} C Q \tag{2.43}$$

with $G_F/\sqrt{2} = g_2^2/(8M_W^2)$ where $G_F = 1.166\,378\,5(6) \times 10^{-5}\,\mathrm{GeV}^{-2}$ is the Fermi constant [8]. Without the inclusion of QCD corrections $C = 1$. One may now add QCD corrections to the charm quark decay. Formally this leads to an additional operator with the same Dirac structure as above but a different colour structure. We refer to Ref. [21] for more details on the calculation. The takeaway is that one must calculate the charm decay in the full theory, which includes the W boson, and the effective theory in which it is absent. By demanding the two amplitudes to be equal the Wilson coefficient may be fixed, this process is called matching. The QCD corrections will lead to UV divergences which need to be removed by a renormalisation. In contrast to the full theory it is now also necessary to perform an additional renormalisation of the operator Q itself. After this renormalisation all quantities are finite in the EFT and the Wilson coefficient will have the general form

$$C(\mu) = c_1 + c_2 a_\mu \ln\left(\frac{M_W^2}{\mu^2}\right) + \ldots \tag{2.44}$$

where the c_i are constants. In this EFT the W boson is absent. The only object containing information about the high energy physics is the Wilson coefficient. Furthermore, the Wilson coefficient is scheme dependent through the choice of the operator renormalisation. As before this scheme dependence is unphysical and observables will not be sensitive to it. Lastly, the Wilson coefficient contains logarithms involving the renormalisation scale μ and the heavy scale M_W. Simply setting $\mu = m_c$ will introduce a large logarithm and thus spoil the convergence of the perturbative series. This effect may be remedied by employing the renormalisation group. Indeed the Wilson coefficient satisfies an RGE similar to the quark masses. We will come back to this in Sec. 3.3.2.

Throughout this work we will apply the RGE of the strong coupling constant, the quark masses, and the Wilson coefficients as well as certain properties of the scale dependence of observables.

2.3. Gauge Boson Decay

2.3.1. Gauge Boson Correlators

We are interested in the QCD corrections to HSN decay. From Eq. (2.17) and (2.18) we see that leptons and thus also HSN only couple to quarks through the electroweak gauge bosons. Hadronic decays of the heaviest lepton $\ell = \tau$ or of HSN are thus fully described by the hadronic decays of the virtual gauge bosons.

The central object describing on- and off-shell gauge boson decay is the two-point correlation function of the currents $j^\mu_{ij,V} = \overline{\psi}_i \gamma^\mu \psi_j$ and $j^\mu_{ij,A} = \overline{\psi}_i \gamma^\mu \gamma_5 \psi_j$

$$\begin{aligned}
\Pi^{\mu\nu}_{ij,V/A}(q, m_i, m_j, \mu, \alpha_s) &= i \int \mathrm{d}x\, e^{iqx} \langle 0|\hat{T}\{j^\mu_{ij,V/A}(x) j^{\nu,\dagger}_{ij,V/A}(0)\}|0\rangle \\
&= (-g_{\mu\nu} q^2 + q_\mu q_\nu)\Pi^{(1)}_{ij,V/A}(q^2) + q_\mu q_\nu \Pi^{(0)}_{ij,V/A}(q^2) \\
&= g_{\mu\nu}\Pi^{[1]}_{ij,V/A}(q^2) + q_\mu q_\nu \Pi^{[2]}_{ij,V/A}(q^2),
\end{aligned} \tag{2.45}$$

where in the second and third line we give the two commonly used decompositions into possible Lorentz structures [47]. Here, q^2 is the invariant mass of the on- or off-shell gauge boson. $\Pi^{(1)}_{ij,V/A}$ is the transversal and $\Pi^{(0)}_{ij,V/A}$ the longitudinal part of the correlator. They are related to the $\Pi^{[1,2]}_{ij,V/A}$ through

$$\Pi^{(1)}_{ij,V/A} = -\frac{\Pi^{[1]}_{ij,V/A}}{q^2}, \qquad \Pi^{(0)}_{ij,V/A} = \Pi^{[2]}_{ij,V/A} + \frac{\Pi^{[1]}_{ij,V/A}}{q^2}. \tag{2.46}$$

Furthermore, the gauge boson correlator satisfies the Ward identity [48–50]

$$q_\mu q_\nu \Pi^{\mu\nu}_{ij,V/A} = q^4 \Pi^{(0)}_{ij,V/A} = (m_j \mp m_i)^2 \Pi^{S/P}_{ij} + (m_j \mp m_i) \langle 0|\overline{\psi}_j \psi_j \mp \overline{\psi}_i \psi_i|0\rangle , \tag{2.47}$$

relating the longitudinal part of the correlator to the quark condensate and the scalar or pseudoscalar correlator

$$\Pi^{S/P}_{ij}(q) = i \int \mathrm{d}x\, e^{iqx} \langle 0|\hat{T}\{j^{S/P}_{ij}(x) j^{S/P\,\dagger}_{ij}(0)\}|0\rangle , \qquad j^{S/P}_{ij} = \bar{\psi}_i(\gamma_5)\psi_j . \tag{2.48}$$

In the chiral limit ($m_q = 0$) this means

$$\Pi^{(0)}_{ij,V/A} = 0 \quad \Rightarrow \quad \Pi^{[2]}_{ij,V/A} = -\frac{\Pi^{[1]}_{ij,V/A}}{q^2} . \tag{2.49}$$

The gauge correlator corresponds to the gauge boson self-energy. By inserting $\hat{\mathbb{1}} = \sum_n \int \prod_{i\in n} \mathrm{d}^3\vec{p}_i/((2\pi)^2 2E_i) |n\rangle \langle n| = \sum_n \int d\Pi_n |n\rangle \langle n|$ into Eq. (2.45) and then taking the imaginary part [32, 50–52]

$$\mathrm{Im}\, \Pi^{\mu\nu}_{ij,V/A} = \frac{1}{2} \sum_n \int \mathrm{d}\Pi_n (2\pi)^4 \delta^{(4)}(q - p_n) \langle 0|j^\mu_{ij,V/A}(0)|n\rangle \langle n|j^{\nu,\dagger}_{ij,V/A}(0)|0\rangle , \tag{2.50}$$

we see that the imaginary part of the correlator is, up to coupling constants and the contraction with remaining Lorentz structures, proportional to the sum of all decay rates of the gauge boson into final states $|n\rangle$. This is the optical theorem.

QCD corrections to the correlator can be calculated by including gauge boson self-energy diagrams with gluons. In Fig. 2.2 we show examples of such contributions. All of these corrections are important as they can have a sizeable impact on the prediction of the τ and Z lifetime. These corrections have been calculated up to $\mathcal{O}(\alpha_s^4)$ in the chiral limit ($m_q = 0$) for both the W and the Z correlator [53–55] and quadratic quark mass corrections are available at $\mathcal{O}(\alpha_s^3)$ for W and Z [56–59]. The W and Z correlators may be expressed as a series in the strong coupling constant $\alpha_s(\mu)$. In this work we write all of these corrections in terms of

$$a_\mu = \frac{\alpha_s(\mu)}{\pi} . \tag{2.51}$$

In the following we state the known results for both the charged and the neutral gauge boson correlator in the chiral limit as well as their quark mass corrections.

2.3.2. W Boson Correlator

The W correlator $\Pi^{(J)}_{ij,V/A}$ may be decomposed into a massless part and a massive part scaling with the quark masses. Including corrections quadratic in the quark masses the correlator is given by [58]

$$\Pi^{(1+0)}_{ij,V/A} = \hat{\Pi}^{(1+0)}_{ij,V/A} + \frac{N_c}{16\pi^2} \frac{m^2_{i,j}}{-q^2} \Pi^{(1+0)}_{ij,V/A,2} , \tag{2.52}$$

$$\Pi^{(0)}_{ij,V/A} = \frac{N_c}{16\pi^2} \frac{m^2_{i,j}}{-q^2} \Pi^{(0)}_{ij,V/A,2} , \tag{2.53}$$

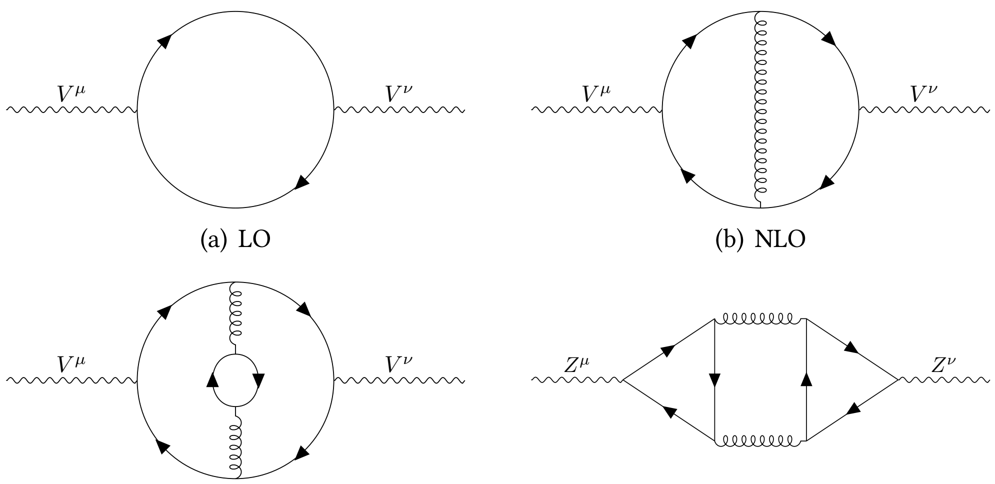

(a) LO (b) NLO

(c) NNLO (d) NNLO - Z only

Figure 2.2.: Examples of gauge boson self-energy diagrams contributing to the QCD corrections for $V = W, Z$. The fourth diagram is only present if the gauge boson is a Z, for W bosons this diagram does not exist.

where $N_c = 3$ is the number of colours, $m_{i,j} = m_{i,j}(\mu)$ is the heavier running quark mass in the $\overline{\text{MS}}$-scheme of the two quarks i and j, and with $\Pi^{(1+0)}_{ij,V/A}(q^2) = \Pi^{(1)}_{ij,V/A}(q^2) + \Pi^{(0)}_{ij,V/A}(q^2)$. The first term in the $\Pi^{(1+0)}_{ij,V/A}(q^2)$ part of the correlator is the massless correction. Due to the Ward identity (Eq. (2.47)) there is no massless longitudinal contribution.

The massless part $\hat{\Pi}^{(1+0)}_{ij,V/A}$ as a series in a_μ reads [60]

$$\hat{\Pi}^{(1+0)}_{ij,V/A}(s) = -\frac{N_c}{12\pi^2} \sum_{n=0}^{\infty} a_\mu^n \sum_{k=1}^{n+1} c_{n,k} \ln^k\left(\frac{-s}{\mu^2}\right), \qquad s = q^2, \tag{2.54}$$

where the branch cut is understood to be taken as $s \longrightarrow s + i\delta$ leading to $\ln(-s/\mu^2 - i\delta) = \ln(s/\mu^2) - i\pi$. The $c_{n,1}$ coefficients are [53, 61–66]

$$c_{0,1} = c_{1,1} = 1, \tag{2.55}$$

$$c_{2,1} = -\left(\frac{11}{12} - \frac{2}{3}\zeta_3\right)n_f + \frac{365}{24} - 11\zeta_3, \tag{2.56}$$

$$\begin{aligned} c_{3,1} = &\left(\frac{151}{162} - \frac{19}{27}\zeta_3\right)n_f^2 - \left(\frac{7847}{216} - \frac{262}{9}\zeta_3 + \frac{25}{9}\zeta_5\right)n_f \\ &+ \frac{87029}{288} - \frac{1103}{4}\zeta_3 + \frac{275}{6}\zeta_5, \end{aligned} \tag{2.57}$$

$$\begin{aligned} c_{4,1} = &\left(\frac{203}{324}\zeta_3 + \frac{5}{18}\zeta_5 - \frac{6131}{5832}\right)n_f^3 \\ &+ \left(-\frac{40655}{864}\zeta_3 + \frac{5}{6}\zeta_3^2 - \frac{260}{27}\zeta_5 + \frac{1045381}{15552}\right)n_f^2 \\ &+ \left(\frac{12205}{12}\zeta_3 - 55\zeta(3)^2 + \frac{29675}{432}\zeta_5 + \frac{665}{72}\zeta_7 - \frac{13044007}{10368}\right)n_f \end{aligned}$$

$$-\frac{7315}{48}\zeta_7+\frac{65945}{288}\zeta_5+\frac{5445}{8}\zeta_3^2-\frac{5693495}{864}\zeta_3+\frac{144939499}{20736}, \tag{2.58}$$

with n_f being the number of active flavours and $\zeta_n \equiv \zeta(n)$ is the Riemann ζ-function. The remaining $c_{n,k}$ coefficients are related to the $c_{n,1}$ coefficients through the renormalisation group (RG) invariant Adler function [67]

$$D^{(1+0)}(s) = -s\frac{d}{ds}\Pi^{(1+0)}_{ij,V/A}(s), \qquad \mu^2\frac{d}{d\mu^2}D^{(1+0)}_{ij,V/A}(s) = 0, \tag{2.59}$$

leading to

$$c_{2,2} = -\frac{\beta_0}{2}c_{1,1} \tag{2.60}$$

$$c_{3,3} = \frac{\beta_0^2}{3}c_{1,1}, \qquad c_{3,2} = -\frac{\beta_1}{2}c_{1,1} - \beta_0 c_{2,1} \tag{2.61}$$

$$\begin{aligned} c_{4,4} &= -\frac{\beta_0^3}{4}c_{1,1}, \qquad c_{4,3} = \frac{5}{6}\beta_1\beta_0 c_{1,1} + \beta_0^2 c_{2,1}, \\ c_{4,2} &= -\frac{1}{2}\big(\beta_2 c_{1,1} + 2\beta_1 c_{2,1} + 3\beta_0 c_{3,1}\big), \end{aligned} \tag{2.62}$$

where all $c_{n,k} = 0$ if $n \neq 0$ and $k > n$. For our calculation of the HSN decay rate we will need the imaginary part of the massless correlator

$$\begin{aligned} \mathrm{Im}\,\hat{\Pi}^{(1+0)}_{ij,V/A}(s) &= -\frac{1}{12\pi^2}\sum_{n=0}^{\infty} a_\mu^n \sum_{k=1}^{n+1} c_{n,k}\mathrm{Im}\,\ln^k\left(\frac{-s}{\mu^2}\right) \\ &= \frac{1}{12\pi}\Bigg\{1 + a_\mu + a_\mu^2\big[c_{2,1} + 2c_{2,2}\ell_{s\mu^2}\big] + a_\mu^3\Big[c_{3,1} + 2c_{3,2}\ell_{s\mu^2} - \Big(\pi^2 - 3\ell^2_{s\mu^2}\Big)c_{3,3}\Big] \\ &\quad + a_\mu^4\Big[c_{4,1} + 2c_{4,2}\ell_{s\mu^2} - \Big(\pi^2 - 3\ell^2_{s\mu^2}\Big)c_{4,3} - \Big(4\pi^2\ell_{s\mu^2} - 4\ell^3_{s\mu^2}\Big)c_{4,4}\Big]\Bigg\} \end{aligned} \tag{2.63}$$

where we have used $\ell_{s\mu^2} = \ln(s/\mu^2)$.

The quark mass corrections to the correlator read [47, 57–59, 68–71]

$$\begin{aligned} \Pi^{(1+0)}_{ij,V/A,2} = &-4\Bigg(1 + a_\mu\left[\frac{7}{3} - 2\ell_{-s\mu^2}\right] \\ &+ a_\mu^2\Bigg[n_f\left(-\frac{1}{6}\ell^2_{-s\mu^2} + \frac{2}{3}\ell_{-s\mu^2} - \frac{2}{9}\zeta_3 - \frac{25}{24}\right) + \frac{19}{4}\ell^2_{-s\mu^2} - \frac{39}{2}\ell_{-s\mu^2} \\ &\qquad + \frac{359}{54}\zeta_3 - \frac{520}{27}\zeta_5 + \frac{15331}{432}\Bigg] \\ &+ a_\mu^3\Bigg[n_f^2\left(-\frac{1}{54}\ell^3_{-s\mu^2} + \frac{1}{9}\ell^2_{-s\mu^2} + \ell_{-s\mu^2}\left(-\frac{2}{27}\zeta_3 - \frac{95}{324}\right) + \frac{19}{81}\zeta_3 + \frac{2131}{11664}\right) \\ &\qquad + n_f\Bigg(\frac{17}{18}\ell^3_{-s\mu^2} - \frac{491}{72}\ell^2_{-s\mu^2} + \left(\frac{899}{162}\zeta_3 - \frac{520}{81}\zeta_5 + \frac{16007}{648}\right)\ell_{-s\mu^2} \\ &\qquad\quad - \frac{52}{27}\zeta_3^2 - \frac{3997}{486}\zeta_3 + \frac{3875}{243}\zeta_5 - \frac{\pi^4}{108} - \frac{68135}{1944}\Bigg) \end{aligned}$$

$$
\begin{aligned}
&-\frac{95}{8}\ell^3_{-s\mu^2}+\frac{1055}{12}\ell^2_{-s\mu^2}+\left(-\frac{1795}{36}\zeta_3+\frac{1300}{9}\zeta_5-\frac{8153}{24}\right)\ell_{-s\mu^2}\\
&+\frac{653}{18}\zeta_3^2+\frac{29333}{648}\zeta_3-\frac{138695}{324}\zeta_5+\frac{79835}{648}\zeta_7+\frac{2629301}{5184}\Bigg]\Bigg),
\end{aligned}
\tag{2.64}
$$

with $\ell_{-s\mu^2}=\ln(-s/\mu^2)$. These corrections were originally calculated for the analysis of τ decays where the above correlator is the contribution of $ij=us$. There is also a contribution of the heavier quark only appearing in gluon self-energy corrections corresponding to $ij=ud$. This effect, however, is numerically small and we neglect it. The longitudinal part of the correlator[1] reads [47–49, 56–59, 71–74]

$$
\begin{aligned}
\Pi^{(0)}_{ij,V/A,2}=&-4\Bigg(-\frac{1}{2}\ell_{-s\mu^2}+a_\mu\left[\frac{1}{2}\ell^2_{-s\mu^2}-\frac{17}{6}\ell_{-s\mu^2}\right]\\
&+a_\mu^2\Bigg[n_f\left(\frac{1}{36}\ell^3_{-s\mu^2}-\frac{11}{36}\ell^2_{-s\mu^2}+\left(\frac{65}{48}-\frac{1}{3}\zeta_3\right)\ell_{-s\mu^2}\right)\\
&\qquad-\frac{19}{24}\ell^3_{-s\mu^2}+\frac{53}{6}\ell^2_{-s\mu^2}+\left(\frac{39}{4}\zeta_3-\frac{10801}{288}\right)\ell_{-s\mu^2}\Bigg]\\
&+a_\mu^3\Bigg[n_f^2\left(\frac{1}{432}\ell^4_{-s\mu^2}-\frac{11}{324}\ell^3_{-s\mu^2}+\left(\frac{275}{1296}-\frac{1}{18}\zeta_3\right)\ell^2_{-s\mu^2}+\left(\frac{1}{6}\zeta_3-\frac{15511}{23328}\right)\ell_{-s\mu^2}\right)\\
&\qquad+n_f\Bigg(-\frac{17}{144}\ell^4_{-s\mu^2}+\frac{277}{144}\ell^3_{-s\mu^2}+\left(\frac{59\zeta_3}{24}-\frac{11651}{864}\right)\ell^2_{-s\mu^2}\\
&\qquad\quad+\left(-\frac{131}{9}\zeta_3+\frac{25}{18}\zeta_5+\frac{\pi^4}{216}+\frac{46147}{972}\right)\ell_{-s\mu^2}\Bigg)\\
&\qquad+\frac{95}{64}\ell^4_{-s\mu^2}-\frac{3535}{144}\ell^3_{-s\mu^2}+\left(\frac{49349}{288}-\frac{585}{16}\zeta_3\right)\ell^2_{-s\mu^2}\\
&\qquad\quad+\left(\frac{109735}{432}\zeta_3-\frac{815}{24}\zeta_5-\frac{6163613}{10368}\right)\ell_{-s\mu^2}\Bigg]+C^{(0)}_\Pi(a_\mu)\Bigg),
\end{aligned}
\tag{2.65}
$$

here we comprised all constant terms into $C^{(0)}_\Pi(a_\mu)$

$$
C^{(0)}_\Pi(a_\mu)=1+a_\mu\left[\frac{131}{24}-2\zeta_3\right]+a_\mu^2\left[n_f\left(-\frac{511}{216}+\frac{2}{3}\zeta_3\right)+\frac{17645}{288}-\frac{353}{12}\zeta_3-\frac{1}{8}\zeta_4+\frac{25}{6}\zeta_5\right],
\tag{2.66}
$$

which is known completely up to $\mathcal{O}(\alpha_s^2)$.

2.3.3. Z Boson Correlator

For the Z correlator it is common to consider the Z boson contribution to the R ratio

$$
R(s)=\frac{\sigma(e^+e^-\to\text{hadrons})}{\sigma(e^+e^-\to\mu^+\mu^-)},
\tag{2.67}
$$

[1]We obtain $\Pi^{(0)}_{ij,V/A,2}$ by using the notation presented in Ref. [59]. In their notation $\Pi^{(0)}_{ij,V/A,2}=3/(-16\pi^2q^2)(\Pi_2^{[2]}-\Pi_2^{[1]})$ where $\Pi_2^{[1]}$ follows from Ref. [57].

instead of the correlator itself. The Z contribution to $R(s)$ is connected to the correlator through [54, 75]

$$-N_c \frac{s}{12\pi} R(s) = \mathrm{Im} \sum_{ij} g_{i,V/A} g_{j,V/A} \Pi^{[1]}_{ij,V/A}(-s - i\delta), \tag{2.68}$$

here $g_{q,V} = T_3^q - 2Q_q \sin^2\theta_w$ and $g_{q,A} = T_3^q$ are the couplings of the Z boson to the quark q, and

$$R(s) = \sum_i g_{i,V}^2 R_V^{\mathrm{NS}} + \sum_i g_{i,A}^2 R_A^{\mathrm{NS}} + \left(\sum_i g_{i,V}\right)^2 R_V^{\mathrm{S}} + \left(\sum_i g_{i,A}\right)^2 R_{\Delta_t}^{\mathrm{S},A}. \tag{2.69}$$

The contributions here are grouped up according to the respective topology of the diagrams from which they stem. They may be decomposed into a massive and a massless part [76]

$$\sum_i g_{i,V}^2 R_V^{\mathrm{NS}} = \sum_i g_{i,V}^2 R^{\mathrm{NS}} + \mathrm{Im}\, \frac{m_q^2}{\pi s}\left(\sum_i g_{i,V}^2 R_2 + g_{q,V}^2 R_{q,2}^V\right), \tag{2.70}$$

$$\sum_i g_{i,A}^2 R_A^{\mathrm{NS}} = \sum_i g_{i,A}^2 R^{\mathrm{NS}} + \mathrm{Im}\, \frac{m_q^2}{\pi s}\left(\sum_i g_{i,A}^2 R_2 + g_{q,A}^2 R_{q,2}^A\right). \tag{2.71}$$

Here we denote the heavy quark by q with the mass $m_q(\mu)$. The non-singlet (NS) contributions are equal in the chiral limit and come from so-called bubble diagrams (Fig. 2.2(a)-2.2(c)). Up to the coupling constants these contributions are the same for the W and the Z boson. Including quark mass corrections both the vector and axial vector NS contributions receive the same contribution R_2 and then additionally terms which are different between vector $R_{q,2}^V$ and axial vector $R_{q,2}^A$ part. In contrast to the W correlator the Z correlator also receives contributions from triangle diagrams (Fig. 2.2(d)). For the vector singlet (S) part $R_{\mathrm{V}}^{\mathrm{S}}$ this is no issue as like the NS contributions it is related to a conserved current in the chiral limit and receives no renormalisation. $R_{\mathrm{V}}^{\mathrm{S}}$ starts at $\mathcal{O}(\alpha_s^3)$ and receives no quadratic quark mass corrections at this order [75]. The axial singlet contribution $R_{\Delta_t}^{\mathrm{S,A}}$ is anomalous. The SM is anomaly free and all SM particles carry quantum numbers in such a way that the anomaly cancels [32]. However, the cancellation of the anomalous contributions is not perfect in processes like Z decay and in order to calculate Z decay it is necessary to integrate out the top quark while preserving the anomaly cancellation of the SM [77–79]. This has been done and we quote the known results [80, 81]

$$\begin{aligned} R_{\Delta_t}^{\mathrm{S,A}} &= n_f C_h^2 R^{\mathrm{NS}} - 2(C_h R^{\mathrm{NS}} + n_f C_h R_A^{\mathrm{S}}) + R_A^{\mathrm{S}} + 2 n_f C_\psi R_A^{\mathrm{S}} + 2 C_\psi R^{\mathrm{NS}} \\ &= -2C_h + R_A^{\mathrm{S}} + \mathcal{O}(\alpha_s^3), \end{aligned} \tag{2.72}$$

here R_A^{S} is the contribution from triangle diagrams with only light quarks in the loop and starts at $\mathcal{O}(\alpha_s^2)$. The coefficients C_h and C_ψ are Wilson coefficients (WC) coming from integrating out the top quark. For our calculation we include the axial singlet contributions up to $\mathcal{O}(\alpha_s^2)$; in the second line above we write $R_{\Delta_t}^{\mathrm{S,A}}$ at $\mathcal{O}(\alpha_s^2)$ where we used that $C_h \sim \mathcal{O}(\alpha_s^2)$ and $C_\psi \sim \mathcal{O}(\alpha_s^3)$. The WC C_h reads [80, 81]

$$C_h(\mu) = (a_\mu^{(6)})^2\left[\frac{1}{8} - \frac{1}{2}\ln\left(\frac{\mu^2}{m_t(\mu)^2}\right)\right]. \tag{2.73}$$

In the WC the strong coupling constant is defined in the six-flavour theory. Formally this means $a_\mu^{(6)}$ should be decoupled to the $n_f = 5$ flavour theory for Z decay and $a_\mu^{(4)}$ or $a_\mu^{(3)}$ for the HSN decay case. At $O(\alpha_s^2)$ this yields no contribution as $a_\mu^{(n_f)} = a_\mu^{(n_f-1)} + O(\alpha_s^2)$. The same argument holds for the running quark mass $m_t(\mu) = m_t(m_t) + O(\alpha_s)$.

The functions R^{NS}, R_V^{S}, and R_A^{S} as an expansion in a_μ are [81]

$$R^{\mathrm{NS}} = 1 + \sum_{i\geq 1}^{j\leq i} a_\mu^i r_{i,j}^{\mathrm{NS}} \ln^j\left(\frac{\mu^2}{s}\right), \tag{2.74}$$

$$R_V^{\mathrm{S}} = \sum_{i\geq 3}^{j\leq i} a_\mu^i r_{i,j}^{\mathrm{S},V} \ln^j\left(\frac{\mu^2}{s}\right), \tag{2.75}$$

$$R_A^{\mathrm{S}} = \sum_{i\geq 2}^{j\leq i} a_\mu^i r_{i,j}^{\mathrm{S},A} \ln^j\left(\frac{\mu^2}{s}\right). \tag{2.76}$$

The non-singlet coefficients $r_{i,j}^{\mathrm{NS}}$ are equal to the $c_{n,k}$ up to the terms resulting from the imaginary part [53]

$$r_{1,0}^{NS} = c_{1,1}, \tag{2.77}$$

$$r_{2,0}^{NS} = c_{2,1}, \tag{2.78}$$

$$r_{3,0}^{NS} = c_{3,1} - \pi^2\frac{\beta_0^2}{3}c_{1,1}, \tag{2.79}$$

$$r_{4,0}^{NS} = c_{4,1} - \pi^2\left[\frac{5}{6}\beta_0\beta_1 c_{1,1} + \beta_0^2 c_{2,1}\right]. \tag{2.80}$$

The remaining $r_{i,j}^{NS}$ are related to the $r_{i,0}^{NS}$ through the RGE

$$\mu^2\frac{d}{d\mu^2}R^{\mathrm{NS}} = \mu^2\frac{d}{d\mu^2}R_V^{\mathrm{S}} = 0, \tag{2.81}$$

leading to

$$r_{2,1}^{NS} = \beta_0 r_{1,0}^{NS}, \tag{2.82}$$

$$r_{3,2}^{NS} = \beta_0^2 r_{1,0}^{NS}, \quad r_{3,1}^{NS} = \beta_1 r_{1,0}^{NS} + 2\beta_0 r_{2,0}^{NS}, \tag{2.83}$$

$$r_{4,3}^{NS} = \beta_0^3 r_{1,0}^{NS}, \quad r_{4,2}^{NS} = \frac{1}{2}\left(5\beta_1\beta_0 r_{1,0}^{NS} + 6\beta_0^2 r_{2,0}^{NS}\right), \quad r_{4,1}^{NS} = \beta_2 r_{1,0}^{NS} + 2\beta_1 r_{2,0}^{NS} + 3\beta_0 r_{3,0}^{NS}. \tag{2.84}$$

Similarly the vector singlet coefficients are given by [55, 65, 66]

$$r_{3,0}^{S,V} = \frac{55}{216} - \frac{5}{9}\zeta_3, \tag{2.85}$$

$$r_{4,0}^{S,V} = n_f\left(-\frac{745}{1296} + \frac{65}{72}\zeta_3 + \frac{5}{18}\zeta_3^2 - \frac{25}{36}\zeta_5\right) + \frac{5795}{576} - \frac{8245}{432}\zeta_3 - \frac{55}{12}\zeta_3^2 + \frac{2825}{216}\zeta_5, \tag{2.86}$$

$$r_{4,1}^{S,V} = 3\beta_0 r_{3,0}^{S,V}. \tag{2.87}$$

At $\mathcal{O}(\alpha_s^2)$ the axial singlet coefficients are [80, 82, 83]

$$r_{2,0}^{S,A} = -\frac{17}{6}, \qquad r_{2,1}^{S,A} = -2\gamma_0^{\psi}, \tag{2.88}$$

where $r_{2,1}^{S,A}$ follows from the RGE

$$\mu^2 \frac{d}{d\mu^2} R_A^S = 2\gamma^{\psi}(R^{NS} + n_f R_A^S). \tag{2.89}$$

The anomalous dimension matrix (ADM) is given by [35, 77, 80, 84]

$$\gamma^{\psi} = -\gamma_0^{\psi} a_\mu^2 - \gamma_1^{\psi} a_\mu^3 + \mathcal{O}(a_\mu^4) = -\frac{1}{2}a_\mu^2 - \left[\frac{85}{48} + \frac{1}{72}n_f\right]a_\mu^3 + \mathcal{O}(a_\mu^4). \tag{2.90}$$

The quark mass corrections are known logarithmically up to $\mathcal{O}(\alpha_s^3)$ (see e.g. Ref. [76]). For our calculations we also require the constant terms in the massive parts of the correlators. The constant parts are available up to α_s^2. We use the results of Ref. [57] which are based on Refs. [71, 72, 74]. The universal quark mass correction is given by

$$R_2 = a_\mu^2\left[-\frac{32}{3} + 8\zeta_3\right]. \tag{2.91}$$

The vector corrections are

$$R_{q,2}^V = a_\mu\left[-12\ell_{-s\mu^2}\right] + a_\mu^2\left[n_f\left(-\ell_{-s\mu^2}^2 + \frac{13}{3}\ell_{-s\mu^2}\right) + \frac{57}{2}\ell_{-s\mu^2}^2 - \frac{253}{2}\ell_{-s\mu^2}\right] + C_\Pi^{q,V} \tag{2.92}$$

and the constant part reads

$$C_\Pi^{q,V} = 6 + 16a_\mu + a_\mu^2\left[-\frac{95}{12}n_f + \frac{19691}{72} + \frac{124}{9}\zeta_3 - \frac{1045}{9}\zeta_5\right]. \tag{2.93}$$

The axial vector quark mass corrections are

$$\begin{aligned} R_{q,2}^A = 6\ell_{-s\mu^2} &+ a_\mu\left[-6\ell_{-s\mu^2}^2 + 22\ell_{-s\mu^2}\right] \\ &+ a_\mu^2\left[n_f\left(-\frac{1}{3}\ell_{-s\mu^2}^3 + \frac{8}{3}\ell_{-s\mu^2}^2 + \left(-\frac{151}{12} + 4\zeta_3\right)\ell_{-s\mu^2}\right)\right. \\ &\left. + \frac{19}{2}\ell_{-s\mu^2}^3 - \frac{155}{2}\ell_{-s\mu^2}^2 + \left(\frac{8221}{24} - 117\zeta_3\right)\ell_{-s\mu^2}\right] + C_\Pi^{q,A}, \end{aligned} \tag{2.94}$$

with the constant part being

$$\begin{aligned} C_\Pi^{q,A} = -6 &+ a_\mu\left[-\frac{107}{2} + 24\zeta_3\right] \\ &+ a_\mu^2\left[n_f\left(\frac{857}{36} - \frac{32}{3}\zeta_3\right) - \frac{3241}{6} + 387\zeta_3 + \frac{3}{2}\zeta_4 - 165\zeta_5\right]. \end{aligned} \tag{2.95}$$

This concludes the summary of the necessary functions needed for our calculation. We use the correlators to calculate HSN decay to hadrons.

2.4. Sterile Neutrinos

Starting in 1968 the Homestake experiment, a radiochemical experiment first measuring the solar neutrino flux, was carried out [85]. The measured solar neutrino flux was significantly below the Standard Solar Model prediction [86]; this discrepancy was dubbed the Solar Neutrino Problem. In 1990 the water Cherenkov experiment Kamiokande-II also observed a solar neutrino flux below the theory prediction [87]. Furthermore, the radiochemical solar neutrino experiments GALLEX [88, 89] and SAGE [90, 91] had measured the solar neutrino flux in agreement with both the Homestake and the Kamiokande-II experiments. Pontecorvo and Gribov already proposed in 1967 and 1968 that a discrepancy in expected and measured solar neutrino fluxes might be explained by neutrino oscillations [92, 93]. The neutrino oscillations were then confirmed, in a model-independent way, by the water Cherenkov experiment Super-Kamiokande [94] detecting atmospheric neutrino oscillations and the Sudbury Neutrino Observatory experiment [95, 96] confirming the solar neutrino mixing. For these discoveries Takaaki Kajita and Arthur B. McDonald were awarded the Nobel Prize in Physics 2015 [97, 98]. The discovery of neutrino oscillations is remarkable as the oscillation frequency depends on the squared mass difference $\Delta m_{ij}^2 = m_i^2 - m_j^2$ of the two neutrinos i and j. As outlined in Sec. 2.1 the SM does not account for neutrino masses. This is a flaw and facilitates the need for an extension of the SM.

By construction there are no right-handed neutrino fields ν_R in the SM. The inclusion of such a right-handed field ν_R is hence a natural beyond Standard Model (BSM) physics extension (here we follow Refs. [99, 100]). This extension immediately allows us to write down a Dirac-type mass term

$$\mathcal{L}_Y^\nu = -y_\nu \overline{L}_L \widetilde{\Phi} \nu_R + \text{h.c.} = -\frac{v}{\sqrt{2}} y_\nu \overline{\nu}_L \nu_R + \text{h.c.}, \tag{2.96}$$

we can identify $m_D = v y_\nu / \sqrt{2}$ as the Dirac mass. Here we have made the assumption that the corresponding Yukawa matrix is already diagonal. This is however not true. A neutrino mass sector would need to be diagonalised analogously to the quark sector giving rise to the Pontecorvo-Maki-Nakagawa-Sakata (PMNS) matrix, describing the flavour changes of neutrinos attributed to neutrino oscillations [101–103]. Neutrino oscillation effects scale with the product of the squared mass difference Δm_{ij}^2 and the source-detector distance L. We are interested in HSN produced at colliders, specifically with masses $m_N \sim 2\,\text{GeV}$. At colliders the source-detector distances are small meaning neutrino oscillations are strongly suppressed and we can safely neglect them for the remainder of this work. A right-handed neutrino would be a complete singlet with respect to the gauge group i.e. $(\mathbf{1}, \mathbf{1}, 0)$. In particular it is uncharged under $\text{U}(1)_Y$ which allows us to add a Majorana mass term [104]

$$\mathcal{L}_M = -\frac{1}{2} M_R (\overline{\nu}_R^c \nu_R + \overline{\nu}_R \nu_R^c), \tag{2.97}$$

where $\nu_R^c = -i\gamma^2 \nu_R^*$. The Majorana mass term breaks lepton number conservation. Only ν_R is uncharged under $\text{U}(1)_Y$ hence in this model the term $M_L \overline{\nu}_L^c \nu_L$ is forbidden. The full mass term then reads

$$\mathcal{L}_\mathcal{M}^\nu = \mathcal{L}_Y^\nu + \mathcal{L}_M = -\frac{1}{2} \left(\overline{\nu}_L, \overline{\nu}_R^c \right) \mathcal{M}_\nu \begin{pmatrix} \nu_L^c \\ \nu_R \end{pmatrix} + \text{h.c.}, \quad \mathcal{M}_\nu = \begin{pmatrix} 0 & m_D \\ m_D & M_R \end{pmatrix}, \tag{2.98}$$

which we can diagonalise by an SO(2) rotation

$$\mathcal{R}(\theta)\mathcal{M}_\nu\mathcal{R}^T(\theta) = \text{diag}(m_-, m_+), \quad \mathcal{R}(\theta) = \begin{pmatrix} \cos\theta & -\sin\theta \\ \sin\theta & \cos\theta \end{pmatrix}, \tag{2.99}$$

where the rotation angle satisfies $\tan(2\theta) = 2m_D/M_R$. The mass eigenvalues are

$$m_\pm = \frac{M_R \pm \sqrt{M_R^2 + 4m_D^2}}{2}. \tag{2.100}$$

For large M_R satisfying $M_R \gg m_D$ this leads to (seesaw mechanism):

$$m_+ = M_R + O\left(\frac{m_D^2}{M_R}\right), \qquad m_- = -\frac{m_D^2}{M_R} + O\left(\frac{m_D^4}{M_R^3}\right), \tag{2.101}$$

and the mass term becomes

$$\mathcal{L}_\mathcal{M}^\nu = -\frac{1}{2}m_-\overline{\nu'}_L\nu_L'^c - \frac{1}{2}m_+\overline{N}_R^c N_R + \text{h.c.}, \tag{2.102}$$

where we have introduced the fields in the mass basis

$$\begin{pmatrix} \nu_L' \\ N_R^c \end{pmatrix} = \mathcal{R}(\theta)\begin{pmatrix} \nu_L \\ \nu_R^c \end{pmatrix}, \tag{2.103}$$

with ν_L' being the light mass state and N_R^c being the heavy mass state. We connect ν_L' to the SM neutrino mass state and refer to N_R^c as the heavy sterile neutrino (HSN). The sign of m_- may be accounted for by a field redefinition of ν_L' [100]. Inverting Eq. (2.103) we identify the SM neutrino in the interaction basis as

$$\nu_L = \nu_L' \cos\theta + N_R^c \sin\theta, \tag{2.104}$$

meaning the SM neutrino in the interaction basis is almost entirely the SM neutrino in the mass basis with a small component of an HSN since the mixing angle θ is small.

The mechanism described here is called the seesaw mechanism [9–13], more precisely a seesaw mechanism of type I. Provided M_R is large it naturally explains small neutrino masses. We outlined the seesaw mechanism for a single neutrino generation, however, the mechanism is straightforwardly extended to more neutrino generations (cf. e.g. [99]).

Phenomenologically Eq. (2.104) leads to a modification of the charged-current and neutral-current interactions in Eqs. (2.18), and (2.17)

$$\begin{aligned} \mathcal{L}_\text{NC} &\supset \frac{g_2}{2\cos\theta_w}\bar{\nu}\gamma^\mu P_L \nu Z_\mu \\ &= \frac{g_2}{2\cos\theta_w}\bigg[\cos^2\theta\,\overline{\nu'}\gamma^\mu P_L\nu' + \sin\theta\cos\theta\,\overline{N}\gamma^\mu P_L\nu' \\ &\qquad + \cos\theta\sin\theta\,\overline{\nu'}\gamma^\mu P_L N + \sin^2\theta\,\overline{N}\gamma^\mu P_L N\bigg]Z_\mu \end{aligned} \tag{2.105}$$

$$\begin{aligned} \mathcal{L}_\text{CC} &\supset \frac{g_2}{\sqrt{2}}\bar{\nu}_i\gamma^\mu P_L\ell_i W_\mu^+ + \text{h.c.} \\ &= \frac{g_2}{\sqrt{2}}\bigg[\cos\theta\,\overline{\nu'}\gamma^\mu P_L\ell + \sin\theta\,\overline{N}\gamma^\mu P_L\ell\bigg]W_\mu^+ + \text{h.c.} \end{aligned} \tag{2.106}$$

When considering more than one neutrino generation there could also be mixing between different generations of the HSN. Including mixing between HSN and ν_e and or ν_μ can influence e.g. the Fermi constant and would require full electroweak fits [105]. We do not study mixing between different HSN and only allow HSN to interact with one SM lepton flavour. In particular we will be interested in interactions of HSN with τ leptons and ν_τ neutrinos as in general interactions with the third generation are the least probed ones. SM neutrinos and sterile neutrinos introduced through the seesaw mechanism of type I are of Majorana type. Dirac type sterile neutrinos could be effectively realised e.g. in an inverse seesaw mechanism (where the lepton number breaking parameter is typically small) [100]. In the next chapters we will be agnostic to the model i.e. we only assume a sterile neutrino interaction of the form in Eqs. (2.105), and (2.106) and make no other assumptions about the underlying model introducing the sterile neutrino. This also means we will primarily treat the HSN as a Dirac neutrino. Going from a Dirac HSN to a Majorana HSN amounts to multiplying the respective observable by a factor of two because a single Dirac field corresponds to two Majorana fields [106, 107].

3. Heavy Sterile Neutrino Decay

3.1. Decay Rate

3.1.1. Tree-Level Decay Rate

Tree-level decay rates of HSN decay have been calculated in the literature [107–114]. They follow from the Feynman rules obtained from Eq. (2.105), and (2.106). Here we state the different tree-level decay rates of HSN; our results here are in agreement with Ref. [107]. Throughout this thesis we have used `Mathematica` and the package `FeynCalc` [115–118]. The charged-current decay rate into a pair of up- and down-type quarks u' and d' is

$$\Gamma(N \to \ell^- u' \bar{d}') = N_c \frac{G_F^2 m_N^5 |V_{N\ell}|^2 |V_{u'd'}|^2}{192\pi^3} \times 12 \int_{(x_{u'}+x_{d'})^2}^{(1-x_\ell)^2} \frac{\mathrm{d}x}{x}(1 + x_\ell^2 - x)(x - x_{u'}^2 - x_{d'}^2)\sqrt{\lambda(1, x, x_\ell^2)\lambda(x, x_{u'}^2, x_{d'}^2)}, \tag{3.1}$$

where G_F is the Fermi constant, $V_{N\ell} = \sin\theta_{N\ell}$ is the mixing angle between N and ν_ℓ, $V_{u'd'}$ is the CKM matrix element, m_N is the HSN mass, $x_i = m_i/m_N$, and $\lambda(a, b, c) = (a-b-c)^2 - 4bc$ is the Källén function. Setting $N_c = V_{u'd'} = 1$ the leptonic decay rate $N \to \ell_\alpha \bar{\ell}_\beta \nu_\beta$ follows immediately

$$\Gamma(N \to \ell_\alpha \bar{\ell}_\beta \nu_\beta) = \frac{G_F^2 m_N^5 |V_{N\ell}|^2}{192\pi^3} \times 12 \int_{x_\beta^2}^{(1-x_\alpha)^2} \frac{\mathrm{d}x}{x}(1 + x_\alpha^2 - x)(x - x_\beta^2)\sqrt{\lambda(1, x, x_\alpha^2)\lambda(x, x_\beta^2, 0)}, \tag{3.2}$$

with $x_\alpha = m_{\ell_\alpha}/m_N$ and $\alpha \neq \beta$, so that there is no Z diagram. The neutral-current decay rate, for $\nu \neq f$, reads

$$\Gamma(N \to \nu f \bar{f}) = N_c \frac{G_F^2 m_N^5 |V_{N\ell}|^2}{192\pi^3} \times \int_{4x_q^2}^{1} \mathrm{d}x\,(1-x)^2 \sqrt{1 - \frac{4x_f^2}{x}} \left[g_V^2 (2x+1)\left(1 + 2\frac{x_f^2}{x}\right) + g_A^2\left(\left(2x - \frac{1}{2}\right)\left(1 - 4\frac{x_f^2}{x}\right) + \frac{3}{2}\right)\right], \tag{3.3}$$

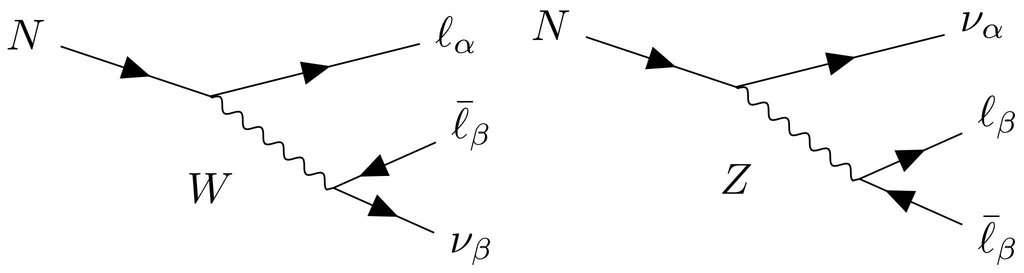

(a) charged-current decay (b) neutral-current decay

Figure 3.1.: Decay of an HSN into leptons at tree-level. If all leptons carry the same flavour the two diagrams interfere.

here $g_V = T_3 - 2Qs_w^2$ where $s_w^2 = \sin^2\theta_w$, $g_A = T_3$, and $x_f = m_f/m_N$. After performing the integration the neutral-current decay rate becomes

$$\begin{aligned}\Gamma(N \to \nu_\alpha f_\beta \bar{f}_\beta) = {} & N_c \frac{G_F^2 m_N^5 |V_{N\ell}|^2}{192\pi^3} \\ & \times \Bigg[\frac{\sqrt{1-4x_f^2}}{2} \Big(g_V^2 (1 - 10x_f^2 + 18x_f^4 - 36x_f^6) + g_A^2 (1 - 18x_f^2 - 22x_f^4 + 12x_f^6) \Big) \\ & \quad - 24 \Big(g_V^2 x_f^6 (2 - 3x_f^2) + g_A^2 x_f^4 (2 - 2x_f^2 + x_f^4) \Big) \ln\left(\frac{2x_f}{1 + \sqrt{1 - 4x_f^2}} \right) \Bigg]. \end{aligned} \tag{3.4}$$

The decay rate into three neutrinos is found by setting $x_f \to 0$ and accounting for an additional interference term if $\alpha = \beta$:

$$\Gamma(N \to \nu_\alpha \nu_\beta \bar{\nu}_\beta) = \frac{G_F^2 m_N^5 |V_{N\ell}|^2}{768\pi^3} (1 + \delta_{\alpha\beta}). \tag{3.5}$$

Furthermore, there is an interference between charged- and neutral-current decays if the leptons are all of the same flavour $N \to \ell_\alpha \bar{\ell}_\alpha \nu_\alpha$ (see Fig. 3.1)

$$\begin{aligned} & \Gamma(N \to \nu_\alpha \ell_\alpha \bar{\ell}_\alpha) \\ & = \frac{G_F^2 m_N^5 |V_{N\ell}|^2}{192\pi^3} \times \Bigg[\sqrt{1-4x_\ell^2} \Bigg(\left(\frac{g_V^2}{2} + g_V \right) (1 - 10x_\ell^2 + 18x_\ell^4 - 36x_\ell^6) \\ & \quad + \left(\frac{g_A^2}{2} + g_A \right) (1 - 18x_\ell^2 - 22x_\ell^4 + 12x_\ell^6) + 1 - 14x_\ell^2 - 2x_\ell^4 - 12x_\ell^6 \Bigg) \\ & \quad - 24 \Bigg(\left(g_V^2 + 2g_V \right) x_\ell^6 (2 - 3x_\ell^2) \\ & \quad + \left(g_A^2 + 2g_A \right) x_\ell^4 (2 - 2x_\ell^2 + x_\ell^4) + x_\ell^4 (2 - 2x_\ell^4) \Bigg) \ln\left(\frac{2x_\ell}{1 + \sqrt{1 - 4x_\ell^2}} \right) \Bigg]. \end{aligned} \tag{3.6}$$

We neglect the effect of the cosine of the mixing angle $\cos^2\theta_{N\ell} = 1 - |V_{N\ell}|^2 \approx 1$ as it is sub-leading.

3.1.2. Hadronic Decay Rate

To calculate the inclusive decay rate of HSN decaying into hadrons (X) we follow the same approach taken to calculate inclusive hadronic τ decays [119–122]. By including higher order corrections in α_s to the decay rate into quarks we can calculate the inclusive HSN decay rate into hadrons. This is an accurate description provided sufficiently many orders in α_s are included. The inclusive decay rate of HSN into hadrons is then given by the following integral over the correlator

$$\begin{aligned}\Gamma(N \to \ell X) &= \frac{G_F^2 m_N^5 |V_{N\ell}|^2}{192\pi^3} \\ &\times 12\pi \int_0^{(1-x_\ell)^2} \mathrm{d}x \sqrt{\lambda(1,x,x_\ell^2)} \Bigg[\Big((1+x_\ell^2-x)(1+2x+x_\ell^2) - 4x_\ell^2 \Big) \mathrm{Im}\Pi^{(1+0)}(m_N^2 x) \\ &\qquad - 2x(1+x_\ell^2-x)\mathrm{Im}\Pi^{(0)}(m_N^2 x) \Bigg], \end{aligned} \tag{3.7}$$

where we integrate over $x = s/m_N^2$ and with $x_\ell = m_\ell/m_N$. Differently than in τ decays we have included the dependence on the final state lepton mass. Setting the final state lepton mass to zero we return to the known τ decay result. Furthermore it is possible to express Eq. (3.7) in terms of a contour integration around the origin at zero with radius $|x| = (1 - x_\ell)^2$ [122–125] (see Fig. 3.2)

$$\begin{aligned}\Gamma(N \to \ell X) &= \frac{G_F^2 m_N^5 |V_{N\ell}|^2}{192\pi^3} \\ &\times 6\pi i \oint_{|x|=(1-x_\ell)^2} \mathrm{d}x \sqrt{\lambda(1,x,x_\ell^2)} \Bigg[\Big((1+x_\ell^2-x)(1+2x+x_\ell^2) - 4x_\ell^2 \Big) \Pi^{(1+0)}(m_N^2 x) \\ &\qquad - 2x(1+x_\ell^2-x)\Pi^{(0)}(m_N^2 x) \Bigg]. \end{aligned} \tag{3.8}$$

We use the the charged- and neutral-current correlators stated in Sec. 2.3.2 and 2.3.3 to calculate the inclusive HSN decay rate.

3.2. W Boson Mediated Decay

3.2.1. Decay Rate

We calculate the charged-current HSN decay rate in the chiral limit fully analytically up to $\mathcal{O}(\alpha_s^3)$. At $\mathcal{O}(\alpha_s^4)$ we employ a series representation of the Källén function. The massive corrections are caluclated fully analytically up to $\mathcal{O}(\alpha_s^2)$ and at $\mathcal{O}(\alpha_s^3)$ we use the series representation.

First we decompose the decay rate into the massless and the massive part and then we further divide the massive part into the respective $J = 1 + 0$ and $J = 0$ parts:

$$\Gamma(N \to \ell X) = \frac{G_F^2 m_N^5 |V_{N\ell}|^2}{192\pi^3} \left[\mathcal{R}_0^{(1+0)} + \mathcal{R}_2^{(1+0)} + \mathcal{R}_2^{(0)} \right], \tag{3.9}$$

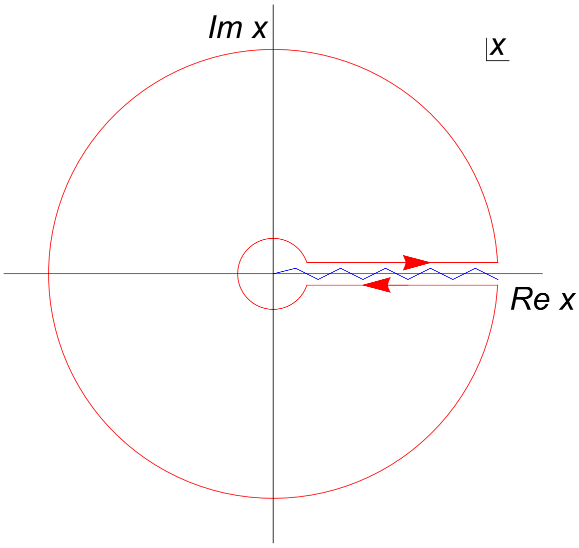

Figure 3.2.: Integration contour in the complex plane. The jagged blue line on the abscissa indicates the branch cut running from zero to infinity and stemming from $\ln(-x)$. There is a pole at the origin coming from the mass corrections m_q^2/x which is avoided by this contour.

where the functions $\mathcal{R}_i^{(J)}$ are given as

$$\mathcal{R}_0^{(1+0)} = 12\pi \int_0^{(1-x_\ell)^2} \mathrm{d}x \sqrt{\lambda(1,x,x_\ell^2)} \times \left((1+x_\ell^2-x)(1+2x+x_\ell^2)-4x_\ell^2\right) \operatorname{Im}\Pi_0^{(1+0)}(m_N^2 x), \tag{3.10}$$

$$\mathcal{R}_2^{(1+0)} = -6\pi i \oint_{|x|=(1-x_\ell)^2} \mathrm{d}x \sqrt{\lambda(1,x,x_\ell^2)} \times \left((1+x_\ell^2-x)(1+2x+x_\ell^2)-4x_\ell^2\right) \frac{N_c x_{m_N}^2 \Pi_2^{(1+0)}(m_N^2 x)}{16\pi^2 x}, \tag{3.11}$$

$$\mathcal{R}_2^{(0)} = 6\pi i \oint_{|x|=(1-x_\ell)^2} \mathrm{d}x\, 2x(1+x_\ell^2-x)\sqrt{\lambda(1,x,x_\ell^2)}\, \frac{N_c x_{m_N}^2 \Pi_2^{(0)}(m_N^2 x)}{16\pi^2 x}, \tag{3.12}$$

where $x_{m_N} = m_{i,j}(m_N)/m_N$. The integration contour corresponds to the large circle in Fig. 3.2 and goes from $(1-x_\ell)^2 + i0^+$ to $(1-x_\ell)^2 + i0^-$ and is therefore not a closed contour on the Riemann sheet of the logarithm. Here we have defined

$$\Pi_0^{(1+0)} = 2(|V_{ud}|^2 + |V_{us}|^2 + \ldots)\,\hat{\Pi}_{ij,V}^{(1+0)}, \tag{3.13}$$

$$\Pi_2^{(1+0)} = 2|V_{ij}|^2\,\Pi_{ij,V,2}^{(1+0)}, \tag{3.14}$$

$$\Pi_2^{(0)} = 2|V_{ij}|^2\,\Pi_{ij,V,2}^{(0)}, \tag{3.15}$$

where we used that the massless correlator is equal for all flavours i and j and that the vector and axial-vector contributions are equal in magnitude. The sum of the CKM elements runs up to V_{ij} where one of the two quarks i or j is the heaviest quark kinematically accessible. We neglect effects of heavy quarks runnning only in loops, e.g. we neglect heavy quark effects in $\Pi^{(1+0)}_{ud,V,2}$ as they are numerically small. $\mathcal{R}_0^{(1+0)}$ is discussed in Sec. 3.2.2, the quark-mass corrections contained in $\mathcal{R}_2^{(1+0)}$ and $\mathcal{R}_2^{(0)}$ are presented in Sec. 3.2.3.

3.2.2. Chiral Limit Corrections

The charged-current corrections in the chiral limit have been published in Ref. [126]; here we outline their calculation again.

Using the imaginary part of the massless correlator given in Eq. (2.63) and setting $\mu = m_N$ the following integrals will appear in $\mathcal{R}_0^{(1+0)}$

$$I_k = \int\limits_0^{(1-x_\ell)^2} dx \left((1+x_\ell^2-x)(1+2x+x_\ell^2) - 4x_\ell^2\right)\sqrt{\lambda(1,x,x_\ell^2)}\,\ln^k(x). \tag{3.16}$$

We have calculated these integrals analytically up to $k = 2$ in terms of dilogarithm and trilogarithm functions:

$$I_0 = \frac{1}{2}\left(1 - 8x_\ell^2 + 8x_\ell^6 - x_\ell^8 - 12x_\ell^4\ln(x_\ell^2)\right), \tag{3.17}$$

$$\begin{aligned} I_1 = &-\frac{19}{24} + \frac{13}{3}x_\ell^2 - 12\zeta_2 x_\ell^4 - \frac{13}{3}x_\ell^6 + \frac{19}{24}x_\ell^8 \\ &+ \left(-3x_\ell^4 - 4x_\ell^6 + \frac{1}{2}x_\ell^8\right)\ln(x_\ell^2) \\ &+ \left(1 - 8x_\ell^2 + 8x_\ell^6 - x_\ell^8\right)\ln(1-x_\ell^2) + 12x_\ell^4\mathrm{Li}_2(x_\ell^2), \end{aligned} \tag{3.18}$$

$$\begin{aligned} I_2 = &\frac{265}{144} - \frac{151}{18}x_\ell^2 - 12(\zeta_2 + 2\zeta_3)x_\ell^4 + \left(\frac{151}{18} - 16\zeta_2\right)x_\ell^6 + \left(-\frac{265}{144} + 2\zeta_2\right)x_\ell^8 \\ &+ \left(-\frac{19}{6} + \frac{52}{3}x_\ell^2 - 48\zeta_2 x_\ell^4 - \frac{52}{3}x_\ell^6 + \frac{19}{6}x_\ell^8 + 48x_\ell^4\,\mathrm{Li}_2(x_\ell^2)\right)\ln(1-x_\ell^2) \\ &+ (2 - 16x_\ell^2 + 16x_\ell^6 - 2x_\ell^8)\ln^2(1-x_\ell^2) \\ &+ \Bigg(-x_\ell^2 + \frac{15}{2}x_\ell^4 + \frac{23}{3}x_\ell^6 - \frac{19}{12}x_\ell^8 \\ &\qquad + (-1 + 8x_\ell^2 - 8x_\ell^6 + x_\ell^8)\ln(1-x_\ell^2) + 24x_\ell^4\ln^2(1-x_\ell^2) - 12x_\ell^4\,\mathrm{Li}_2(x_\ell^2)\Bigg)\ln(x_\ell^2) \\ &+ (-1 + 8x_\ell^2 + 12x_\ell^4 + 8x_\ell^6 - x_\ell^8)\,\mathrm{Li}_2(x_\ell^2) \\ &+ 24x_\ell^4\,\mathrm{Li}_3(x_\ell^2) + 48x_\ell^4\,\mathrm{Li}_3(1-x_\ell^2). \end{aligned} \tag{3.19}$$

For $k \geq 3$ we calculate I_k with the help of a series representation that we derived. The n-th derivative of the square root of the Källén function can be written as

$$\frac{\mathrm{d}^n}{\mathrm{d}x^n}\sqrt{\lambda(1,x,x_\ell^2)} = \sum_{j=0}^{\lfloor \frac{n}{2} \rfloor} (-1)^{n-j} \left(-\frac{1}{2}\right)_{n-j} (2j-1)!! \binom{n}{2j} \times \frac{\left(\lambda'(1,x,x_\ell^2)\right)^{n-2j} \left(\lambda''(1,x,x_\ell^2)\right)^{j}}{\left(\lambda(1,x,x_\ell^2)\right)^{\frac{2(n-j)-1}{2}}}, \tag{3.20}$$

where $\lfloor n \rfloor$ is the floor function of n, which is defined as the largest integer less than or equal to n. $(a)_n = a(a+1)(a+2)\cdot \ldots \cdot (a+n-1)$ is the Pochhammer symbol and

$$\lambda(1,x,x_\ell^2) = x^2 - 2x(1+x_\ell^2) + (1-x_\ell^2)^2, \tag{3.21}$$

$$\lambda'(1,x,x_\ell^2) = \frac{\mathrm{d}\lambda(1,x,x_\ell^2)}{\mathrm{d}x} = 2x - 2(1+x_\ell^2), \tag{3.22}$$

$$\lambda''(1,x,x_\ell^2) = \frac{\mathrm{d}^2\lambda(1,x,x_\ell^2)}{\mathrm{d}x^2} = 2. \tag{3.23}$$

For an arbitrary upper limit the integral I_k can then be written as

$$\begin{aligned} I_k(x_\ell^2, a) &\equiv \int_0^a dx \left((1+x_\ell^2 - x)(1+2x+x_\ell^2) - 4x_\ell^2\right)\sqrt{\lambda(1,x,x_\ell^2)}\ln^k(x) \\ &= \sum_{n=0}^{\infty} \frac{1}{n!} A_n(x_\ell^2) B_{n,k}(x_\ell^2, a), \end{aligned} \tag{3.24}$$

where the function $A_n(x_\ell^2)$ is

$$\begin{aligned} A_n(x_\ell^2) &\equiv \left.\frac{\mathrm{d}^n}{\mathrm{d}x^n}\sqrt{\lambda(1,x,x_\ell^2)}\right|_{x=0} \\ &= \sum_{j=0}^{\lfloor \frac{n}{2} \rfloor} (-1)^{j} \left(-\frac{1}{2}\right)_{n-j} (2j-1)!! \binom{n}{2j} 2^{n-j} (1+x_\ell^2)^{n-2j} (1-x_\ell^2)^{1-2(n-j)}, \end{aligned} \tag{3.25}$$

and $B_{n,k}(x_\ell^2, a)$ is given by

$$\begin{aligned} B_{n,k}(x_\ell^2, a) &\equiv \int_0^a dx \left((1+x_\ell^2 - x)(1+2x+x_\ell^2) - 4x_\ell^2\right) x^n \ln^k(x) \\ &= -2I_{n+2,k}(a) + (1+x_\ell^2) I_{n+1,k}(a) + (1-x_\ell^2)^2 I_{n,k}(a). \end{aligned} \tag{3.26}$$

The remaining integrals in this expression can be calculated in a closed form

$$
\begin{aligned}
I_{n,k}(a) &\equiv \int_0^a dx\, x^n \ln^k x \\
&= a^{n+1} \sum_{l=0}^{k} (-k)_l (n+1)^{-l-1} \ln^{k-l} a.
\end{aligned} \tag{3.27}
$$

This completes the calculation of all I_k integrals and $\mathcal{R}_0^{(1+0)}$ in terms of them reads

$$
\begin{aligned}
\mathcal{R}_0^{(1+0)} &= 2N_c(|V_{ud}|^2 + |V_{us}|^2 + ...) \\
\times &\Bigg\{ I_0 + a_{m_N} I_0 + a_{m_N}^2 \left[c_{2,1} I_0 + 2c_{2,2} I_1\right] + a_{m_N}^3 \left[c_{3,1} I_0 + 2c_{3,2} I_1 - \left(\pi^2 I_0 - 3I_2\right) c_{3,3}\right] \\
&+ a_{m_N}^4 \left[c_{4,1} I_0 + 2c_{4,2} I_1 - \left(\pi^2 I_0 - 3I_2\right) c_{4,3} - \left(4\pi^2 I_1 - 4I_3\right) c_{4,4}\right] \Bigg\},
\end{aligned} \tag{3.28}
$$

where all $I_k = I_k(x_\ell^2, (1-x_\ell)^2)$. In our calculation we have used the analytic integrals Eqs. (3.17)-(3.19) and only employed our series representation for the I_3 integral, however it is also possible to use the series representation for all integrals.

In addition we have also calculated the integrated spectrum of the inclusive HSN decay by evaluating the integral in Eq. (3.16) for an arbitrary upper integration limit $s_{\max}$

$$
\begin{aligned}
\Gamma_{\text{cut}}(N \to \ell X) &= \int_0^{s_{\max}} \mathrm{d}s \, \frac{d\Gamma(N \to \ell X)}{ds}, \quad s_{\max} \in [\mathcal{O}(1\,\text{GeV}), (m_N - m_\ell)^2], \\
&= \int_0^{x_{\max}} dx \, \frac{d\Gamma(N \to \ell X)}{\mathrm{d}x},
\end{aligned} \tag{3.29}
$$

with $x_{\max} = s_{\max}/m_N^2$. Neglecting quark mass corrections, $\Gamma_{\text{cut}}(N \to \ell X)$ immediately follows from the chiral part of Eq. (3.9) (i.e. $\mathcal{R}_0^{(1+0)}$ in Eq. (3.28)) and replacing the I_k by I_k^{cut}. We have calculated analytically closed-form expressions for I_k^{cut} up to $k = 2$. These expressions are rather lengthy, for this reason we only state the result for $I_0^{\text{cut}} - I_0$ here and relegate the rest of the expressions to Appendix A.

$$
\begin{aligned}
I_0^{\text{cut}} - I_0 =& \frac{1}{2}\Bigg(- \left(x_{\max}^2 + 7\right) x_\ell^2 - (x_{\max} + 7) x_\ell^4 + x_\ell^6 \\
&+ (x_{\max} - 1)^2 (x_{\max} + 1)\Bigg)\left(x_{\max} - (x_\ell + 1)^2\right) X_r - 24 x_\ell^4 \text{ArcTanh}(X_r),
\end{aligned} \tag{3.30}
$$

where we used $X_r = \sqrt{(x_{\max} - (1-x_\ell)^2)/(x_{\max} - (1+x_\ell)^2)}$.

3.2.3. Quark Mass Corrections

Both $\mathcal{R}_2^{(1+0)}$ and $\mathcal{R}_2^{(0)}$ are obtained from the correlators in Eqs. (2.64) and (2.65) respectively.

We start by discussing $\mathcal{R}_2^{(0)}$ as it is closer to the discussion of the massless term. The quark mass correction terms all scale with the ratio of the quark mass squared over the square of the transferred momentum and thus introduce an additional pole $1/x$. In $\mathcal{R}_2^{(0)}$ this pole is absorbed by the prefactor $2x$ making it possible to calculate the integral on the real axis. Terms constant with respect to x in $\Pi_2^{(0)}$, i.e. terms without branch cuts, do not contribute as a consequence of Cauchy's integral theorem. The remaining terms scaling with logarithms $\ln^k(-x)$ will however contribute. The integrals appearing in $\mathcal{R}_2^{(0)}$ are of the form ($\mu = m_N$)

$$I_k^{(0),c} = \frac{1}{2\pi i} \oint\limits_{|x|=(1-x_\ell)^2} \mathrm{d}x\, 2x(1 + x_\ell^2 - x)\sqrt{\lambda(1, x, x_\ell^2)}\, \frac{\ln^k(-x)}{x}. \tag{3.31}$$

Since there is no singularity in this integral, we can relate it to an integration on the real axis through

$$I_1^{(0),c} = I_0^{(0)}, \tag{3.32}$$

$$I_2^{(0),c} = 2I_1^{(0)}, \tag{3.33}$$

$$I_3^{(0),c} = -\pi^2 I_0^{(0)} + 3I_2^{(0)}, \tag{3.34}$$

$$I_4^{(0),c} = -4\pi^2 I_1^{(0)} + 4I_3^{(0)}, \tag{3.35}$$

with the integral $I_k^{(0)}$ being

$$I_k^{(0)} = \int\limits_0^{(1-x_\ell)^2} \mathrm{d}x\, 2(1 + x_\ell^2 - x)\sqrt{\lambda(1, x, x_\ell^2)}\, \ln^k(x), \tag{3.36}$$

and for $k \leq 2$ we find

$$I_0^{(0)} = \frac{2}{3}(1 - x_\ell^2)^3 \tag{3.37}$$

$$\begin{aligned} I_1^{(0)} = \frac{1}{9}\big(&6x_\ell^4(-3 + x_\ell^2)\ln(x_\ell^2) \\ &+ (1 - x_\ell^2)(-11 + 10x_\ell^2 - 11x_\ell^4 + 12(1 - x_\ell^2)^2 \ln(1 - x_\ell^2))\big) \end{aligned} \tag{3.38}$$

$$\begin{aligned} I_2^{(0)} = \frac{85}{27} - \frac{41}{9}x_\ell^2 + \left(\frac{41}{9} - 8\zeta_2\right)x_\ell^4 + \left(-\frac{85}{27} + \frac{8}{3}\zeta_2\right)x_\ell^6 \\ + \frac{4}{9}(1 - x_\ell^2)(-11 + 10x_\ell^2 - 11x_\ell^4 + 6(1 - x_\ell^2)^2 \ln(1 - x_\ell^2)) \ln(1 - x_\ell^2) \\ + \frac{2}{9}(-6x_\ell^2 + 15x_\ell^4 - 11x_\ell^6 - 6(1 - x_\ell^2)^3 \ln(1 - x_\ell^2)) \ln(x_\ell^2) \\ - \frac{4}{3}(1 + x_\ell^2)(1 - 4x_\ell^2 + x_\ell^4)\mathrm{Li}_2(x_\ell^2). \end{aligned} \tag{3.39}$$

The calculation for $k \geq 3$ follows analogously as in the massless corrections

$$I_k^{(0)}(x_\ell^2, a) = \sum_{n=0}^{\infty} \frac{1}{n!} A_n(x_\ell^2) B_{n,k}^{(0)}(x_\ell^2, a), \tag{3.40}$$

$$B_{n,k}^{(0)}(x_\ell^2, a) = 2(1 + x_\ell^2) I_{n,k}(a) - 2I_{n+1,k}(a). \tag{3.41}$$

Then, $\mathcal{R}_2^{(0)}$ in terms of $I_k^{(0),c}$, reads

$$\mathcal{R}_2^{(0)} = -2N_c|V_{ij}|^2 x_{m_N}^2 \frac{3}{4}\Pi_{ij,V,2}^{(0)}\Bigg|_{\ln^k(-x)\to I_k^{(0),c}}^{C_\Pi^{(0)}\to 0}. \tag{3.42}$$

For $\mathcal{R}_2^{(1+0)}$ it is helpful to break the integration apart into one part containing the pole and another part not containing any poles ($\mu = m_N$)

$$\begin{aligned}
I_k^{(1+0),c} &= \frac{1}{2\pi i}\oint\limits_{|x|=(1-x_\ell)^2} dx\left((1-x+x_\ell^2)(1+2x+x_\ell^2)-4x_\ell^2\right)\sqrt{\lambda(1,x,x_\ell^2)}\,\frac{\ln^k(-x)}{x} \\
&= \frac{1}{2\pi i}\oint\limits_{|x|=(1-x_\ell)^2} dx(-2x^2+(1+x_\ell^2)x)\sqrt{\lambda(1,x,x_\ell^2)}\,\frac{\ln^k(-x)}{x} \\
&\quad + \frac{(1-x_\ell^2)^2}{2\pi i}\oint\limits_{|x|=(1-x_\ell)^2} dx\sqrt{\lambda(1,x,x_\ell^2)}\,\frac{\ln^k(-x)}{x} \\
&\equiv I_k^{(1+0),r} + I_k^{(1+0),p}.
\end{aligned} \tag{3.43}$$

The integrand of the first integral $I_k^{(1+0),r}$ again contains no poles and may be evaluated on the real axis (and is integrable at $x = 0$). It reads

$$I_1^{(1+0),r} = I_0^{(1+0)}, \tag{3.44}$$

$$I_2^{(1+0),r} = 2I_1^{(1+0)}, \tag{3.45}$$

$$I_3^{(1+0),r} = -\pi^2 I_0^{(1+0)} + 3I_2^{(1+0)}, \tag{3.46}$$

where

$$I_k^{(1+0)} = \int\limits_0^{(1-x_\ell)^2} dx(-2x+(1+x_\ell^2))\sqrt{\lambda(1,x,x_\ell^2)}\,\ln^k(x), \tag{3.47}$$

and

$$I_0^{(1+0)} = \frac{1}{6}(1 - 15x_\ell^2 + 15x_\ell^4 - x_\ell^6 - 6(x_\ell^2 + x_\ell^4)\ln(x_\ell^2)) \tag{3.48}$$

$$\begin{aligned} I_1^{(1+0)} = \frac{1}{36}\bigg(& - 17 + 3(37 - 24\zeta_2)x_\ell^2 - 3(24\zeta_2 + 37)x_\ell^4 + 17x_\ell^6 + 6(x_\ell^2 - 15)x_\ell^4\ln(x_\ell^2) \\ & - 12(-1 + 15x_\ell^2 - 15x_\ell^4 + x_\ell^6)\ln(1 - x_\ell^2) + 72(x_\ell^2 + x_\ell^4)\mathrm{Li}_2(x_\ell^2)\bigg) \end{aligned} \tag{3.49}$$

$$\begin{aligned} I_2^{(1+0)} = {} & \frac{151}{108} + \left(- \frac{151}{108} + \frac{2}{3}\zeta_2\right)x_\ell^6 + \left(\frac{227}{36} - 10\zeta_2 - 4\zeta_3\right)x_\ell^4 - \left(\frac{227}{36} + 4\zeta_3\right)x_\ell^2 \\ & + \frac{1}{9}\left(- 17 + (111 - 72\zeta_2)x_\ell^2 - 3(37 + 24\zeta_2)x_\ell^4 + 17x_\ell^6\right)\ln(1 - x_\ell^2) \\ & - \frac{2}{3}\left(- 1 + 15x_\ell^2 - 15x_\ell^4 + x_\ell^6\right)\ln^2(1 - x_\ell^2) \\ & + \frac{1}{18}\ln(x_\ell^2)\bigg(- 6x_\ell^2 + 105x_\ell^4 - 17x_\ell^6 \\ & \quad + 6\ln(1 - x_\ell^2)\Big(- 1 + 15x_\ell^2 - 15x_\ell^4 + x_\ell^6 + 12(x_\ell^2 + x_\ell^4)\ln(1 - x_\ell^2)\Big)\bigg) \\ & - \frac{1}{3}(1 + x_\ell^2)\Big(1 - 16x_\ell^2 + x_\ell^4 + 6x_\ell^2\big(\ln(x_\ell^2) - 4\ln(1 - x_\ell^2)\big)\Big)\mathrm{Li}_2(x_\ell^2) \\ & + 4(x_\ell^2 + x_\ell^4)\big(\mathrm{Li}_3(x_\ell^2) + 2\mathrm{Li}_3(1 - x_\ell^2)\big). \end{aligned} \tag{3.50}$$

We have calculated the integral $I_k^{(1+0),p}$ containing the pole up to $k \leq 2$:

$$I_0^{(1+0),p} = (1 - x_\ell^2)^3, \tag{3.51}$$

$$I_1^{(1+0),p} = (1 - x_\ell^2)^2\Big(x_\ell^2\ln(x_\ell^2) - (1 - x_\ell^2)\big(1 - 2\ln(1 - x_\ell^2)\big)\Big), \tag{3.52}$$

$$\begin{aligned} I_2^{(1+0),p} = {} & \frac{1}{6}(1 - x_\ell^2)^2\bigg(12 - 30\zeta_2 + \left(- 12 + 18\zeta_2\right)x_\ell^2 \\ & + 24(1 - x_\ell^2)\ln^2(1 - x_\ell^2) - 24(1 - x_\ell^2)\ln(1 - x_\ell^2) \\ & + 6\ln(x_\ell^2)\left(- 2x_\ell^2 + 2(1 + x_\ell^2)\ln(1 - x_\ell) - (3 - x_\ell^2)\ln(1 - x_\ell^2)\right) \\ & - 12(1 + x_\ell^2)\left(3\mathrm{Li}_2(-x_\ell) + \mathrm{Li}_2(x_\ell) + \mathrm{Li}_2\left(- \frac{1 - x_\ell}{1 + x_\ell}\right) - \mathrm{Li}_2\left(\frac{1 - x_\ell}{1 + x_\ell}\right)\right)\bigg). \end{aligned} \tag{3.53}$$

For the remaining integral $I_3^{(1+0),\,p}$ we find

$$\begin{aligned}
I_3^{(1+0),\,p} &= \frac{(1-x_\ell^2)^2}{2\pi i} A_0(x_\ell^2) \oint\limits_{|x|=(1-x_\ell)^2} \mathrm{d}x \frac{\ln^3(-x)}{x} \\
&\quad + \frac{(1-x_\ell^2)^2}{2\pi i} \oint\limits_{|x|=(1-x_\ell)^2} \mathrm{d}x \sum_{n=1}^{\infty} \frac{A_n(x_\ell^2)}{n!} x^{n-1} \ln^3(-x) \\
&= (1-x_\ell^2)^2 A_0(x_\ell^2)\big(-2\pi^2 + 8\ln^2(1-x_\ell)\big)\ln(1-x_\ell) \\
&\quad + (1-x_\ell^2)^2 \sum_{n=1}^{\infty} \frac{A_n(x_\ell^2)}{n!} \Big[-\pi^2 I_{n-1,0} + 3 I_{n-1,2}\Big].
\end{aligned} \tag{3.54}$$

The calculations above allow us to compactly write down $\mathcal{R}_2^{(1+0)}$:

$$\mathcal{R}_2^{(1+0)} = 2N_c |V_{ij}|^2 x_{m_N}^2 \frac{3}{4} I_0^{(1+0),\,p} \Pi_{ij,\,V,\,2}^{(1+0)} \bigg|_{\ln^k(-x) \to \frac{I_k^{(1+0),\,c}}{I_0^{(1+0),\,p}}} . \tag{3.55}$$

Any dependence on the renormalisation scale μ can be reconstructed employing standard RGE techniques (see Sec. 2.2).

3.3. Z Boson Mediated Decay

3.3.1. Decay Rate

The neutral-current hadronic HSN decay rate follows immediately from Eq. (3.7) by setting $x_\ell = 0$ since $\ell = \nu$:

$$\begin{aligned}
\Gamma(N \to \nu X) &= \frac{G_F^2 m_N^5 |V_{N\ell}|^2}{192\pi^3} \\
&\quad \times 12\pi \int_0^1 \mathrm{d}x\, (1-x)^2 \Big[(1+2x)\mathrm{Im}\Pi^{(1+0)}(m_N^2 x) - 2x \mathrm{Im}\Pi^{(0)}(m_N^2 x)\Big],
\end{aligned} \tag{3.56}$$

where $\Pi^{(J)} = \sum_{ij} g_{i,\,V/A} g_{j,\,V/A} \Pi_{ij,\,V/A}^{(J)}$. We can use Eq. (2.46) to write the decay rate in the form

$$\begin{aligned}
\Gamma(N \to \nu X) &= \frac{G_F^2 m_N^5 |V_{N\ell}|^2}{192\pi^3} \\
&\quad \times 12\pi \int_0^1 \mathrm{d}x\, (1-x)^2 \bigg(\mathrm{Im}\Pi^{(0)}(m_N^2 x) + \bigg(-\frac{(1+2x)m_N^2}{x}\bigg)\mathrm{Im}\Pi^{[1]}(m_N^2 x)\bigg).
\end{aligned} \tag{3.57}$$

We can express this in terms of the R ratio commonly used for Z decay by employing Eq. (2.68) and the decay rate becomes

$$\Gamma(N \to \nu X) = \frac{G_F^2 m_N^5 |V_{N\ell}|^2}{192\pi^3} \int_0^1 \mathrm{d}x\, (1-x)^2 \Big((1+2x) N_c R(m_N^2 x) + 12\pi \mathrm{Im}\Pi^{(0)}(m_N^2 x)\Big). \tag{3.58}$$

As in the charged-current case we split this up as

$$\Gamma(N \to \nu X) = \frac{G_F^2 m_N^5 |V_{N\ell}|^2}{192\pi^3}\left[\mathcal{R}_0 + \mathcal{R}_2 + \mathcal{R}_2^{(0),Z}\right], \tag{3.59}$$

where the three functions are given by

$$\mathcal{R}_0 = N_c \int_0^1 \mathrm{d}x\,(1-x)^2(1+2x) \\ \times \left[\sum_i (g_{i,V}^2 + g_{i,A}^2) R^{\mathrm{NS}} + \left(\sum_i g_{i,V}\right)^2 R_V^{\mathrm{S}} + \left(\sum_i g_{i,A}\right)^2 R_{\Delta_t}^{\mathrm{S},A}\right] \tag{3.60}$$

$$\mathcal{R}_2 = N_c \frac{i}{2} \oint_{|x|=1} \mathrm{d}x\,(1-x)^2(1+2x)\frac{x_q^2}{\pi x}\left[\sum_i (g_{i,V}^2 + g_{i,A}^2) R_2 + g_{q,V}^2 R_{q,2}^V + g_{q,A}^2 R_{q,2}^A\right], \tag{3.61}$$

$$\mathcal{R}_2^{(0),Z} = -6\pi i \oint_{|x|=1} \mathrm{d}x\,(1-x)^2 \frac{N_c x_q^2}{4\pi^2 x} g_{q,A}^2 \Pi_{qq,A,2}^{(0)}(m_N^2 x), \tag{3.62}$$

where $x_q = m_q(\mu)/m_N$. We have stated $\Pi_{ij,A,2}^{(0)}$ in Eq. (2.65). In contrast to the charged-current case only the axial-vector longitudinal correlator contributes. This is a consequence of the Ward identity in Eq. (2.47), which implies $\Pi_{ij,V/A,2}^{(0)} \propto (m_j \mp m_i)^2$. For the neutral-current decay $m_i = m_j = m_q$ and the vector contribution vanishes whereas the axial vector contribution survives. Furthermore, to accommodate the poles coming from the quark mass contributions we have written $\mathcal{R}_2$ and $\mathcal{R}_2^{(0),Z}$ as an integral around the complex contour $|x| = 1$ in complete analogy to the charged-current case.

3.3.2. Chiral Limit Corrections

The neutral-current decays receive contributions from anomalous triangle diagrams. In Sec. 2.3.3 we stated the known results of the neutral-current gauge boson correlator, or as it is more commonly used $R(s)$. In the calculation of $R(s)$ all of the effects of the anomalous triangle diagrams are accounted for in $R_{\Delta_t}^{S,A}$. The remnants of the anomalous triangle diagrams, i.e. the top quark which is integrated out, are logarithms $\ln(\mu^2/m_t^2)$ in the WC. For Z decays setting $\mu = M_Z$ leads $\ln(M_Z^2/m_t^2) \approx -1.2$ which is still small [81]. However, in our case we are interested in decays of HSN with masses $m_N \sim \mathcal{O}(2\,\mathrm{GeV})$. This means we will eventually end up with logarithms where $\mu = m_N$, which are quite large $\ln(m_N^2/m_t^2) \approx -8.8$. Naturally, these large logarithms should be resummed. This has been studied in the context of Z decays [80].

For our calculation it proves to be helpful to perform a basis transformation from the operator basis employed in Ref. [80] to the operator basis used in Ref. [127] with the operators and the WC in the latter being

$$\mathcal{H}^{(5)} = C_b Q_b + C_{\mathrm{sg}} Q_{\mathrm{sg}} + Q_{\mathrm{nsg}}, \tag{3.63}$$

where

$$Q_b = \frac{1}{2}\bar{b}\gamma^\mu\gamma_5 b, \tag{3.64}$$

$$Q_{\text{sg}} = \frac{1}{2}\left[\bar{u}\gamma^\mu\gamma_5 u + \bar{d}\gamma^\mu\gamma_5 d + \bar{c}\gamma^\mu\gamma_5 c + \bar{s}\gamma^\mu\gamma_5 s\right], \tag{3.65}$$

$$Q_{\text{nsg}} = \frac{1}{2}\left[-\bar{u}\gamma^\mu\gamma_5 u + \bar{d}\gamma^\mu\gamma_5 d - \bar{c}\gamma^\mu\gamma_5 c + \bar{s}\gamma^\mu\gamma_5 s\right]. \tag{3.66}$$

Here the Wilson coefficients are

$$C_b(\mu) = 1 + C_{\text{sg}}(\mu), \qquad C_{\text{sg}}(\mu) = -\frac{1}{2}a_\mu^2 \ln\left(\frac{m_t^2}{\mu^2}\right). \tag{3.67}$$

Observables are unaffected by any change of basis, however, WC and matrix elements will in general be different individually in different bases. These differences stem from differences in the renormalisation scheme [128]. In Ref. [127] the scheme dependence stems from the choice of the operator renormalisation. We denote this scheme the L-scheme since it produces the same ADM as in the work of Larin in Ref. [35]; the ADM is given by

$$\begin{aligned}\gamma_A &= a_\mu^2\gamma_A^{(1)} + a_\mu^3\gamma_A^{(2)} \\ &= a_\mu^2 + \left[\frac{59}{12} - \frac{1}{18}n_f\right]a_\mu^3.\end{aligned} \tag{3.68}$$

In the approach taken in Ref. [80] the scheme dependence is encoded in the choice of the "Larin factor" which is a finite renormalisation of the axial vector current. We denote this scheme the CK-scheme. In the CK-scheme the Larin factor is chosen differently than in Ref. [35] and hence produces a different ADM than the one in the L-scheme [128, 129].[1]

In the L-scheme we obtain

$$\begin{aligned}R_{\Delta_t}^{\text{S, A}} &= (C_b^2 - 1)R^{\text{NS}} + R_{A,\text{L}}^{\text{S}} + \mathcal{O}(\alpha_s^3) \\ &= 2C_{\text{sg}} + R_{A,\text{L}}^{\text{S}} + \mathcal{O}(\alpha_s^3),\end{aligned} \tag{3.69}$$

with $R_{A,\text{L}}^{\text{S}} = r_{2,0,\text{L}}^{S,A} + r_{2,1,\text{L}}^{S,A}\ln(\mu^2/s)$. Here the WC C_b and C_{sg} are scheme dependent. Both the functions $R_{A,\text{L}}^{\text{S}}$ and R_A^{S} (introduced in Eqs. (2.76) and (2.88)) are scheme dependent and their scheme dependence manifests only in the constant part as $R_A^{\text{S}} = r_{2,0}^{S,A} + r_{2,1}^{S,A}\ln(\mu^2/s)$ and $r_{2,1,\text{L}}^{S,A} = r_{2,1}^{S,A} = -2\gamma_0^\psi$ which is scheme independent. To show this we derive the scheme dependence of the ADM explicitly from the renormalisation constants. As mentioned in Sec 2.2 in addition to the renormalisation of the fields and the coupling constants it is necessary to also renormalise the effective operators. To that end the scheme dependence manifests as a difference in the renormalisation prescription of the two composite operators in question

$$C_1^0 Z_1 Q^R = C_2^0 Z_2 Q^R. \tag{3.70}$$

[1] In Ref. [128] this is called the n-normalisaton whereas we call it the CK-scheme. The n-normalisation/CK-scheme amounts to choosing the Larin factors of the singlet and non-singlet operators equal (see also Refs. [81, 130]). We thank K. G. Chetyrkin for his explanations of the scheme dependence.

Instead of understanding this as a renormalisation of the effective operator Q we may also interpret it as a renormalisation of the WC

$$C_1^R Z_1 Q^0 = C_2^R Z_2 Q^0. \tag{3.71}$$

The difference in the renormalisation schemes is then given by a finite renormalisation z_{fin}

$$Z_1 = z_{\text{fin}} Z_2, \tag{3.72}$$

where the finite renormalisation factor z_{fin} has the general form

$$z_{\text{fin}} = 1 + a_\mu^2 \hat{s}, \tag{3.73}$$

and starts at $\mathcal{O}(\alpha_s^2)$ because the axial singlet contributions also first start at $\mathcal{O}(\alpha_s^2)$. We define the ADM as

$$\gamma = Z \frac{\mathrm{d}Z^{-1}}{\mathrm{d}\ln\mu}. \tag{3.74}$$

Differentiating both sides of Eq. (3.72) with respect to $\mathrm{d}/\mathrm{d}\ln\mu$ leads to [21, 131]

$$\gamma_1 - \gamma_2 = 4\beta_0 \hat{s} a_\mu^3. \tag{3.75}$$

We see that the leading part of the ADM is scheme independent while the next-to-leading-order part of the ADM is scheme dependent. Explicitly calculating the difference of the ADM in the L-scheme and the CK-scheme[2] fixes the scheme constant $\hat{s}$

$$\gamma_A^{(1)} - 2\gamma_0^\psi = 0, \qquad \gamma_A^{(2)} - 2\gamma_1^\psi = 4\beta_0 \hat{s} \Leftrightarrow \hat{s} = \frac{1}{8}. \tag{3.76}$$

Furthermore, Eq. (3.72) relates a WC in one scheme to another scheme. The two WC in different schemes are related to each other through the finite renormalisation $C_1 z_{\text{fin}} = C_2$. Applying this transformation to the WC in the L-scheme yields

$$C_b z_{\text{fin}} = 1 + C_{\text{sg}} + a_\mu^2 \hat{s} = 1 + a_\mu^2 \left[\frac{1}{8} + \frac{1}{2}\ln\left(\frac{\mu^2}{m_t^2}\right)\right]. \tag{3.77}$$

Since $R_{\Delta_t}^{\text{S, A}}$ is an observable it follows that $R_{A,\text{L}}^{\text{S}}$ is connected to R_A^{S} through the scheme transformation

$$R_{A,\text{L}}^{\text{S}} = R_A^{\text{S}} + 2a_\mu^2 \hat{s}. \tag{3.78}$$

The two WC C_{sg} and $-C_h$ should be related to each other through the finite renormalisation yet we observe that this is not the case.[3] The constant term in $-C_h$ carries the opposite sign than the one we predict from the scheme transformation of C_{sg}. The origin of this

[2]The additional factor of 2 in front of γ_i^ψ is there to account for the different choice of definition of the ADM with respect to $\gamma_A^{(i)}$ which was defined with $\mathrm{d}/\mathrm{d}\mu$.

[3]The extra minus in front of C_h is there due to a difference in the definitions of the WC in the L-scheme and the CK-scheme. Including the sign in front of C_h leads to the logarithms being in agreement in both schemes.

inconsistency is unknown to us. Despite this the evolution of the WC remains manifestly scheme independent. In the L-scheme the WC $\vec{C} = (C_b, C_{\mathrm{sg}})^T$ obeys the RGE [127]

$$\mu \frac{d}{d\mu}\vec{C} = \gamma_Z^T \vec{C}, \tag{3.79}$$

where the ADM is

$$\begin{aligned}\gamma_Z &= a_\mu^2 \gamma_{(1)} + a_\mu^3 \gamma_{(2)} \\ &= a_\mu^2 \begin{pmatrix} \gamma_A^{(1)} & \gamma_A^{(1)} \\ (n_f-1)\gamma_A^{(1)} & (n_f-1)\gamma_A^{(1)} \end{pmatrix} + a_\mu^3 \begin{pmatrix} \gamma_A^{(2)} & \gamma_A^{(2)} \\ (n_f-1)\gamma_A^{(2)} & (n_f-1)\gamma_A^{(2)} \end{pmatrix}.\end{aligned} \tag{3.80}$$

The solution of Eq. (3.79) is straightforward since $[\gamma_Z(\mu_1), \gamma_Z(\mu_2)] = 0$ (in general this is not the case cf. [131]) and is given by the evolution matrix

$$\begin{aligned}\hat{U}^{(n_f)}(\mu,\mu_0) &= \exp\left\{ \int_{a_{\mu_0}}^{a_\mu} da \frac{\gamma_Z^T(a)}{\beta(a)} \right\} \\ &= \mathbb{1} + \frac{\gamma_{(1)}^T}{2\beta_0}(a_{\mu_0} - a_\mu) + \frac{\left(\gamma_{(1)}^T\right)^2}{8\beta_0^2}(a_{\mu_0} - a_\mu)^2 + \frac{\beta_0\gamma_{(2)}^T - \beta_1\gamma_{(1)}^T}{4\beta_0^2}(a_{\mu_0}^2 - a_\mu^2),\end{aligned} \tag{3.81}$$

such that the WC at a scale μ is

$$\begin{aligned}\vec{C}(\mu) &= \hat{U}^{(n_f)}(\mu,\mu_0)\vec{C}(\mu_0) \\ &= \begin{pmatrix} C_b(\mu_0) + \frac{\gamma_A^{(1)}}{2\beta_0}\Delta_{a_{\mu_0},a_\mu} + \frac{n_f\left(\gamma_A^{(1)}\right)^2}{8\beta_0^2}\Delta^2_{a_{\mu_0},a_\mu} + \frac{\beta_0\gamma_A^{(2)} - \beta_1\gamma_A^{(1)}}{4\beta_0^2}\Delta_{a^2_{\mu_0},a^2_\mu} \\ C_{\mathrm{sg}}(\mu_0) + \frac{\gamma_A^{(1)}}{2\beta_0}\Delta_{a_{\mu_0},a_\mu} + \frac{n_f\left(\gamma_A^{(1)}\right)^2}{8\beta_0^2}\Delta^2_{a_{\mu_0},a_\mu} + \frac{\beta_0\gamma_A^{(2)} - \beta_1\gamma_A^{(1)}}{4\beta_0^2}\Delta_{a^2_{\mu_0},a^2_\mu} \end{pmatrix} + \mathcal{O}(\alpha_s^3),\end{aligned} \tag{3.82}$$

where we defined $\Delta_{a,b} = a - b$. The evolution is scheme dependent but the scheme dependence drops out in the terms proportional to $a_{\mu_0}^2$ between $\gamma_A^{(2)}$ and $\vec{C}(\mu_0)$. The only scheme dependent objects in this evolution are the WC at its initial value and the ADM $\gamma_A^{(2)}$. They mutually compensate the scheme dependence at the scale μ_0

$$\begin{aligned}\frac{\beta_0\gamma_A^{(2)}}{4\beta_0^2}\Delta_{a^2_{\mu_0},a^2_\mu} + C_b(\mu_0) &\to \frac{\gamma_A^{(2)} - 4\beta_0\hat{s}}{4\beta_0}\Delta_{a^2_{\mu_0},a^2_\mu} + C_b(\mu_0)(1 + a_{\mu_0}^2\hat{s}) + \mathcal{O}(\alpha_s^3) \\ &= \frac{\gamma_A^{(2)}}{4\beta_0}\Delta_{a^2_{\mu_0},a^2_\mu} + C_b(\mu_0) + a_\mu^2\hat{s} + \mathcal{O}(\alpha_s^3) \\ &\sim C_b(\mu) + a_\mu^2\hat{s},\end{aligned} \tag{3.83}$$

in agreement with Eq. (3.77); the remaining scheme dependence at the scale μ should be compensated by the scheme dependence of R_A^{S}.

For the remainder of this work we use

$$r_{2,0,\mathrm{L}}^{S,A} = r_{2,0}^{S,A} + 2\hat{s} = -\frac{31}{12}. \tag{3.84}$$

Because of the inconsistency discussed above, the scheme dependence does not fully cancel. Nevertheless, the numerical impact on the decay rate by changing either the constant part of the WC or $R^{\mathrm{S}}_{A,\mathrm{L}}$ by $\pm\hat{s}$ is negligible. When evolving from the high scale $\mu = M_Z$ down to the low scale $\mu \approx 2\,\mathrm{GeV}$ we have to include quark threshold effects. However, the benefit of doing the evolution in the L-scheme is that all of these quark threshold effects are of the form $\hat{M}(\mu_q) = \mathbb{1} + a^2_{\mu_q}(1/2)\ln(m_q^2/\mu_q^2)$ [127]. We set the scale $\mu_q = m_q$ and all of these effects vanish. The WC evolved down to the three flavour scale then becomes

$$\vec{C}^{(3)}(\mu) = \hat{U}^{(3)}(\mu, m_c)\hat{U}^{(5)}(m_b, M_Z)\vec{C}^{(5)}(M_Z), \tag{3.85}$$

where $\hat{U}^{(4)}(m_c, m_b) = \mathbb{1}$ since for four flavours the ADM is zero i.e. the axial singlet contribution vanishes since the full $\mathrm{SU}(2)$ doublet of charm and strange is present. Numerically the WC evaluates to

$$\begin{aligned}
C^{(3)}_{\mathrm{sg}}(\mu) =& -\frac{1}{2}\left(a^{(5)}_{M_Z}\right)^2 \ln\left(\frac{m_t^2}{M_Z^2}\right) \\
&+ \frac{6}{23}\Delta_{a^{(5)}_{M_Z},a^{(5)}_{m_b}} + \frac{90}{529}\Delta^2_{a^{(5)}_{M_Z},a^{(5)}_{m_b}} + \frac{2797}{6348}\Delta_{(a^{(5)}_{M_Z})^2,(a^{(5)}_{m_b})^2} \\
&+ \frac{2}{9}\Delta_{a^{(3)}_{m_c},a^{(3)}_{\mu}} + \frac{2}{27}\Delta^2_{a^{(3)}_{m_c},a^{(3)}_{\mu}} + \frac{107}{324}\Delta_{(a^{(3)}_{m_c})^2,(a^{(3)}_{\mu})^2} \\
=& -0.011 + 0.034 - 0.241 a^{(3)}_{\mu} - 0.256\left(a^{(3)}_{\mu}\right)^2,
\end{aligned} \tag{3.86}$$

where the first constant in the last line is the numerical value at the five flavor threshold and the remaining values are from the three flavor threshold. At the τ scale the WC is very small

$$C^{(3)}_{\mathrm{sg}}(m_\tau) = -0.004. \tag{3.87}$$

The numerically dominant axial singlet contribution comes entirely from $R^{\mathrm{S}}_{A,L}$. For our calculation of the decay rate we use

$$R^{\mathrm{S,A}}_{\Delta_t} = 2C^{(3)}_{\mathrm{sg}}(\mu) + R^{\mathrm{S}}_{A,\mathrm{L}}(\mu) + \mathcal{O}(\alpha_s^3), \tag{3.88}$$

and set below the charm threshold $n_f = 3$ as well as the strong coupling constant to $a^{(3)}_{\mu}$. Above the charm threshold $n_f = 4$ with $R^{\mathrm{S,A}}_{\Delta_t} = 0$ and we use $a^{(4)}_{\mu}$.

The occurring integrals are of the form

$$J^0_k = \int_0^1 \mathrm{d}x\,(1-x)^2(1+2x)\ln^k\left(\frac{\mu^2}{m_N^2 x}\right), \tag{3.89}$$

if we set $\mu = m_N$ then they all follow immediately from Eqs. (3.17)-(3.19) as $J^0_k(\mu = m_N) = (-1)^k \lim_{x_\ell\to 0} I_k$. Keeping the dependence on the renormalisation scale the integrals are given by

$$J_0^0 = \frac{1}{2}, \tag{3.90}$$

$$J_1^0 = \frac{19}{24} + \frac{1}{2}\ln\left(\frac{\mu^2}{m_N^2}\right), \tag{3.91}$$

$$J_2^0 = \frac{265}{144} + \frac{19}{12}\ln\left(\frac{\mu^2}{m_N^2}\right) + \frac{1}{2}\ln^2\left(\frac{\mu^2}{m_N^2}\right), \tag{3.92}$$

$$J_3^0 = \frac{3355}{576} + \frac{265}{48}\ln\left(\frac{\mu^2}{m_N^2}\right) + \frac{19}{8}\ln^2\left(\frac{\mu^2}{m_N^2}\right) + \frac{1}{2}\ln^3\left(\frac{\mu^2}{m_N^2}\right), \tag{3.93}$$

which leads to the compact form of $\mathcal{R}_0$

$$\mathcal{R}_0 = N_c J_0^0 \left[\sum_i (g_{i,V}^2 + g_{i,A}^2) R^{\mathrm{NS}} + \left(\sum_i g_{i,V}\right)^2 R_V^{\mathrm{S}} + \left(\sum_i g_{i,A}\right)^2 R_{\Delta_t}^{\mathrm{S},A} \right]\Bigg|_{\ln^k\left(\frac{\mu^2}{m_N^2 x}\right) \to \frac{J_k^0}{J_0^0}} \tag{3.94}$$

3.3.3. Quark Mass Corrections

The integrals appearing in $\mathcal{R}_2$ and $\mathcal{R}_2^{(0),Z}$ are given by

$$\begin{aligned} J_k^2 &= J_k^{2,r} + J_k^{(0),Z} \\ &= \frac{1}{2\pi i}\oint\limits_{|x|=1} \mathrm{d}x\, \frac{2x(1-x)^2}{x}\ln^k\left(-\frac{\mu^2}{m_N^2 x}\right) + \frac{1}{2\pi i}\oint\limits_{|x|=1} \mathrm{d}x\, \frac{(1-x)^2}{x}\ln^k\left(-\frac{\mu^2}{m_N^2 x}\right). \end{aligned} \tag{3.95}$$

As for the massless case the integrals here are simply related to the integrals presented for the charged-current case $J_k^2(\mu = m_N) = (-1)^k \lim_{x_\ell \to 0} I_k^{(1+0),c}$. For the neutral-current we keep the dependence on renormalisation scale which leads to

$$J_1^{2,r} = -\frac{2}{3}, \tag{3.96}$$

$$J_2^{2,r} = -\frac{22}{9} - \frac{4}{3}\ln\left(\frac{\mu^2}{m_N^2}\right), \tag{3.97}$$

$$J_3^{2,r} = -\frac{85}{9} + \frac{2}{3}\pi^2 - \frac{22}{3}\ln\left(\frac{\mu^2}{m_N^2}\right) - 2\ln^2\left(\frac{\mu^2}{m_N^2}\right), \tag{3.98}$$

and the integrals involving the pole evaluate to

$$J_0^{(0),Z} = 1, \tag{3.99}$$

$$J_1^{(0),Z} = \frac{3}{2} + \ln\left(\frac{\mu^2}{m_N^2}\right), \tag{3.100}$$

$$J_2^{(0),Z} = \frac{7}{2} - \frac{1}{3}\pi^2 + 3\ln\left(\frac{\mu^2}{m_N^2}\right) + \ln^2\left(\frac{\mu^2}{m_N^2}\right), \tag{3.101}$$

$$J_3^{(0),Z} = \frac{45}{4} - \frac{3}{2}\pi^2 + \left(\frac{21}{2} - \pi^2\right)\ln\left(\frac{\mu^2}{m_N^2}\right) + \frac{9}{2}\ln^2\left(\frac{\mu^2}{m_N^2}\right) + \ln^3\left(\frac{\mu^2}{m_N^2}\right). \tag{3.102}$$

Using these integrals we write $\mathcal{R}_2$ and $\mathcal{R}_2^{(0),Z}$ in the compact form

$$\mathcal{R}_2 = -N_c x_q^2 J_0^2 \left[\sum_i \left(g_{i,V}^2 + g_{i,A}^2\right) R_2 + g_{q,V}^2 R_{q,2}^V + g_{q,A}^2 R_{q,2}^A \right]\Bigg|_{\ln^k\left(-\frac{\mu^2}{m_N^2 x}\right) \to \frac{J_k^2}{J_0^2}}, \tag{3.103}$$

$$\mathcal{R}_2^{(0),Z} = 3 N_c x_q^2 J_0^{(0),Z} g_{q,A}^2 \Pi_{qq,A,2}^{(0)} \Bigg|_{\ln^k\left(-\frac{\mu^2}{m_N^2 x}\right) \to \frac{J_k^{(0),Z}}{J_0^{(0),Z}}}. \tag{3.104}$$

We conclude the calculation of the quark mass corrections by commenting on the singlet contributions. Quark mass corrections to the vector singlet contribution start at $O(m_q^4)$ [75, 76]. The quadratic quark mass corrections to the axial singlet contribution vanish. We can see this by looking at the diagram in Fig. 2.2(d). We are interested in quadratic quark mass corrections involving the charm quark. The axial singlet diagram will be proportional to a function $f(m_i^2, m_j^2)$ which is symmetric in its two arguments. For four flavours all massless contributions vanish and only the quark mass effects contribute. Therefore, including the axial couplings the whole massive four flavour correction will be proportional to

$$\begin{aligned} R_{\Delta_t}^{S,A,2}(n_f = 4) &\propto f(m_c^2, m_c^2) - f(m_c^2, m_s^2) - f(m_s^2, m_c^2) + f(m_s^2, m_s^2) \\ &= m_c^2 \Big(2f'(0,0) - f'(0,0) - f'(0,0) \Big) + O(m_c^4) = 0 + O(m_c^4), \end{aligned} \tag{3.105}$$

where we used $f'(x, y) = \partial_x f = \partial_y f$.

4. Heavy Sterile Neutrino Phenomenology

4.1. $\mathrm{SU}(2)$ Limit

We start our discussion of the phenomenology of hadronic HSN decays by studying the $\mathrm{SU}(2)$ limit. Setting the Weinberg angle θ_w to zero eliminates the contributions from the hypercharge gauge boson. In this limit the charged-current rate should be roughly double the neutral-current rate. This is satisfied when taking the limit of large HSN masses

$$\begin{aligned}
\lim_{\substack{m_N\to\infty\\ \theta_w\to 0}} \frac{\Gamma(N\to\ell X)}{\Gamma(N\to\nu X)} &= \lim_{\theta_w\to 0} \frac{2(|V_{ud}|^2+|V_{us}|^2+\ldots)}{\sum_i \left(g_{i,V}^2+g_{i,A}^2\right)} \\
&= \begin{cases} 2|V_{ud}|^2 & \approx 1.90 \quad \text{for } n_f = 2 \\ |V_{ud}|^2+|V_{us}|^2+|V_{cd}|^2+|V_{cs}|^2 & \approx 2.00 \quad \text{for } n_f = 4 \end{cases}, \qquad (4.1)
\end{aligned}$$

which coincides with the $\mathrm{SU}(2)$ limit value of 2 if one takes into account that $V_{ud} = 1$ in a theory with $n_f = 2$. This ratio is affected by the non-zero Weinberg angle as

$$\begin{aligned}
\lim_{m_N\to\infty} \frac{\Gamma(N\to\ell X)}{\Gamma(N\to\nu X)} &= \frac{2(|V_{ud}|^2+|V_{us}|^2+\ldots)}{\sum_i \left(g_{i,V}^2+g_{i,A}^2\right)} \\
&= \begin{cases} \frac{2|V_{ud}|^2}{1-s_w^2+\frac{20}{9}s_w^4} & \approx 2.89 \quad \text{for } n_f = 2 \\ \frac{2(|V_{ud}|^2+|V_{us}|^2+|V_{cd}|^2+|V_{cs}|^2)}{2-4s_w^2+\frac{40}{9}s_w^4} & \approx 3.04 \quad \text{for } n_f = 4 \end{cases}. \qquad (4.2)
\end{aligned}$$

In Fig. 4.1 we show the ratio of charged- and neutral-current decay for $n_f = 4$. It approaches the predicted value.

4.2. Inclusive Hadronic HSN Decay Rate

4.2.1. Charged-Current Decay

We first presented the calculation of the charged-current HSN decay rate in the chiral limit in Ref. [126].

We are interested in the HSN mass region which permits a perturbative description. For small HSN masses we expect a poor perturbative behaviour, as here $\alpha_s(m_N)$ will be large and thus spoil the convergence of the perturbative series. By contrast, large HSN masses should permit a good pertubative description. Furthermore, at an HSN mass of $m_N \geq m_D + m_\ell$ the decay into charmed final states becomes accessible. The decay rate calculated through perturbative methods cannot be trusted near the charm resonance

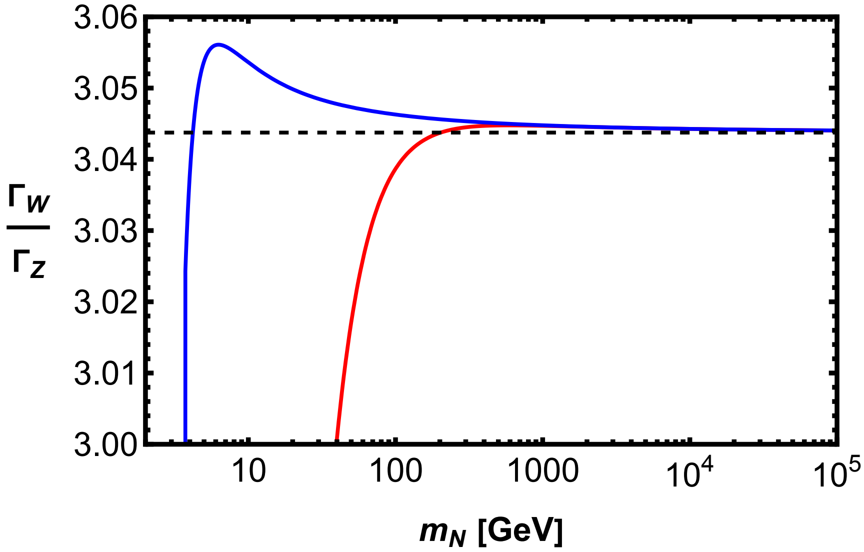

Figure 4.1.: Ratio of the charged-current and neutral-current decay rate denoted $\Gamma_W = \Gamma(N \to \ell X)$ and $\Gamma_Z = \Gamma(N \to \nu X)$ respectively. The blue curve belongs to $\ell = \mu$ and the red one to $\ell = \tau$. The dashed line corresponds to the value 3.04375. Both curves approach the limit.

region as here non-perturbative effects dominate the decay rate. We can increase the accuracy of our calculation through the inclusion of the finite quark mass effects (we neglect the quark mass effects of $q = u, d, s$ as they are all small). The inclusion of the charm mass effects will increase the accuracy of our calculation i.e. it allows us to gauge the HSN mass region allowing for a perturbative description more precisely. Nevertheless, even with the inclusion of the charm mass effects a reliable perturbative description close to or even at the charm resonance remains impossible.

We employ the correlators used for τ decays. Kinematically τ and HSN decay are equal up to the mass of the final state lepton, which is a neutrino in the τ case or a charged lepton in the HSN case. In the limit of vanishing lepton mass we reproduce the same coefficients as in τ decays [53, 58, 59]:

$$\begin{aligned}
&\lim_{x_\ell \to 0} \Gamma(N \to \ell X) = N_c \frac{G_F^2 m_N^5 |V_{N\ell}|^2}{192\pi^3} \\
&\times \left[(|V_{ud}|^2 + |V_{us}|^2) \left(1 + a_{m_N} + 5.202 a_{m_N}^2 + 26.366 a_{m_N}^3 + 127.079 a_{m_N}^4 \right) \right. \\
&\left. - 8 |V_{us}|^2 \frac{(m_s(m_N))^2}{m_N^2} \left(1 + 5.333 a_{m_N} + 46.000 a_{m_N}^2 + 435.286 a_{m_N}^3 \right) \right].
\end{aligned} \tag{4.3}$$

We write the massive corrections above in terms of the strange quark mass only to emphasise this is the value of the coefficients of the perturbative series for $n_f = 3$. At

$n_f = 4$ flavours the coefficients change

$$
\begin{aligned}
\lim_{x_\ell \to 0} \Gamma(N \to \ell X) = N_c \frac{G_F^2 m_N^5 |V_{N\ell}|^2}{192\pi^3} \\
\times \Bigg[(|V_{ud}|^2 + |V_{us}|^2 + |V_{cd}|^2 + |V_{cs}|^2) \\
\times \left(1 + a_{m_N} + 4.823 a_{m_N}^2 + 19.592 a_{m_N}^3 + 58.547 a_{m_N}^4\right) \\
- 8(|V_{cd}|^2 + |V_{cs}|^2) \frac{(m_c(m_N))^2}{m_N^2} \left(1 + 5.333 a_{m_N} + 43.785 a_{m_N}^2 + 378.996 a_{m_N}^3\right) \Bigg]. \qquad (4.4)
\end{aligned}
$$

For an HSN with $m_N = 5\,\text{GeV}$ and $\ell = \tau$ the coefficients change drastically

$$
\begin{aligned}
\lim_{x_\ell \to m_\tau/5\,\text{GeV}} \Gamma(N \to \ell X) = N_c \frac{G_F^2 m_N^5 |V_{N\ell}|^2}{192\pi^3} \\
\times \Bigg[(|V_{ud}|^2 + |V_{us}|^2 + |V_{cd}|^2 + |V_{cs}|^2) \\
\times 0.402 \cdot \left(1 + a_{m_N} + 5.967 a_{m_N}^2 + 33.385 a_{m_N}^3 + 164.721 a_{m_N}^4\right) \\
- 8(|V_{cd}|^2 + |V_{cs}|^2) \frac{(m_c(m_N))^2}{m_N^2} \\
\times 0.027 \cdot \left(1 + 5.605 a_{m_N} + 53.487 a_{m_N}^2 + 536.696 a_{m_N}^3\right) \Bigg]. \qquad (4.5)
\end{aligned}
$$

A τ lepton in the final state reduces the total decay rate and thus the convergence of the perturbative rate is worse.

In Figs. 4.2 and 4.3 we show the HSN decay rates for $\ell = \mu,\ \tau$ below the charm threshold (we use $\alpha_s^{(5)}(M_Z) = 0.1183$ which we obtain from the weighted average of all measurements listed in the PDG [8] excluding the one obtained through τ decays and running it down to the relevant scale using `RunDec` [132, 133]; in Appendix B we list the numerical values of the quantities and constants we use throughout this work). The case of $\ell = e$ is qualitatively similar to $\ell = \mu$ and hence we omit it. In both cases we see the different $\mathcal{O}(\alpha_s^n)$ corrections have a sizeable impact on the decay rate. In Figs. 4.2(b) and 4.3(b) we show the decay rates normalised to the leading order decay rate. For small HSN masses the convergence is poor as it is expected since $\alpha_s(m_N)$ is not a small parameter for small HSN masses. For heavier HSN masses the strong coupling constant becomes smaller and the quality of the perturbative series improves. Looking at the scaling of the decay rate with respect to the renormalisation scale μ in Figs. 4.4 and 4.5 we fix a mass threshold of the HSN for which the perturbative description is applicable by demanding that the decay rate is insensitive to the renormalisation scale i.e. the decay rate is flat with respect to μ. The decay rate is an observable and should thus not depend on the renormalisation scale. In practice it does scale with the renormalisation scale as we can only include a finite number of terms in the perturbative series. This remaining renormalisation scale dependence can be used to estimate an uncertainty. Nevertheless, the more orders in α_s are included the less

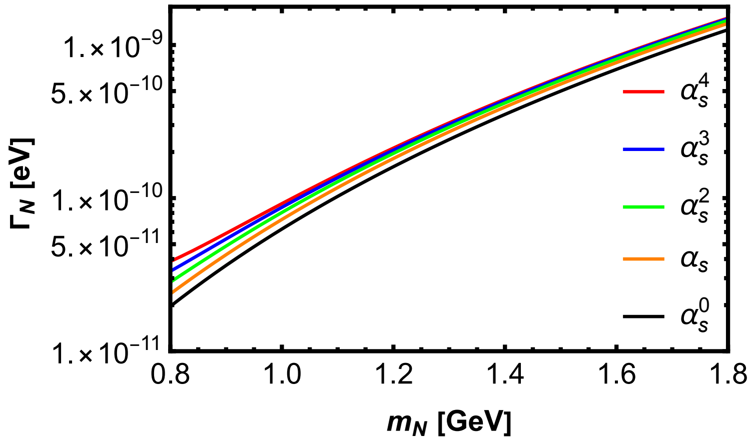

(a) Inclusive decay rate at different orders in α_s.

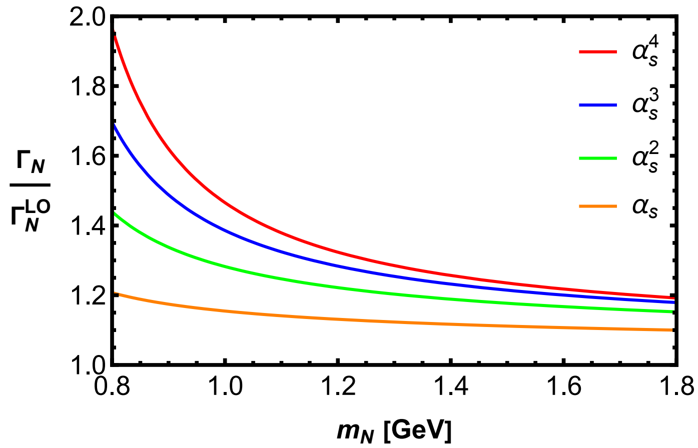

(b) Inclusive decay normalised to the LO.

Figure 4.2.: Decay rate $\Gamma_N = \Gamma(N \to \mu X)$. Here the mixing angle is $|V_{N\mu}| = 10^{-3}$.

the decay rate should be sensitive to the renormalisation scale. This is what we observe. For $\ell = \mu$ in Fig. 4.4 the decay rate scales strongly with the renormalisation scale for HSN masses $m_N \leq 1.2\,\text{GeV}$. At $m_N = 1.5\,\text{GeV}$ the highest order $\mathcal{O}(\alpha_s^4)$ corrections start to flatten meaning the decay rate becomes more and more insensitive to the choice of the renormalisation scale. Further increasing the mass the behaviour improves. Thus we can state that the perturbative description of charged-current HSN decays with $\ell = \mu$ is well behaved for HSN masses $m_N \gtrsim 1.5\,\text{GeV}$. This threshold is not to be understood as a hard limit. Instead this limit is to be understood as the perturbative description being well behaved roughly around this HSN mass. Qualitatively the picture is the same for $\ell = \tau$ in Fig. 4.5. For HSN with masses $m_N \leq 2.8\,\text{GeV}$ the decay rate is rather sensitive to the renormalisation scale. For $m_N \gtrsim 3.0\,\text{GeV}$ we observe, as in the muon case, that the highest order correction at $\mathcal{O}(\alpha_s^4)$ leads to a decay rate which is less sensitive to the renormalisation scale. In summary, HSN with masses that do not permit decays into charmed final states permit a well behaved perturbative description of the decay rate for

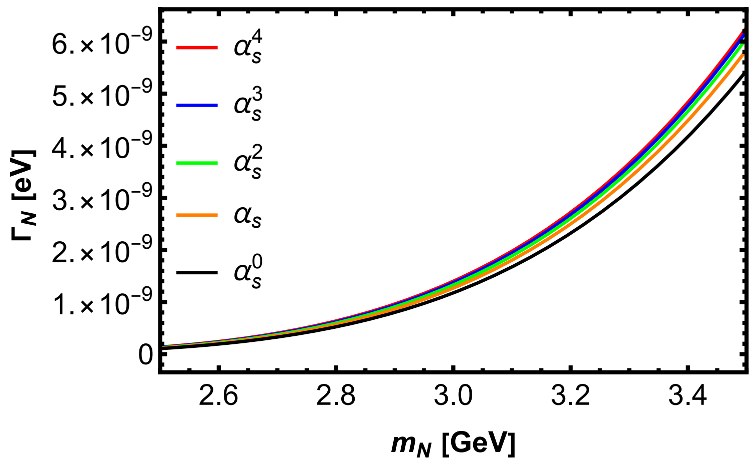

(a) Inclusive decay rate at different orders in α_s.

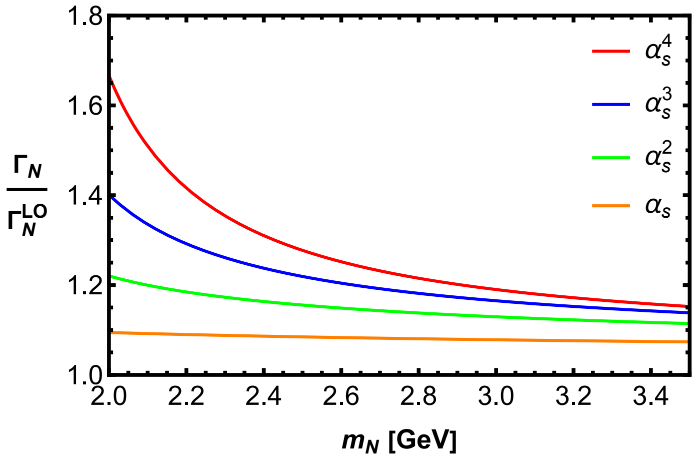

(b) Inclusive decay normalised to the LO.

Figure 4.3.: Decay rate $\Gamma_N = \Gamma(N \longrightarrow \tau X)$. Here the mixing angle is $|V_{N\tau}| = 10^{-3}$

HSN masses

$$1.5\,\text{GeV} \lesssim m_N \quad \ell = e,\ \mu, \tag{4.6}$$
$$3.0\,\text{GeV} \lesssim m_N \quad \ell = \tau. \tag{4.7}$$

It is only possible to arrive at this conclusion by including the $O(\alpha_s^4)$ corrections. Following Figs. 4.4 and 4.5 the thresholds would be significantly weaker if, for example, only the $O(\alpha_s^2)$ corrections were included. We see that the perturbative description would be significantly worse in this case as at the three-loop level the decay rate stays sensitive to the renormalisation scale up to the charmed meson production scale. Thus for an accurate description the inclusion of the highest order corrections plays a crucial role in the robustness of the perturbative description.

HSN with masses $m_N \geq m_{D^+} + m_\ell$ may decay hadronically into charmed final states. At the charm threshold charm final states would be produced resonantly which is a non-perturbative process and defies any perturbative description. The inclusion of the quark

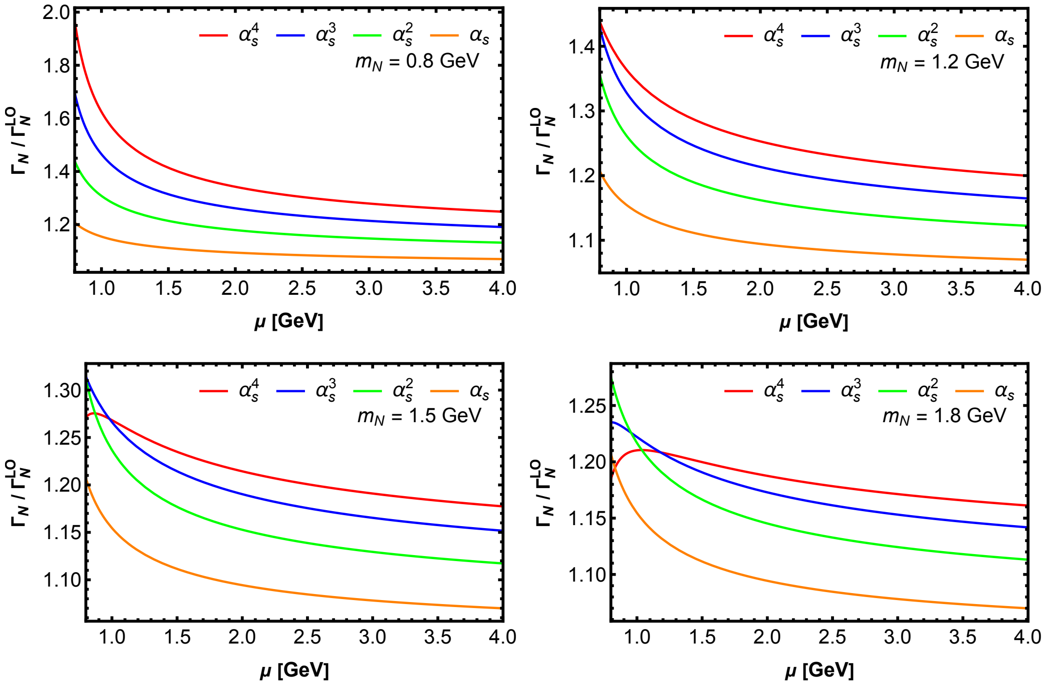

Figure 4.4.: Dependence of the inclusive HSN decay rate $\Gamma_N = \Gamma(N \to \mu X)$ on the renormalisation scale μ for different HSN masses below the charm production threshold.

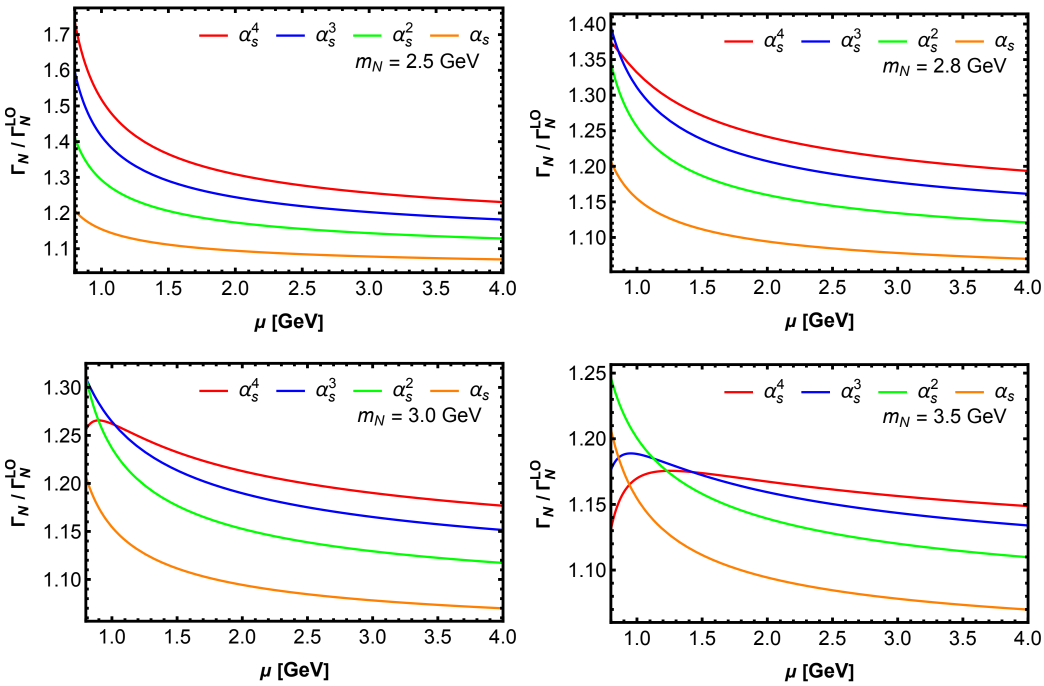

Figure 4.5.: Dependence of the inclusive HSN decay rate $\Gamma_N = \Gamma(N \to \tau X)$ on the renormalisation scale μ for different HSN masses below the charm production threshold.

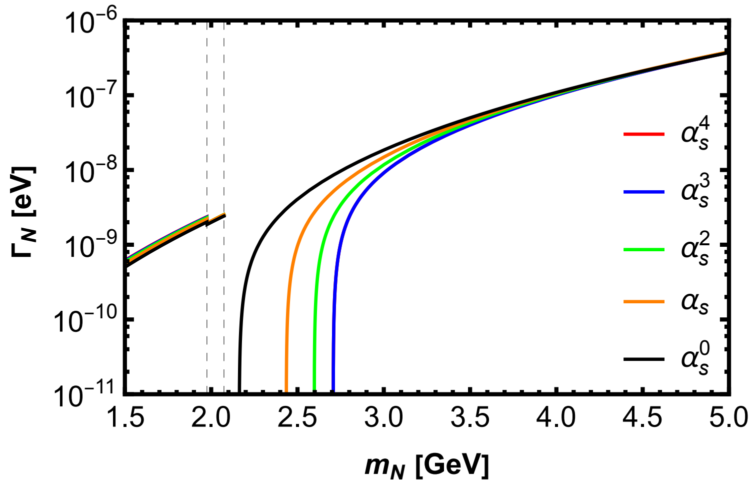

(a) Inclusive decay rate at different orders above the charm production threshold.

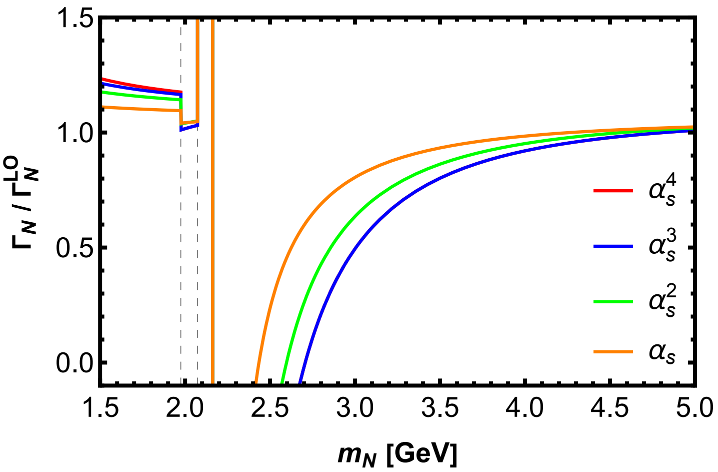

(b) Inclusive decay rate above the charm threshold normalised to the LO.

Figure 4.6.: Decay rate $\Gamma_N = \Gamma(N \to \mu X)$. Here the mixing angle is $|V_{N\mu}| = 10^{-3}$. We show the behaviour induced by the quark mass corrections. The kinks at $m_N = m_{D^+} + m_\mu$ and $m_N = m_{D_s^+} + m_\mu$ are dominated by non-perturbative effects and the decay rate cannot be trusted closely above the thresholds. Above the charm threshold we omit the $O(\alpha_s^4)$ corrections in the massless part of the decay rate because the charm mass corrections come with the opposite sign of the massless corrections and so there are cancellations between the massless and massive parts. For this reason above the charm threshold the red α_s^4 line is absent.

mass corrections improves the accuracy of the perturbative calculation and helps us to make a more precise statement about the mass threshold above which we can perturbatively describe HSN decays beyond the charm threshold. In Figs. 4.6 and 4.7 we show the total charged-current decay rate including HSN masses above the charm production threshold

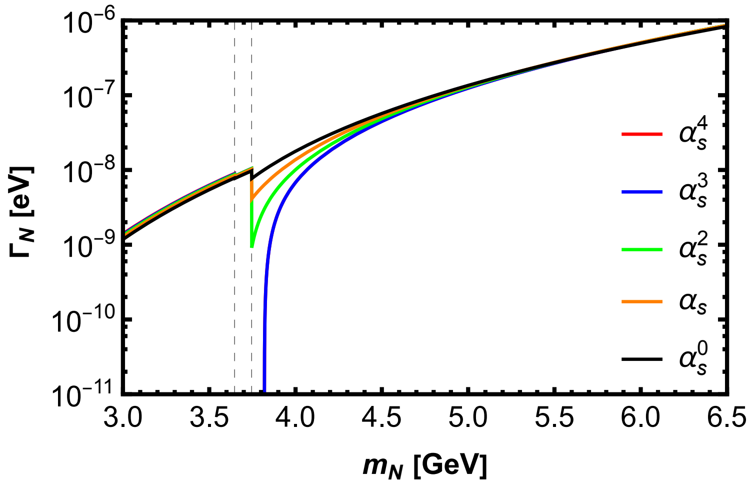

(a) Inclusive decay rate at different orders in $O(\alpha_s)$ above the charm production threshold.

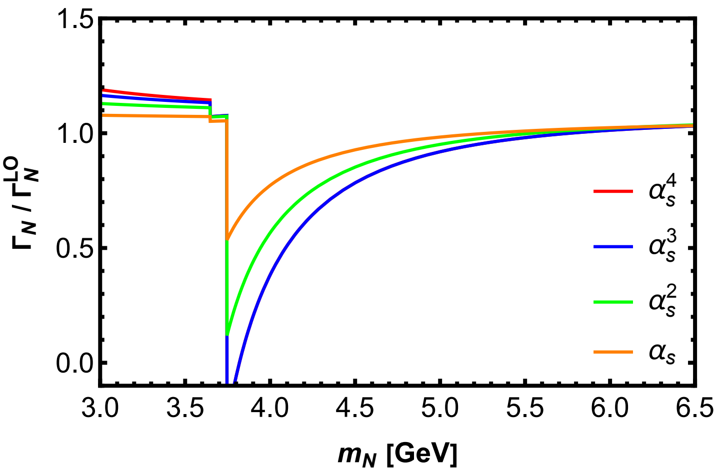

(b) Inclusive decay rate above the charm threshold normalised to the LO.

Figure 4.7.: Decay rate $\Gamma_N = \Gamma(N \to \tau X)$. Here the mixing angle is $|V_{N\tau}| = 10^{-3}$. We show the behaviour induced by the quark mass corrections. The kinks at $m_N = m_{D^+} + m_\tau$ and $m_N = m_{D_s^+} + m_\tau$ are dominated by non-perturbative effects and the decay rate cannot be trusted closely above the thresholds. We omit the $O(\alpha_s^4)$ terms in the massless part of the decay rate above the charm threshold, which is why the red α_s^4 line is absent above the charm threshold (also see Fig. 4.6).

for both $\ell = \mu$ and $\ell = \tau$. Immediately above the charm threshold $m_N = m_{D^+} + m_\ell$ the decay rate strongly decreases. The reason for this is that the quark mass corrections are all negative. In the extreme case the decay rate above the charm threshold becomes negative which is unphysical. The height of the kinks at $m_N = m_{D^+} + m_\ell$ and $m_N = m_{D_s^+} + m_\ell$ scales with the size of the CKM element and thus the D_s^+ contributions are the dominant ones since $|V_{cs}|^2 \gg |V_{cd}|^2$. We observe in Figs. 4.6 and 4.7 that the mass corrections are

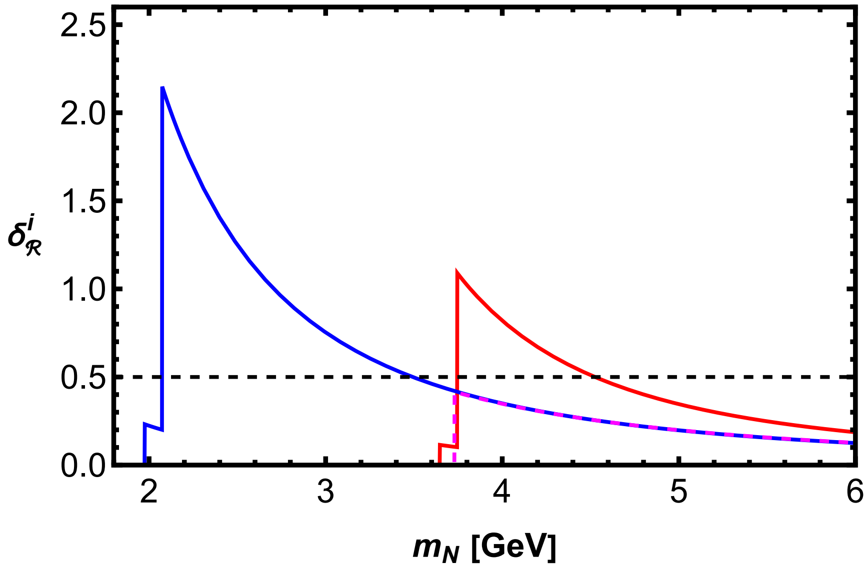

Figure 4.8.: The ratio of the massive corrections to the massless corrections for the charged-current $\delta^{\mathrm{CC}}_{\mathcal{R}}$ given in Eq. (4.8). The blue line belongs to $N \longrightarrow \mu X$ and the red one to $N \longrightarrow \tau X$. The horizontal dashed line marks the 50% threshold. Additionally we show $\delta^{\mathrm{NC}}_{\mathcal{R}}$ (magenta, dot-dashed line) following analogously from Eq. (4.8) with the appropriate neutral-current expressions.

sizeable at each order in α_s. Especially in Fig. 4.6 we see that each order in α_s significantly extends the region in which we cannot trust the perturbative calculation. We also see that while each order in α_s extends the non-perturbative region the relative size of the extension with respect to the previous α_s correction becomes smaller and the higher order massive corrections converge. From Figs. 4.6 and 4.7 it is clear that the higher order QCD corrections play a crucial role in the accuracy of the perturbative description and more importantly in the determination of the non-perturbative region. To determine the mass window in which we can perturbatively describe the decay rate we require the size of the massive corrections to not exceed 50% of the massless corrections i.e.

$$\delta^{\mathrm{CC}}_{\mathcal{R}} = \frac{|\mathcal{R}_2^{(1+0)} + \mathcal{R}_2^{(0)}|}{\mathcal{R}_0^{(1+0)}} \leq 0.5. \tag{4.8}$$

We call this the 50% criterion. In addition, we demand that the mass limit m_N^{lim} obtained from the 50% criterion leads to a decay rate that is still insensitive to the renormalisation scale i.e. the uncertainty coming from varying the renormalisation scale between $m_N^{\mathrm{lim}}/2$ and $2m_N^{\mathrm{lim}}$ is still small (at most around $\mathcal{O}(20\%)$). Fig. 4.8 shows the $\delta^{\mathrm{CC}}_{\mathcal{R}}$ ratio. We see the 50% criterion is fulfilled for HSN masses

$$3.5\,\mathrm{GeV} \lesssim m_N \qquad \ell = e,\, \mu, \tag{4.9}$$

$$4.6\,\mathrm{GeV} \lesssim m_N \qquad \ell = \tau. \tag{4.10}$$

As in the massless case we look at the sensitivity of the decay rate with respect to the renormalisation scale. In Figs. 4.9 and 4.10 we show the decay rates for $\ell = \mu, \tau$ as a

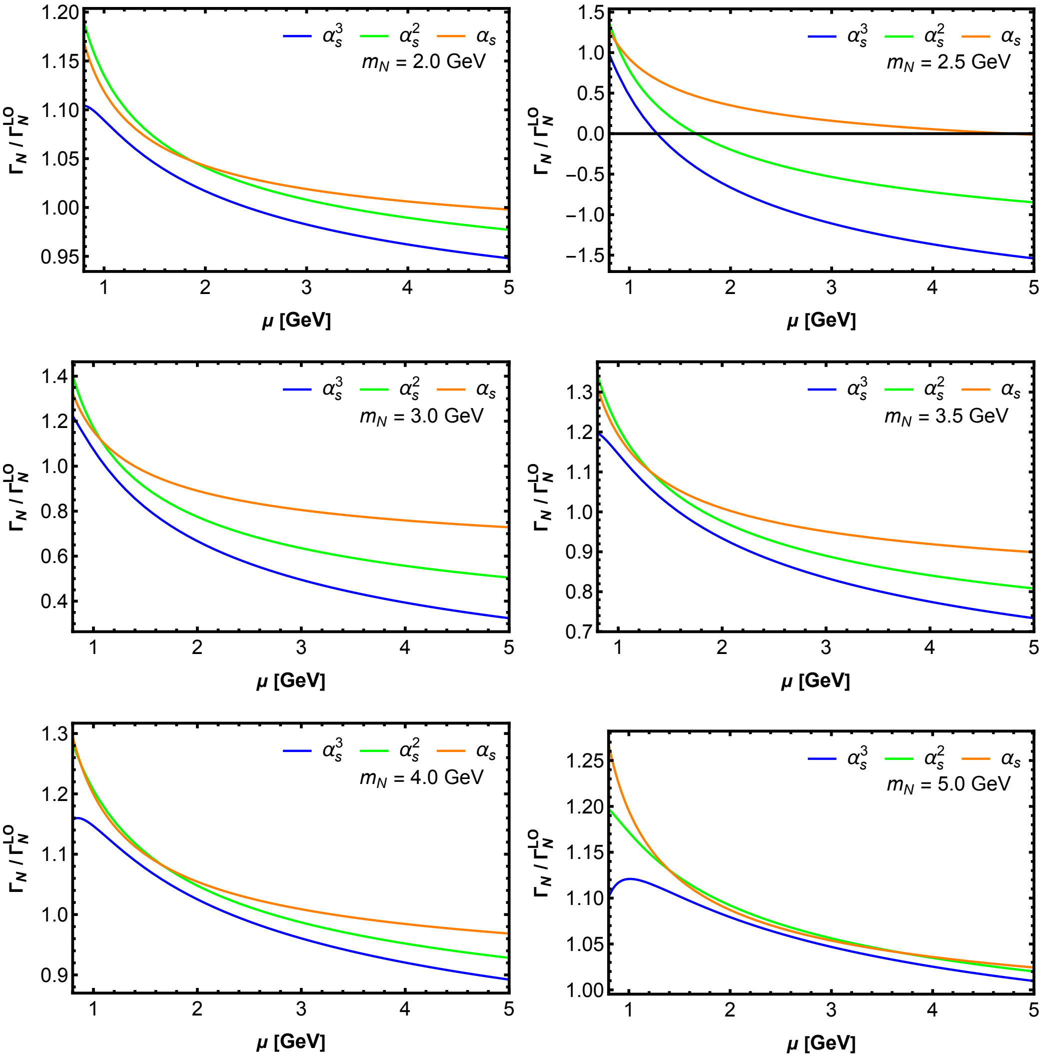

Figure 4.9.: Dependence of the inclusive HSN decay rate $\Gamma_N = \Gamma(N \to \mu X)$ on the renormalisation scale μ for different HSN masses above the charm production threshold.

function of the renormalisation scale μ. Since the quark mass corrections are only available up to $\mathcal{O}(\alpha_s^3)$ we expect poorer behaviour in comparison to the massless case. We let the quark mass run with respect to the renormalisation scale which further introduces a strong dependence on the renormalisation scale. For $\ell = \mu$ we observe for $m_N = 2.0$ GeV that the $\mathcal{O}(\alpha_s^3)$ correction seems to already lead to scale insensitivity. However, this cannot be trusted as in this mass range the decay rate is still very close to the D^+ and D_s^+ threshold and thus the non-perturbative region. For $m_N = 2.5$ GeV the decay rate exhibits a strong sensitivity to the renormalisation scale. Increasing the mass we see the sensitivity to the renormalisation scale decreases. At our mass limit obtained from the 50% criterion $m_N = 3.5$ GeV varying the renormalisation scale between $m_N/2$ and $2m_N$ increases or decreases the decay rate by about 21% and 15% indicating a well behaved perturbative description. This uncertainty further decreases for larger HSN masses. From Fig. 4.10 we see that

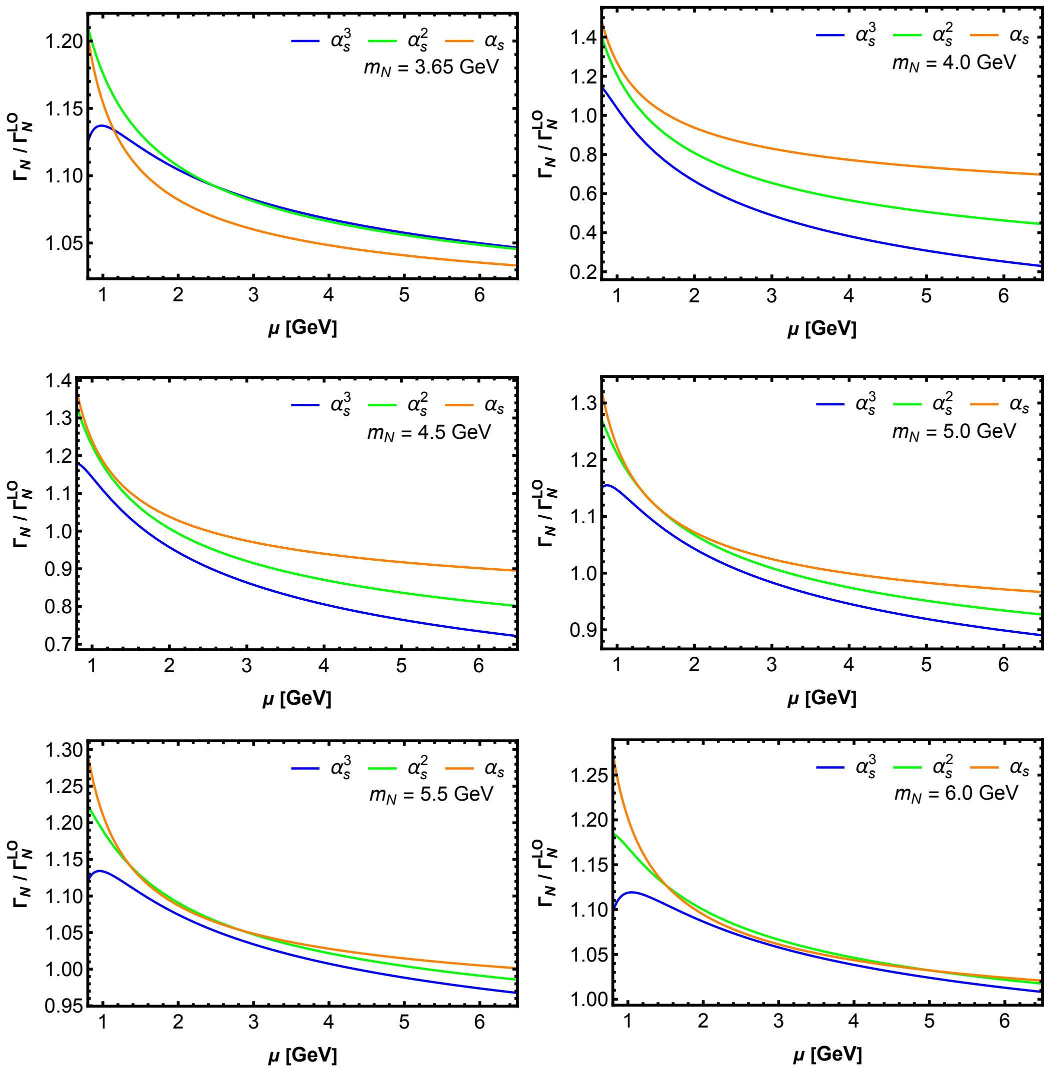

Figure 4.10.: Dependence of the inclusive HSN decay rate $\Gamma_N = \Gamma(N \to \tau X)$ on the renormalisation scale μ for different HSN masses above the charm production threshold.

qualitatively the $\ell = \tau$ case is similar: Near the D^+ threshold and below the D_s^+ threshold the $\mathcal{O}(\alpha_s^3)$ correction seems to lead to a renormalisation scale insensitive decay rate which is however misleading as this is a highly non-perturbative region. Closely above the D_s^+ threshold the decay rate is strongly sensitive to the renormalisation scale and becomes gradually more insensitive to it for larger HSN masses. Varying the renormalisation scale around $m_N = 4.6\,\text{GeV}$ between $m_N/2$ and $2m_N$ changes the decay rate by about 16% and 12%. Therefore we find a perturbative description of HSN decay is valid for the following HSN mass windows:

$$1.5\,\text{GeV} \lesssim m_N < m_{D^+} + m_\ell \quad \wedge \quad 3.5\,\text{GeV} \lesssim m_N \qquad \ell = e,\ \mu, \tag{4.11}$$

$$3.0\,\text{GeV} \lesssim m_N < m_{D^+} + m_\tau \quad \wedge \quad 4.6\,\text{GeV} \lesssim m_N \qquad \ell = \tau. \tag{4.12}$$

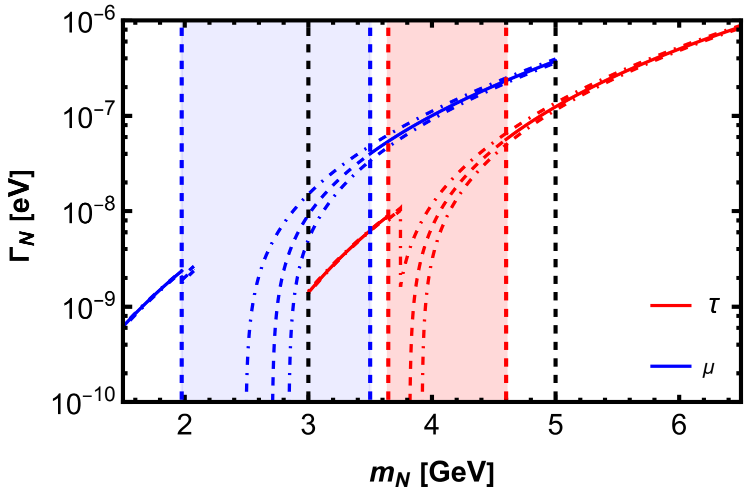

Figure 4.11.: Charged-current HSN decay rate for $\ell = \tau$ (red) and $\ell = \mu$ (blue), here the mixing angle is $|V_{N\ell}| = 10^{-3}$. The coloured regions are the $m_\tau + m_{D^+} \lesssim m_N \lesssim$ 4.6 GeV and $m_\mu + m_{D^+} \lesssim m_N \lesssim 3.5$ GeV mass regions in which a perturbative description of the HSN decay is not applicable. The dot-dashed lines mark the limits of the error band obtained by varying the renormalisation scale between $m_N/2$ (upper dot-dashed line) and $2m_N$ (lower dot-dashed line). The black vertical line at 3.0 GeV delimits the point above which the $\ell = \tau$ decay is perturbatively describable while the dashed black line at 5.0 GeV delimits the end of the $\ell = \mu$ decay rate that we show.

In Fig. 4.11 we show the charged-current decay rate for HSN masses that permit an accurate perturbative description. We added an error band that follows from varying the renormalisation scale between $m_N/2$ and $2m_N$. The larger the HSN mass the smaller this band becomes.

4.2.2. Neutral-Current Decay

In contrast to the charged-current HSN decay there is no equivalent SM process like τ decay for the neutral-current HSN decay to which we could compare it. However, the correlators of the charged- and neutral-current decays are up to the couplings, the mass dependence, and the singlet contributions the same for both decays. Hence we expect the numerical values of the coefficients in the perturbative series and the behaviour of the decay rate to be similar to the charged-current decay. Numerically for $n_f = 3$ flavours the decay rate reads

$$\begin{aligned}\Gamma(N \to \nu X) = N_c \frac{G_F^2 m_N^5 |V_{N\ell}|^2}{192\pi^3} \\ &\times \left[0.513 \cdot \left(1 + a_{m_N} + 5.202 a_{m_N}^2 + 26.265 a_{m_N}^3 + 124.695 a_{m_N}^4\right)\right. \\ &+ 0.006 \cdot \left(1 - 10.578 a_{m_N} - 102.833 a_{m_N}^2\right) \\ &\left. - 3.218 \cdot \frac{(m_s(m_N))^2}{m_N^2}\left(1 + 5.576 a_{m_N} + 49.860 a_{m_N}^2\right)\right]\end{aligned} \tag{4.13}$$

where again we only write the mass corrections in terms of the strange mass to emphasise this is $n_f = 3$. The third line gives the numerical values of the axial singlet contributions. As expected, the absolute values of the coefficients in front of the α_s presented here are comparable in size to the ones in the charged-current decay. In the second line the coefficients are even the same up to α_s^2 since up to this order, excluding the axial singlet contributions, charged- and neutral-current contributions are the same. Starting at $\mathcal{O}(\alpha_s^3)$ the vector singlet contributions appear (and formally also further axial singlet contributions which we neglect). However, these are small and only have a small impact on the decay rate. The quark mass corrections carry the opposite sign of the massless corrections and will reduce the size of the decay rate above the respective flavour threshold. At $n_f = 4$ flavours the decay rate reads

$$\begin{aligned}\Gamma(N \to \nu X) = N_c \frac{G_F^2 m_N^5 |V_{N\ell}|^2}{192\pi^3} \\ &\times \left[0.656 \cdot \left(1 + a_{m_N} + 4.823 a_{m_N}^2 + 19.562 a_{m_N}^3 + 57.876 a_{m_N}^4\right)\right. \\ &\left. - 2.721 \cdot \frac{(m_c(m_N))^2}{m_N^2}\left(1 + 5.804 a_{m_N} + 50.711 a_{m_N}^2\right)\right].\end{aligned} \tag{4.14}$$

Above the charm threshold the full SU(2) doublet is present and hence the axial singlet contribution vanishes.

In Fig. 4.12 we show the neutral-current decay rate below the charm production threshold. As in the charged-current case the convergence of the perturbative series is poor for small HSN masses. We deduce the mass range of HSN permitting a perturbative description by looking at how the decay rate scales with the renormalisation scale. In Fig. 4.13 we show the dependence of the decay rate on the renormalisation scale at different orders in the strong coupling constant. We find that an accurate perturbative description of neutral-current HSN decays is possible for HSN masses

$$1.5\,\text{GeV} \lesssim m_N \qquad \nu = \nu_e,\ \nu_\mu,\ \nu_\tau. \tag{4.15}$$

This is the same limit we found in the charged-current case for $\ell = e,\ \mu$ and aligns with our expectations because the masses of the electron and the muon are almost negligibly small in comparison to the HSN mass and thus the neutral-current decay producing a

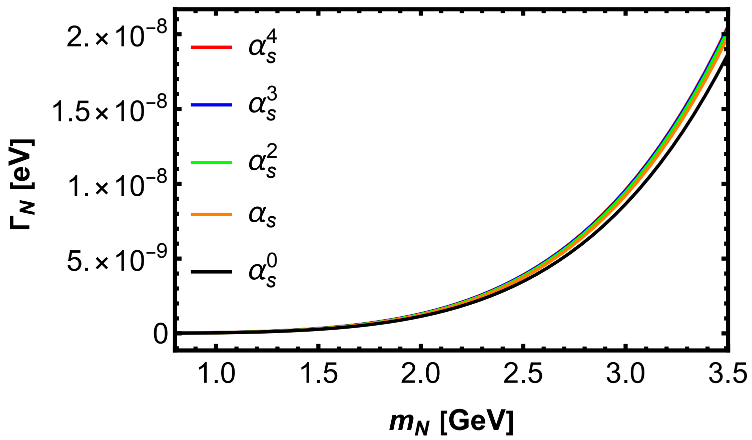

(a) Inclusive decay rate at different orders in α_s.

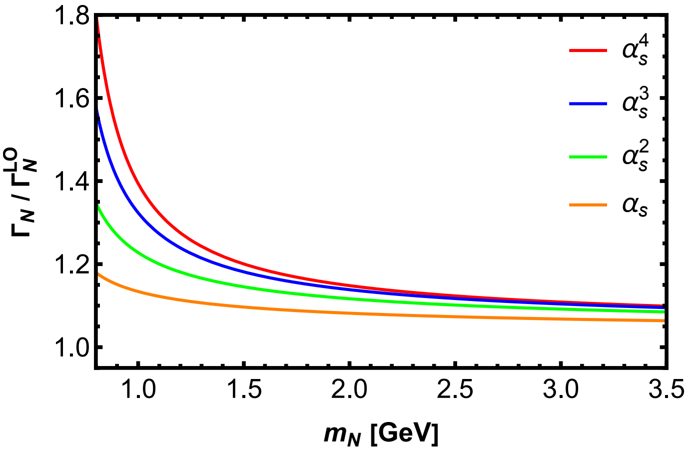

(b) Inclusive decay normalised to the LO.

Figure 4.12.: Decay rate $\Gamma_N = \Gamma(N \to \nu X)$. Here the mixing angle is $|V_{N\ell}| = 10^{-3}$.

SM neutrino instead of a charged lepton in the final state should not differ dramatically from the charged-current. Including the quark mass corrections we show the decay rate above the charm production threshold in Fig. 4.14. At the position of the charm threshold at $m_N = 2m_{D^0}$ there is a kink and the decay rate is reduced through the inclusion of the quark mass corrections. Both the neutral- and charged-current decay rate become smaller through the inclusion of the quark mass corrections. The effect is far stronger in the charged current case than in the neutral-current one. This is because the size of this kink scales with the size of the ratio m_c^2/m_N^2. Whereas in the charged-current case above the charm threshold the HSN mass had to satisfy $m_N \geq m_\ell + m_{D^+}$ in the neutral-current case it must satisfy $m_N \geq 2m_{D^0}$. Since $m_{D^+} \approx m_{D^0}$ we expect the relative size of the kink to be about a fourth of the charged-current decay ones (for $\ell = \mu$). Indeed this is what we observe in Fig. 4.8 where we see the height of the kink of the dot-dashed line is about a fourth of the blue one. Furthermore, we see that the 50% criterion is not a good criterion for the neutral current. To that end we sharpen the criterion to demanding $\delta_{\mathcal{R}}^{\mathrm{NC}} \leq 0.25$ which leads to the mass threshold $m_N \gtrsim 4.6\,\mathrm{GeV}$. In contrast to the charged-current case

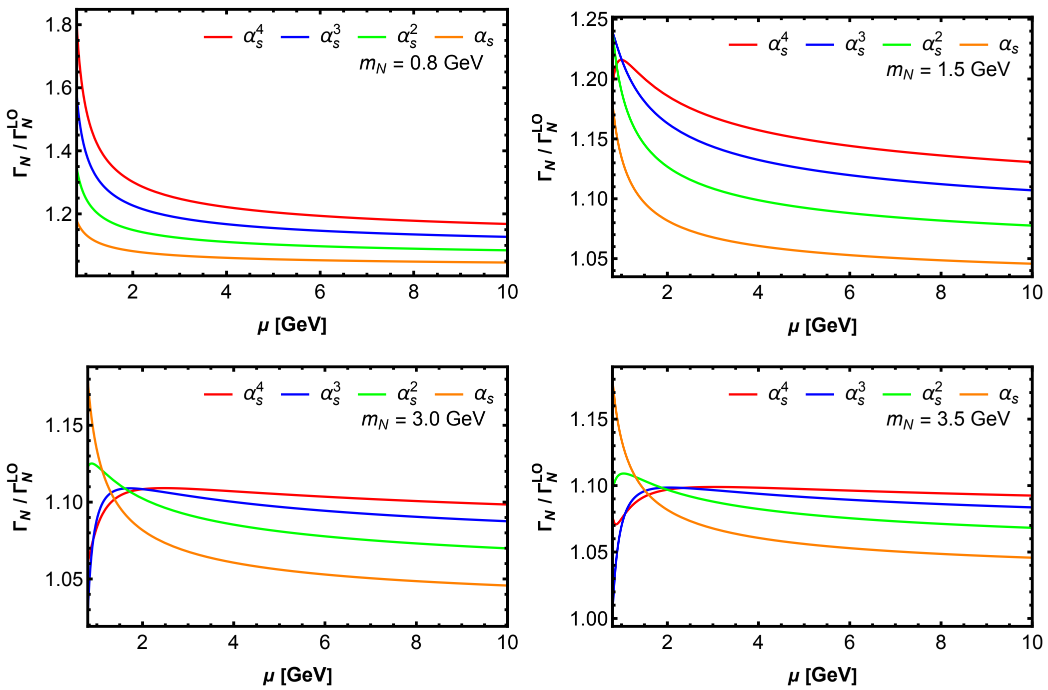

Figure 4.13.: Dependence of the inclusive HSN decay rate $\Gamma_N = \Gamma(N \to \nu X)$ on the renormalisation scale μ for different HSN masses below the charm production threshold.

we only have access to quark mass corrections up to $\mathcal{O}(\alpha_s^2)$. Despite this we see in Fig. 4.15 that the uncertainty induced by varying the renormalisation scale between $m_N/2$ and $2m_N$ for masses $m_N \gtrsim 4.6\,\text{GeV}$ is negligibly small (at the order of a few percent). Here we let the charm quark mass run with respect to the renormalisation scale as well. Therefore we can state that an accurate perturbative description of the neutral-current HSN decay is possible for HSN masses in the window

$$1.5\,\text{GeV} \lesssim m_N < 2m_{D^0} \quad \wedge \quad 4.6\,\text{GeV} \lesssim m_N \qquad \nu = \nu_e,\, \nu_\mu,\, \nu_\tau. \tag{4.16}$$

In Fig. 4.16 we show the inclusive neutral-current decay rate excluding the region of HSN masses that do not permit a perturbative description. We omitted showing the uncertainty coming from varying the renormalisation scale as it is negligibly small.

4.2.3. Total HSN Decay Rate and Branching Fractions

With the hadronic inclusive HSN decay rate calculated we are now in a position to calculate branching ratios. We allow the HSN to mix only with one SM neutrino e.g. $V_{N\tau}$ and set all other mixing angles to zero. The total decay rate then reads

$$\Gamma_N^{\text{tot.}} = \Gamma(N \to \ell X) + \Gamma(N \to \nu X) + \Gamma_N^{\text{lep.}}, \tag{4.17}$$

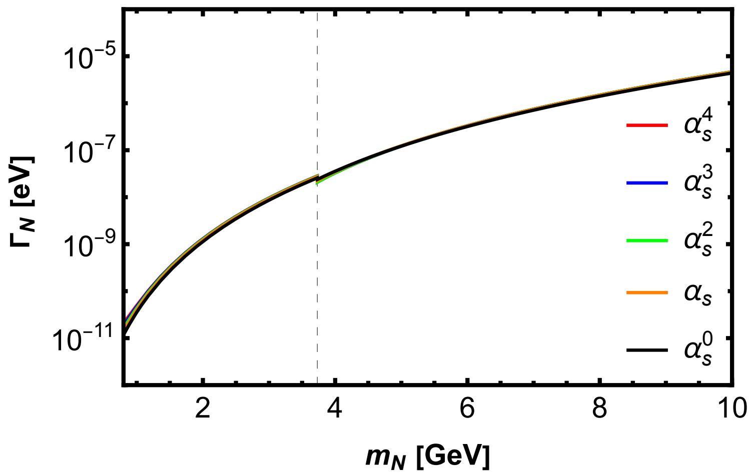

(a) Inclusive decay rate at different orders in α_s.

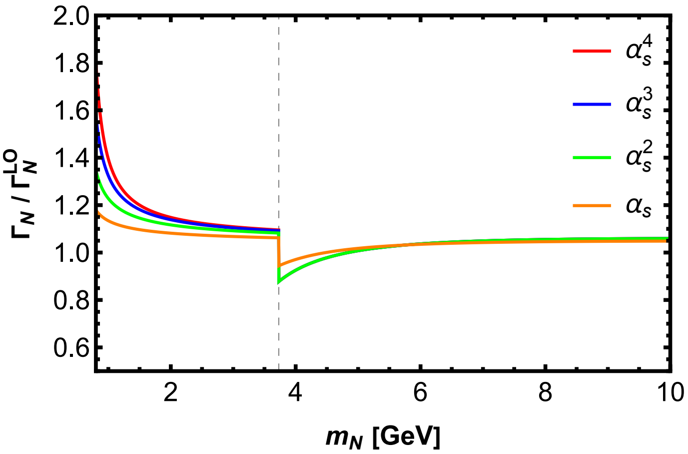

(b) Inclusive decay normalised to the LO.

Figure 4.14.: Decay rate $\Gamma_N = \Gamma(N \to \nu X)$. Here the mixing angle is $|V_{N\ell}| = 10^{-3}$. As before, beyond the charm threshold we omit the $\mathcal{O}(\alpha_s^3)$ and higher order corrections in the massless part of the decay rate, hence the red and blue curves are absent above the charm threshold.

where the leptonic HSN decay rate follows from Eqs. (3.2-3.6) as

$$\Gamma_N^{\text{lep.}} = \Gamma(N \to \nu_\ell \ell \bar{\ell}) + \Gamma(N \to \nu_\beta \nu_\beta \bar{\nu}_\beta) + \sum_{\ell \neq \beta} \Big[\Gamma(N \to \ell \bar{\ell}_\beta \nu_\beta) + \Gamma(N \to \nu_\ell \nu_\beta \bar{\nu}_\beta) \Big]. \tag{4.18}$$

The branching ratios into different final states f are then given by

$$\mathcal{BR}(N \to f) = \frac{\Gamma(N \to f)}{\Gamma_N^{\text{tot.}}}. \tag{4.19}$$

In Fig. 4.17 we show the charged- and neutral current as well as the leptonic decay rate for both $\ell = \mu$ and $\ell = \tau$. The coloured regions are the regions in which a perturbative

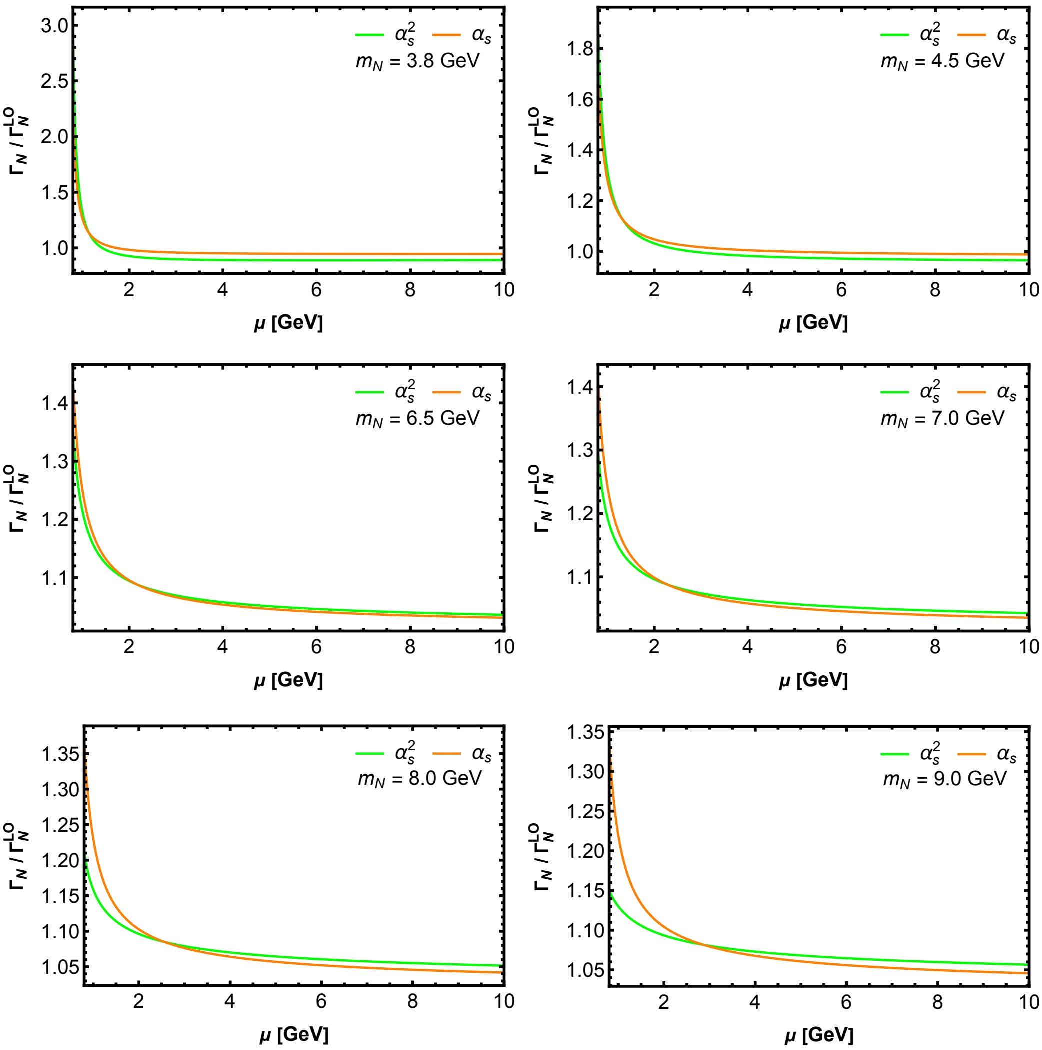

Figure 4.15.: Dependence of the inclusive HSN decay rate $\Gamma_N = \Gamma(N \to \nu X)$ on the renormalisation scale μ for different HSN masses above the charm production threshold.

calculation does not yield a sensible result. The calculation of a branching fraction requires both the charged- and neutral-current decay rate to be calculable at the same time. We can identify three mass windows that permit a perturbative description of both the charged- and neutral-current decay rate for $\ell = \mu$ and two windows for the $\ell = \tau$ case. These windows are

$$
\begin{aligned}
1.5\,\text{GeV} \lesssim m_N < m_{D^+} + m_\mu \quad &\wedge \quad 3.5\,\text{GeV} \lesssim m_N < 2m_{D^0} \\
&\wedge \quad 4.6\,\text{GeV} \lesssim m_N \lesssim 5.0\,\text{GeV} \qquad \ell = \mu, \qquad (4.20)\\
3.0\,\text{GeV} \lesssim m_N < m_{D^+} + m_\tau \quad &\wedge \quad 4.6\,\text{GeV} \lesssim m_N \lesssim 6.5\,\text{GeV} \qquad \ell = \tau. \qquad (4.21)
\end{aligned}
$$

Below $m_N < 3.0\,\text{GeV}$ the charged-current decay $N \to \tau X$ is no longer well behaved. However, for HSN with masses smaller than the tau mass $m_N < m_\tau$ the decay into final

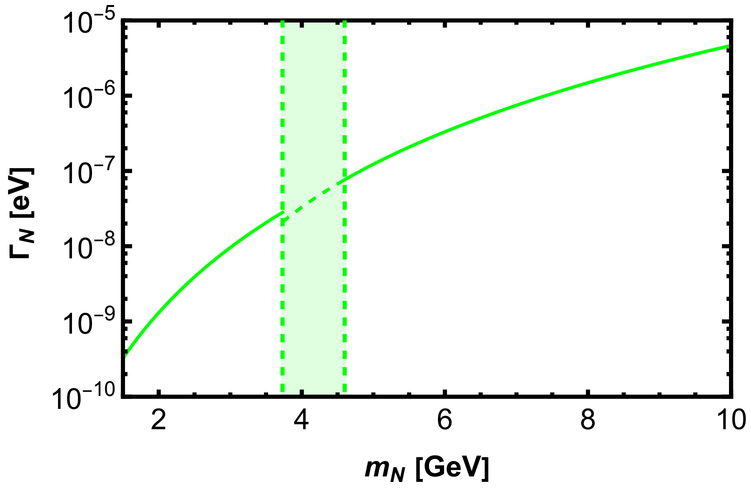

Figure 4.16.: Neutral-current HSN decay rate, here the mixing angle is $|V_{N\ell}| = 10^{-3}$. The coloured region is the $2m_{D^0} \lesssim m_N \lesssim 4.6\,\text{GeV}$ mass region in which a perturbative description of the HSN decay is not applicable.

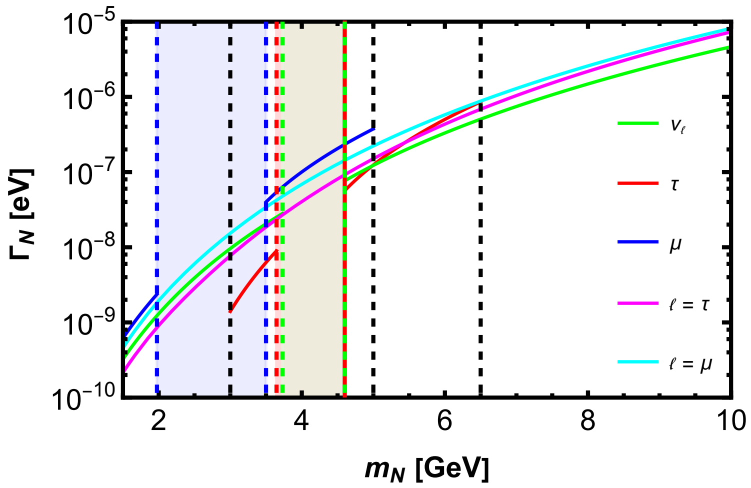

Figure 4.17.: The inclusive hadronic charged-current decay rate $\Gamma(N \to \tau X)$ (red) and $\Gamma(N \to \mu X)$ (blue) as well as the neutral-current HSN decay rate $\Gamma(N \to \nu X)$ (green) together with the leptonic HSN decay rates $\Gamma(N \to \tau \bar{\ell}_\beta \nu_\beta)$ (magenta) and $\Gamma(N \to \mu \bar{\ell}_\beta \nu_\beta)$ (cyan). The coloured regions mark the mass windows in which a perturbative description of the decay rate is not possible. Here the mixing angle is $|V_{N\ell}| = 10^{-3}$

states with τ is no longer possible, but this does not affect the neutral-current decays i.e. in the mass window

$$1.5\,\text{GeV} \lesssim m_N < m_\tau \qquad \ell = \tau, \tag{4.22}$$

it is possible again to calculate a branching fraction with the total decay rate being entirely comprised of the neutral-current and the leptonic decay rate. In Fig. 4.18 we show the branching ratios of the charged- and neutral-current as well as the leptonic contributions for both $\ell = \tau$ and $\ell = \mu$. In the $\ell = \tau$ case for small HSN masses the dominant contribution

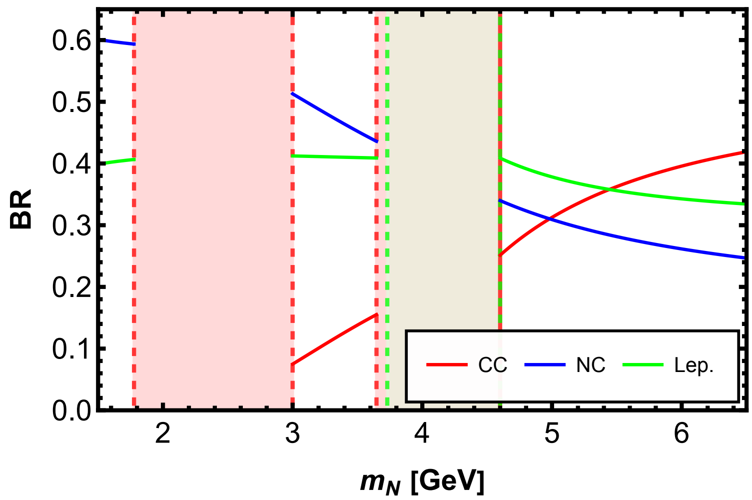

(a) $\ell = \tau$

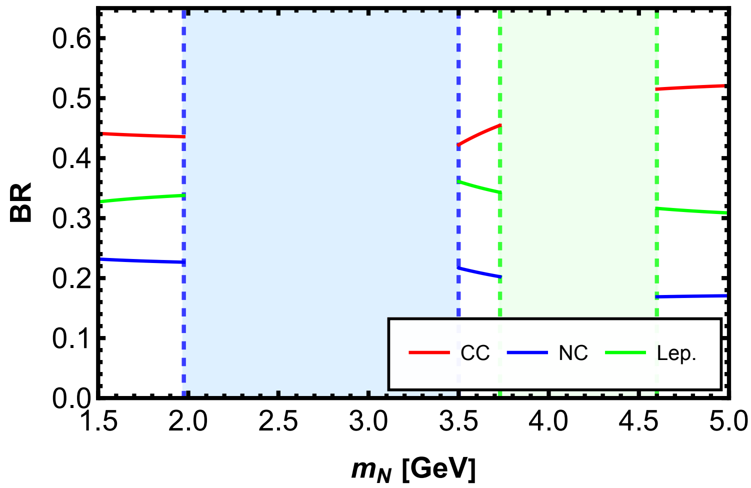

(b) $\ell = \mu$

Figure 4.18.: Here the branching fractions of the charged-current $\mathcal{BR}(N \longrightarrow \ell X)$ (red curve) and neutral-current $\mathcal{BR}(N \longrightarrow \nu_\ell X)$ (blue curve) as well as the leptonic decays $\mathcal{BR}(N \longrightarrow \text{lep.})$ (green curve) are shown for both $\ell = \tau$ and $\ell = \mu$. The red (blue) and green areas are the mass regions in which a perturbative HSN decay description is not reliable (see Eqs. (4.20) to (4.22)), with the red region being excluded due to the charged current for $\ell = \tau$ and the blue region for $\ell = \mu$. The green region is excluded by the neutral current.

is the neutral-current contribution due to the phase space suppression of the charged-current decay rate. Towards larger HSN masses the charged-current decay rate becomes the dominant contribution as expected from the SU(2) limit. Qualitatively this is the same in the $\ell = \mu$ case. However, since the muon is so much lighter than the tau we do not observe any phase space suppression and the charged-current decay is the dominant decay mode for all shown HSN masses. In the $\ell = \mu$ case the leptonic decays are always less abundant than the hadronic decays. This changes in the $\ell = \tau$ case where due to the phase space suppression there is a small mass window $4.6\,\text{GeV} \leq m_N \lesssim 5.5\,\text{GeV}$ where the leptonic decays are more abundant than the hadronic decays.

We may also calculate branching ratios into mesonic final states. The decay rate of an HSN into a scalar meson $P = \pi^+, K^+, D^+, D_s^+$ is given by [107]

$$\Gamma(N \to \ell P) = \frac{G_F^2 m_N^3 |V_{N\ell}|^2}{16\pi} |V_{u'd'}|^2 f_P^2 \left((1 - x_\ell^2)^2 - x_P^2 (1 + x_\ell^2) \right) \sqrt{\lambda(1, x_\ell^2, x_P^2)}, \tag{4.23}$$

where f_P is the respective meson decay constant and $x_i = m_i/m_N$. In Tab. 4.1 we state the values of the decay constants and meson masses that we use. We calculate the pion decay constant from the ratio f_{K^+}/f_{π^+} and the kaon decay constant. In Fig. 4.19 we show the branching ratios into the single meson final states $\mathcal{BR}(N \to \ell\pi^+)$ and $\mathcal{BR}(N \to \ell D_s^+)$ for both $\ell = \tau$ and $\ell = \mu$. We omit decays into kaons K^+ and D^+ mesons as their respective CKM matrix elements are small $|V_{us}|^2 \approx |V_{cd}|^2 \ll |V_{ud}|^2 \approx |V_{cs}|^2$ and hence their branching fractions are negligible in comparison to the pion and D_s meson branching fractions. In both the $\ell = \tau$ and $\ell = \mu$ case the decay into D_s^+ mesons is more common than into pions above the charm threshold. In the $\ell = \tau$ case the branching fraction into a pion or a D_s^+ meson is at the order of $\mathcal{O}(1\%)$. In the $\ell = \mu$ case they are generally a bit larger and below the charm threshold the decay into pions even makes up a sizeable contribution at $\mathcal{O}(8\%)$. These decays are mediated by the charged current. Comparing Figs. 4.19 and 4.18 we see that for $\ell = \tau$ the charged-current decay is only the dominant decay mode for $m_N \gtrsim 5.5\,\text{GeV}$. But even then the decay into a single pion or a D_s^+ meson is subdominant and accordingly decays into multi-hadron final states are dominant. In the $\ell = \mu$ case the charged-current contribution is always the dominant one with the decays into multi-hadron final states being the more common ones.

From the total decay rate we can calculate the proper lifetime of the HSN

$$\tau = \frac{\hbar}{\Gamma_N^{\text{tot.}}}, \tag{4.24}$$

as a function of the mass and the mixing angle. From the proper lifetime we can immediately calculate the proper decay length $c\tau$ of the particle which determines how likely it is to

Table 4.1.: The values of meson masses and decay constants used. The pion decay constant is calculated from the ratio f_{K^+}/f_{π^+} and the kaon decay constant f_{K^+}.

	value	source
m_{π^+}	139.570 39(18) MeV	PDG Online [8]
m_{K^+}	493.677(15) MeV	PDG Online [8]
m_{D^+}	1869.66(5) MeV	PDG Online [8]
$m_{D_s^+}$	1968.35(7) MeV	PDG Online [8]
f_{π^+}	130.5(3) MeV	
f_{K^+}	155.7(3) MeV	FLAG [134–138]
f_{K^+}/f_{π^+}	1.1934(19)	FLAG [134, 135, 137–140]
f_{D^+}	212.0(7) MeV	FLAG [135, 138, 139]
$f_{D_s^+}$	249.9(5) MeV	FLAG [135, 138, 139]

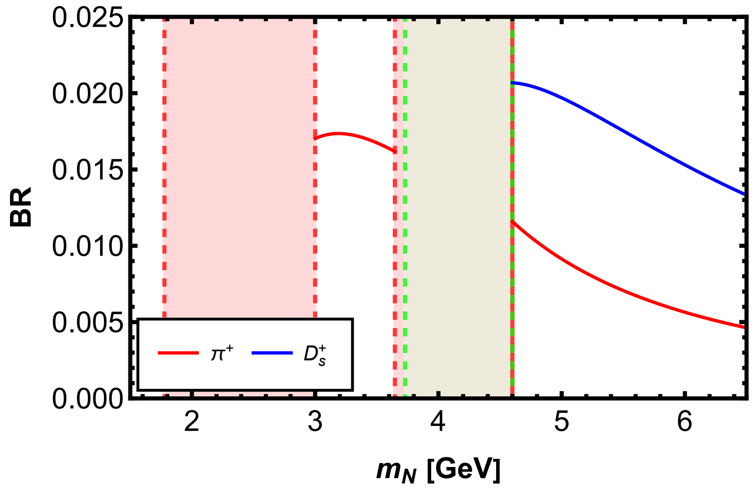

(a) $\ell = \tau$

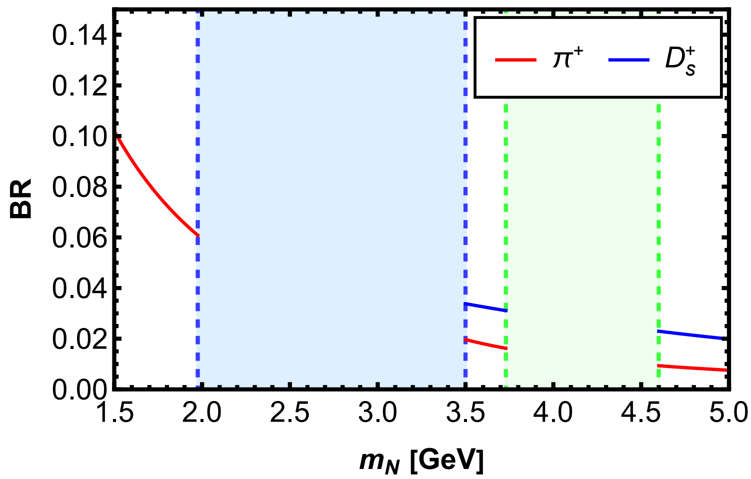

(b) $\ell = \mu$

Figure 4.19.: Branching fractions $\mathcal{BR}(N \longrightarrow \ell P)$ for $P = \pi^+$ mesons (red curve) and $P = D_s^+$ mesons (blue curve) for both $\ell = \tau$ and $\ell = \mu$. The coloured regions are the regions in which a perturbative description is not applicable. The red region is excluded by the charged current for $\ell = \tau$ and the blue region for $\ell = \mu$. The green region is excluded by the neutral current. We do not show the error band obtained from varying the renormalisation scale, because it is small and at most of order 10% (see Fig. 4.11).

decay after propagating a certain distance. This quantity is important for collider studies as it dictates whether the particle most likely decays inside or outside the detector. Short-lived particles only travel a short distance away from the interaction point after production and then decay i.e. the vertex of the decaying particle is close to the center of the detector where it was produced. The longer the lifetime of the particle the longer is its proper decay length. Long-lived particles travel further away from their production origin and may escape the detector without interacting at all. Such signatures can only be detected through missing energy and are rather difficult analyse as they require precise measurements of all other particles produced in the decay in order to reconstruct the momentum of the non interacting particle. The most prominent example of such a particle is a SM neutrino. Particles with lifetimes long enough to propagate away from the initial production point but short enough to still decay inside the detector yield a very interesting signature: a displaced decay vertex. After reconstructing a displaced vertex event one may see tracks appearing a certain distance away from the center of the detector where the decaying particle has been produced. Displaced vertex searches are a powerful way to search for new physics particles and are both experimentally clean, in the sense there is little background, and challenging to reconstruct. To that end we show the proper decay length in Fig. 4.20 for both $\ell = \mu$ and $\ell = \tau$ for different configurations $(m_N, |V_{N\tau}|)$ leading to a proper decay length below certain thresholds. The grey areas are the regions in which we cannot apply the perturbative calculation. The decay rates scale like $\Gamma \propto |V_{N\ell}|^2 m_N^5$. Therefore, smaller mixing angles decrease the decay rate and increase the lifetime. This effect is counteracted by increasing the HSN mass which enlarges the decay rate and thus reduces the proper lifetime. Between these two parameters there is always some configuration such that the proper decay length is below a given limit. Some of these mixing angles have already been excluded by experiments (see Fig. 4.26). We conclude this section by giving explicit values of the branching ratios at different masses as well as the proper lifetime $c\tau$ in Tabs. 4.2 and 4.3. The uncertainty associated to varying the renormalisation scale for the branching ratios and the proper lifetime is small and at most of order 10%.

Table 4.2.: Numerical values of the branching ratio and the proper lifetime for $\ell = \tau$ in the final state. The horizontal lines mark the the gaps where a reliable perturbative description is not possible (see Eq. (4.21) and (4.22)).

m_N [GeV]	$\mathcal{BR}(N \to \tau X)$ [%]	$\mathcal{BR}(N \to \nu_\tau X)$ [%]	$\mathcal{BR}(N \to \text{lep.})$ [%]	$c\tau \cdot \lvert V_{N\tau}\rvert^2$ [m]
1.50 GeV	0.0	60.1	39.9	$3.7 \cdot 10^{-4}$
1.75 GeV	0.0	59.4	40.6	$1.7 \cdot 10^{-4}$
3.00 GeV	7.5	51.3	41.2	$1.1 \cdot 10^{-5}$
3.25 GeV	10.7	48.2	41.1	$6.7 \cdot 10^{-6}$
3.50 GeV	13.8	45.2	40.9	$4.3 \cdot 10^{-6}$
4.60 GeV	25.1	34.0	40.9	$8.8 \cdot 10^{-7}$
4.75 GeV	27.7	32.7	39.5	$7.0 \cdot 10^{-7}$
5.00 GeV	31.3	30.9	37.8	$5.0 \cdot 10^{-7}$
5.25 GeV	34.0	29.4	36.6	$3.6 \cdot 10^{-7}$
5.50 GeV	36.3	28.1	35.6	$2.7 \cdot 10^{-7}$
5.75 GeV	38.1	27.1	34.9	$2.0 \cdot 10^{-7}$
6.00 GeV	39.6	26.2	34.3	$1.6 \cdot 10^{-7}$
6.25 GeV	40.8	25.4	33.8	$1.2 \cdot 10^{-7}$
6.50 GeV	41.9	24.7	33.4	$9.6 \cdot 10^{-8}$

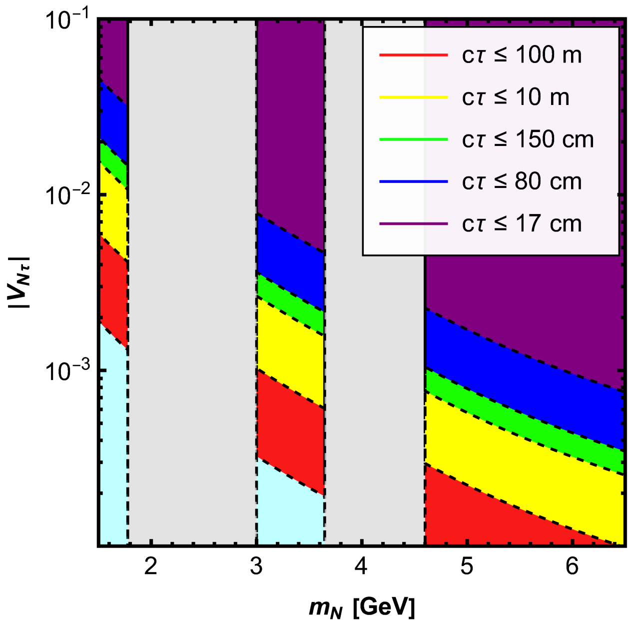

(a) $\ell = \tau$

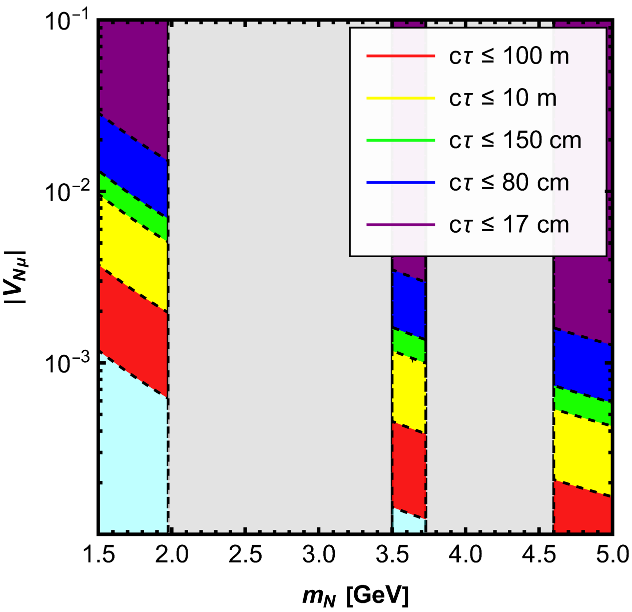

(b) $\ell = \mu$

Figure 4.20.: Proper decay length of an HSN decaying into a $\ell = \tau$ or $\ell = \mu$ final state. The proper decay length values are chosen to permit typical displaced vertex searches [141–143]. In the grey regions a perturbative description of the decay rate is not possible. The light blue region denotes proper decay lengths $c\tau > 100$ m.

4.3. Application to τ Decay

This section and parts of the subsequent discussion of it are based on Ref. [126].

4.3.1. Constraints from the τ lifetime

We can apply our HSN decay calculation to also study hadronic τ decays. For τ decays we can study two different scenarios: (1) the sterile neutrino is lighter than the τ lepton $m_N < m_\tau$. In this scenario the sterile neutrino can be produced in decays like $\tau \to N\ell\bar{\nu}_\ell$. This decay is a different final state than the SM decay and hence there is no interference between these decays. The τ decay rate is then an incoherent sum of the SM and the BSM decay mode. Furthermore, in this case we need to include the cosine of the mixing angle attached to the SM neutrinos. The other scenario is (2) the sterile neutrino is heavier than the τ lepton $m_N > m_\tau$. In this scenario the τ gets a contribution from the sterile neutrino only through the cosine of the mixing angle attached to the SM neutrino.[1] Currently the world average of the τ-lifetime is

$$\tau_\tau^{\text{exp.}} = 290.29 \pm 0.53\,\text{fs} \quad [144] \tag{4.25}$$

and is in agreement with the SM theory prediction

$$\tau_\tau^{\text{SM}} = 288.59 \pm 2.31\,\text{fs} \quad [8, 145]. \tag{4.26}$$

We can constrain the size of the mixing angle $|V_{N\tau}| = |\sin\theta_{N\tau}| = |\sin\theta|$ using the experimentally measured lifetime. The experiment cannot detect the escaping SM neutrino.

[1] To further distinguish the two scenarios we only use the term 'Heavy Sterile Neutrino' (HSN) whenever the sterile neutrino is $m_N \gtrsim m_\tau$. In the case where it is lighter we simply refer to it as a sterile neutrino.

Table 4.3.: Numerical values of the branching ratio and the proper lifetime for $\ell = \mu$ in the final state. The horizontal lines mark the the gaps where a perturbative description is not possible (see Eq. (4.20))

m_N [GeV]	$\mathcal{BR}(N \to \mu X)$ [%]	$\mathcal{BR}(N \to \nu_\mu X)$ [%]	$\mathcal{BR}(N \to \text{lep.})$ [%]	$c\tau \cdot \lvert V_{N\mu}\rvert^2$ [m]
1.50 GeV	44.1	23.2	32.7	$1.4 \cdot 10^{-4}$
1.60 GeV	44.0	23.0	33.0	$1.0 \cdot 10^{-4}$
1.70 GeV	43.8	22.9	33.3	$7.6 \cdot 10^{-5}$
1.80 GeV	43.7	22.8	33.5	$5.7 \cdot 10^{-5}$
1.90 GeV	43.6	22.7	33.6	$4.4 \cdot 10^{-5}$
3.50 GeV	42.2	21.7	36.1	$2.1 \cdot 10^{-6}$
3.60 GeV	43.8	21.0	35.2	$1.8 \cdot 10^{-6}$
3.70 GeV	45.1	20.4	34.5	$1.5 \cdot 10^{-6}$
4.60 GeV	51.5	16.9	31.6	$4.4 \cdot 10^{-7}$
4.70 GeV	51.7	16.9	31.4	$3.9 \cdot 10^{-7}$
4.80 GeV	51.8	17.0	31.2	$3.4 \cdot 10^{-7}$
4.90 GeV	52.0	17.0	31.0	$3.1 \cdot 10^{-7}$
5.00 GeV	52.1	17.1	30.9	$2.7 \cdot 10^{-7}$

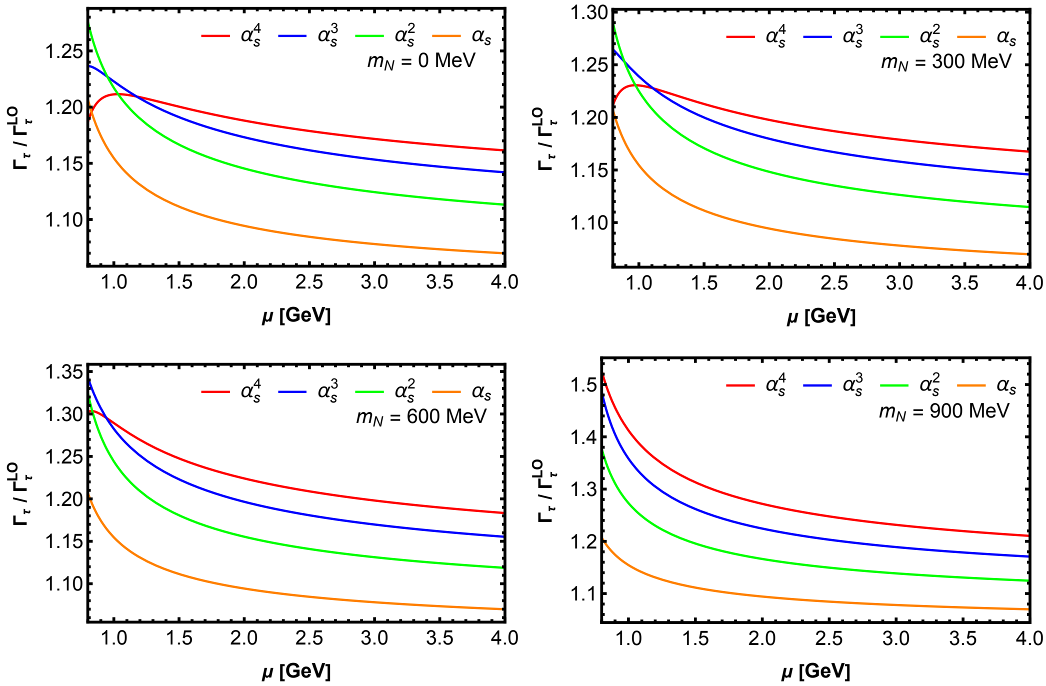

Figure 4.21.: Dependence of the inclusive τ decay rate into a sterile neutrino $\Gamma(\tau \to NX)$ on the renormalisation scale μ for different sterile neutrino masses.

Similarly, if a sterile neutrino is also produced in τ decays then it too would escape undetected like the SM neutrino. However, the sterile neutrino needs to be included in the theory prediction of the lifetime. In this way we can constrain the mixing angle through

$$\tau_\tau^{\text{exp.}} = \frac{1 - \mathcal{B}_\tau^s}{\cos^2\theta\,(1 - \mathcal{B}_\tau^s)\Gamma_\tau^{\text{SM}} + \sin^2\theta\,\Gamma_\tau^N}, \tag{4.27}$$

where Γ_τ^N is the non-strange sterile neutrino contribution to τ decay, i.e. the $\tau \to NX$ decay rate where X is a non-strange hadronic final state, $(1 - \mathcal{B}_\tau^s)\Gamma_\tau^{\text{SM}}$ is the SM width involving leptonic and non-strange hadronic decays, and $\mathcal{B}_\tau^s = 0.0292$ [8] is the branching fraction of τ decays into strange final states. Here we follow the approach of Ref. [8]. In the limit of a vanishing sterile neutrino mass we return to the SM case. While for most cases it is sufficient to neglect the factor $\cos\theta$ in this case it is important to include it. An omission of it would lead to the $m_N \to 0$ limit not reproducing the SM as it should. We calculate the SM decay rate using Eq. (4.26) as $\Gamma_\tau^{\text{SM}} = \hbar/\tau_\tau^{\text{SM}}$. The sterile neutrino decay rate follows from the leptonic decay rate Eq. (3.2) and the charged-current decay rate Eq. (3.9) with the appropriate replacements: $m_N \to m_\tau$, $V_{N\ell} \to 1$, $V_{us} \to 0$, and $x_\ell \to x_N = m_N/m_\tau$. By looking at the dependence on the renormalisation scale of the $\tau \to NX$ decay rate in Fig. 4.21 we can identify the sterile neutrino mass region permitting a well-behaved perturbative description of τ decays (we omit strange mass corrections here). Up to sterile neutrino masses of around 600 MeV the $\mathcal{O}(\alpha_s^4)$ corrections lead to a τ decay rate that remains insensitive to the renormalisation scale. Larger sterile neutrino masses lead to a stronger scale dependence. From this we conclude that a perturbative description of

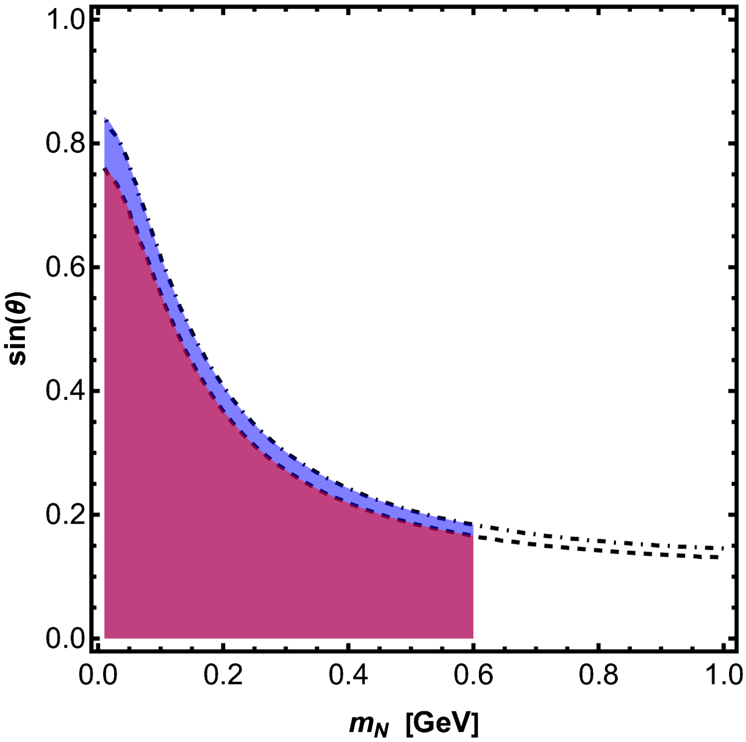

Figure 4.22.: Allowed parameter space in m_N and $\sin\theta$ in agreement with the experimentally measured τ lifetime. The purple region corresponds to the 1σ region and the blue region corresponds to the 3σ region. In the blue region we only varied the experimental value by 3σ. The dashed and dot-dashed lines extend the perturbative result into the region $m_N > 600\,\text{MeV}$ where a reliable perturbative description is no longer possible.

hadronic τ decays into a sterile neutrino requires

$$m_N \lesssim 600\,\text{MeV} \qquad \text{for } \tau \longrightarrow NX. \tag{4.28}$$

Using Eq. (4.27) and neglecting electroweak corrections in Γ_τ^N we can find the parameter space in m_N and $\sin\theta$ consistent with the experimental measurement of the τ lifetime. Fig. 4.22 shows the allowed parameter space. The purple region corresponds to varying the experimental τ lifetime by 1σ and the blue one to varying it by 3σ. In the latter case we do not triple the theoretical uncertainty. We extend the dotted and dot-dashed lines above $m_N = 600\,\text{MeV}$ for illustration only. Above $m_N = 600\,\text{MeV}$ the perturbative calculation is no longer reliable.

We may also employ Eq. (4.27) in the case $m_N > m_\tau$. In this scenario $\Gamma_\tau^N = 0$ and the only effect of the HSN is through the cosine of the mixing angle. We find

$$\sin^2\theta = 1 - \frac{\tau_\tau^{\text{SM}}}{\tau_\tau^{\text{exp.}}} = 0.00586 \pm 0.00816, \tag{4.29}$$

which leads to the sine of the mixing angle at the 1σ level

$$|\sin\theta| \leq 11.8 \cdot 10^{-2} \quad \text{at } 1\sigma. \tag{4.30}$$

4.3.2. Constraints from Leptonic and Semi-Hadronic τ Decays for $m_N > m_\tau$

In the scenario where the sterile neutrino is heavier than the τ lepton we can also study the leptonic decays $\tau \to \nu_\tau \ell \bar{\nu}_\ell$ with $\ell = e, \mu$ and the semi-hadronic decays $\tau \to \nu_\tau \pi^-$ and $\tau \to \nu_\tau K^-$ [113, 146]. In this way we can circumvent the uncertainty associated with the hadronic width in Eq. (4.26). The leptonic and semi-hadronic decay rates are well known and read

$$\begin{aligned}\Gamma(\tau \to \nu_\tau P) =& \cos^2\theta \Gamma_{\text{SM}}(\tau \to \nu_\tau P)\\ =& \frac{G_F^2 m_\tau^3 \cos^2\theta}{16\pi} |V_{uq}|^2 f_P^2 \left(1 - \frac{m_P^2}{m_\tau^2}\right)^2 \left(1 + \delta_{\text{RC}}^{(P)}\right),\end{aligned} \tag{4.31}$$

$$\begin{aligned}\Gamma(\tau \to \nu_\tau \ell \bar{\nu}_\ell) =& \cos^2\theta \Gamma_{\text{SM}}(\tau \to \nu_\tau \ell \bar{\nu}_\ell) = \frac{G_F^2 m_\tau^5 \cos^2\theta}{192\pi^3}\\ &\times \left[\left(1 - 8x_\ell^2 + 8x_\ell^6 - x_\ell^8 - 12x_\ell^4 \ln(x_\ell^2)\right) + \frac{\alpha(m_\tau)}{\pi} H_1 + \frac{\alpha^2(m_\tau)}{\pi^2} H_2\right],\end{aligned} \tag{4.32}$$

here $x_\ell = m_\ell / m_\tau$, $P = K^-, \pi^-$ is a pseudoscalar meson and f_P is the respective meson decay constant, V_{uq} is the associated CKM matrix element, and α is the QED coupling constant. As before, we added a factor $\cos\theta$ to account for the effect of the HSN. The $\delta_{\text{RC}}^{(P)}$ are the radiative QED corrections controlled by the QED coupling constant $\alpha(m_\tau)$ and we use the values $\delta_{\text{RC}}^{(\pi)} = 0.0194 \pm 0.0061$ and $\delta_{\text{RC}}^{(K)} = 0.0204 \pm 0.0062$ presented in Ref. [147] which are based on Refs. [148–151]. The H_i functions comprise the radiative QED corrections for leptonic decays and are given by [152–156]

$$H_1 = \left(\frac{25}{8} - \frac{\pi^2}{2}\right) - (34 + 24\ln x_\ell) x_\ell^2 + 16\pi^2 x_\ell^3 + O(x_\ell^4), \tag{4.33}$$

$$\begin{aligned}H_2 =& \frac{156815}{5184} - \frac{518}{81}\pi^2 - \frac{895}{36}\zeta_3 + \frac{67}{720}\pi^4 + \frac{53}{6}\pi^2 \ln 2\\ &- (0.042 \pm 0.002) - \frac{5}{4}\pi^2 x_\ell + O(x_\ell^2).\end{aligned} \tag{4.34}$$

Now we can use the experimentally measured τ lifetime given in Eq. (4.25) and the experimentally measured branching fractions given in Tab. 4.4 together with the theoretically calculated decay widths to constrain the mixing angle. For the leptonic decays the following

Table 4.4.: Table of the experimentally measured branching ratios as well as the value of the QED coupling constant that we use.

$\mathcal{BR}^{\text{exp.}}(\tau \to \nu_\tau e \bar{\nu}_e)$	$0.1785(4)$	HFLAV [144]
$\mathcal{BR}^{\text{exp.}}(\tau \to \nu_\tau \mu \bar{\nu}_\mu)$	$0.17366(36)$	HFLAV [144]
$\mathcal{BR}^{\text{exp.}}(\tau \to \nu_\tau \pi)$	$0.1082(5)$	HFLAV [144]
$\mathcal{BR}^{\text{exp.}}(\tau \to \nu_\tau K)$	$0.00697(10)$	HFLAV [144]
$1/\alpha(m_\tau)$	$133.50(2)$	[157, 158]

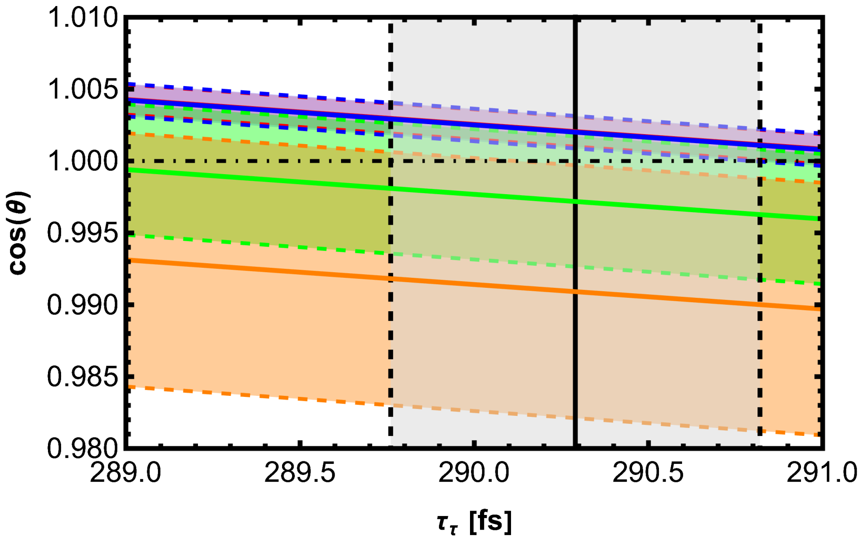

Figure 4.23.: The 1σ bands of the values of the cosines in agreement with the measurements of the τ decay as a function of the τ lifetime. Central values are indicated by the solid lines whereas the dashed lines mark the borders of the 1σ band. The leptonic decays $\tau \longrightarrow \nu_\tau e \bar{\nu}_e$ (blue) and $\tau \longrightarrow \nu_\tau \mu \bar{\nu}_\mu$ (red) prefer unphysical values of the mixing angle whereas the the semi-hadronic decays $\tau \longrightarrow \nu_\tau \pi$ (green) and $\tau \longrightarrow \nu_\tau K$ (orange) allow for physical values of the mixing angle. The experimentally measured τ lifetime is given by the grey band. The area below the horizontal dot-dashed line at $\cos\theta = 1$ is the physical region.

mixing angles are in agreement with the experimental measurements

$$\left(\frac{\mathcal{BR}^{\text{exp.}}(\tau \longrightarrow \nu_\tau e \bar{\nu}_e)}{\tau_\tau^{\text{exp.}}} \cdot \frac{1}{\Gamma_{\text{SM}}(\tau \longrightarrow \nu_\tau e \bar{\nu}_e))}\right)^{1/2} = \cos\theta = 1.00201 \pm 0.00145 \tag{4.35}$$

$$\left(\frac{\mathcal{BR}^{\text{exp.}}(\tau \longrightarrow \nu_\tau \mu \bar{\nu}_\mu)}{\tau_\tau^{\text{exp.}}} \cdot \frac{1}{\Gamma_{\text{SM}}(\tau \longrightarrow \nu_\tau \mu \bar{\nu}_\mu))}\right)^{1/2} = \cos\theta = 1.00205 \pm 0.00139 \tag{4.36}$$

while the semi-hadronic decays permit the mixing angles

$$\left(\frac{\mathcal{BR}^{\text{exp.}}(\tau \longrightarrow \nu_\tau \pi)}{\tau_\tau^{\text{exp.}}} \cdot \frac{1}{\Gamma_{\text{SM}}(\tau \longrightarrow \nu_\tau \pi)}\right)^{1/2} = \cos\theta = 0.99717 \pm 0.00462 \tag{4.37}$$

$$\left(\frac{\mathcal{BR}^{\text{exp.}}(\tau \longrightarrow \nu_\tau K)}{\tau_\tau^{\text{exp.}}} \cdot \frac{1}{\Gamma_{\text{SM}}(\tau \longrightarrow \nu_\tau K))}\right)^{1/2} = \cos\theta = 0.99091 \pm 0.00884. \tag{4.38}$$

We roughly estimated the uncertainties by assuming they are distributed Gaussian and are all uncorrelated.

We see that the leptonic decays yield unphysical mixing angles $\cos\theta > 1$ at the 1σ level. In contrast, the semi-hadronic decays permit physical mixing angles $\cos\theta < 1$ at the 1σ level. Fig. 4.23 shows the corresponding 1σ bands of the cosines of each of the four decays studied here as a function of the τ lifetime. At the 1σ level we find the constraint on the mixing angle from the decay $\tau \longrightarrow \nu_\tau \pi$

$$\tau \longrightarrow \nu_\tau \pi : \qquad |\sin\theta| \leq 12.2 \cdot 10^{-2} \quad \text{at } 1\sigma, \tag{4.39}$$

and the decay into a kaon $\tau \longrightarrow \nu_\tau K$ leads to

$$\tau \longrightarrow \nu_\tau K : \qquad |\sin\theta| = \left(13.5^{+5.4}_{-11.3}\right) \cdot 10^{-2} \quad \text{at } 1\sigma. \tag{4.40}$$

The weighted average of both leptonic decays yields $\cos\theta = 1.00203 \pm 0.00100$ and permits a physical value of the cosine of the mixing angle $\cos\theta \geq 0.99901$ at the 3σ level. This leads to the mixing angle

$$\tau \longrightarrow \nu_\tau \ell \bar{\nu}_\ell \quad \ell = e, \mu \text{ combined} : \qquad |\sin\theta| \leq 4.4 \cdot 10^{-2} \quad \text{at } 3\sigma. \tag{4.41}$$

The combination of the semi-hadronic decays yields $\cos\theta = 0.99582 \pm 0.00410$, which corresponds to the mixing angle

$$\tau \longrightarrow \nu_\tau P, \quad P = \pi, K \text{ combined} : \qquad |\sin\theta| = \left(9.1^{+3.7}_{-7.8}\right) \cdot 10^{-2} \quad \text{at } 1\sigma. \tag{4.42}$$

Combining both the leptonic and semi-hadronic decays the cosine of the mixing angle reads $\cos\theta = 1.00168 \pm 0.00098$ and permits a physical value $\cos\theta \geq 0.99973$ at the 2σ level. This translates to the constraint on the mixing angle

$$\text{leptonic and semi-hadronic combined:} \qquad |\sin\theta| \leq 2.3 \cdot 10^{-2} \quad \text{at } 2\sigma. \tag{4.43}$$

4.3.3. Sterile Neutrinos in Spectra for $m_N < m_\tau$

The detection of light sterile neutrinos in branching ratios of τ decays is very difficult because

$$\Gamma(\tau \longrightarrow \nu_\tau Y) + \Gamma(\tau \longrightarrow NY) = \Gamma_{\text{SM}}(\tau \longrightarrow \nu_\tau Y) + \mathcal{O}\left(\frac{m_N^2}{m_\tau^2} \cdot \sin^2\theta\right), \tag{4.44}$$

where Y denotes any possible final state and for $m_N < m_\tau$. The sterile neutrino may escape the detector similar to a SM neutrino (see Fig. 4.20). However, the non-zero mass of the sterile neutrino leaves an impact on the kinematics of the remaining particles in the decay. Therefore, one may consider precise measurements of the charged lepton energy spectrum

$$\frac{d\Gamma(\tau \longrightarrow \nu \ell \bar{\nu}_\ell)}{dE_\ell} = \frac{G_F^2 m_\tau^4 V_\nu^2}{2\pi^3} F(x_E, x_\ell, x_\nu), \tag{4.45}$$

with $\nu = \nu_\tau, N$ either being a SM or a sterile neutrino, $x_E = E_\ell / m_\tau$, $x_i = m_i / m_\tau$, $V_\nu = \cos\theta$ for SM neutrinos and $V_\nu = \sin\theta$ for sterile neutrinos, and

$$\begin{aligned} F(x_E, x_\ell, x_\nu) = {} & \frac{\sqrt{x_E^2 - x_\ell^2}\left(1 - 2x_E + x_\ell^2 - x_\nu^2\right)^2}{6\left(1 - 2x_E + x_\ell^2\right)^3} \\ & \times \Big[8x_E^3 - 2x_E^2(5 + 5x_\ell^2 + x_\nu^2) \\ & \qquad + x_E(3 + 10x_\ell^2 + 3x_\ell^4 + 3x_\nu^2(1 + x_\ell^2)) - 2x_\ell^2(1 + x_\ell^2 + 2x_\nu^2) \Big]. \end{aligned} \tag{4.46}$$

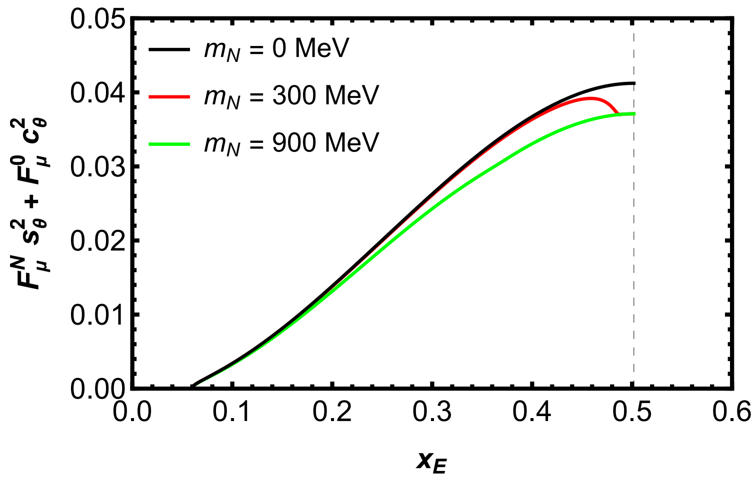

Figure 4.24.: Sum of the F functions $F_\mu^N s_\theta^2 + F_\mu^0 c_\theta^2 = F(E_\mu/m_\tau, x_\mu, x_N)\sin^2\theta + F(E_\mu/m_\tau, x_\mu, 0)\cos^2\theta$. Here $\ell = \mu$ and we use the mixing angle $\sin\theta = 0.32$. The black line belongs to the SM case ($m_N = 0$) whereas the coloured lines show the effect of a non-zero sterile neutrino.

The experiment does not directly detect the neutrino and is therefore blind to whether a SM or a sterile neutrino is produced. Therefore the measured lepton energy spectrum is given by the sum of the two

$$\begin{aligned}\frac{d\Gamma_{\text{lep}}^{\text{exp.}}}{dE_\ell} =& \frac{d\Gamma(\tau \to \nu_\tau \ell \bar{\nu}_\ell)}{dE_\ell} + \frac{d\Gamma(\tau \to N \ell \bar{\nu}_\ell)}{dE_\ell} \\ =& \frac{G_F^2 m_\tau^4 V_\nu^2}{2\pi^3}\Big[F(x_E, x_\ell, x_N)\sin^2\theta + F(x_E, x_\ell, 0)\cos^2\theta\Big].\end{aligned} \tag{4.47}$$

In Fig 4.24 we show $F(E_\mu/m_\tau, x_\mu, x_N)\sin^2\theta + F(E_\mu/m_\tau, x_\mu, 0)\cos^2\theta$ (i.e. $\ell = \mu$) as a function of x_E. The effect of the sterile neutrino is small. At $m_N = 300\,\text{MeV}$ the spectrum almost entirely overlaps with the SM spectrum. Deviations from the SM spectrum are strongest towards the end of the spectrum. In contrast, the larger the mass of the sterile neutrino is the stronger the spectrum deviates from the SM spectrum even for smaller x_E.

Similarly, the hadronic energy spectrum can be derived in an analogous way and reads

$$\frac{d\Gamma(\tau \to \nu X)}{ds} = N_c \frac{G_F^2 m_\tau^3 V_\nu^2 \cdot 2(|V_{ud}|^2 + |V_{us}|^2)}{192\pi^3} S(m_\tau, m_Z) G\big(x, x_\nu\big), \tag{4.48}$$

here electroweak corrections are accounted for in the factor $S(m_\tau, m_Z) = 1.01907$ [158, 159], $x = s/m_\tau^2$, $x_\nu = m_\nu/m_\tau$, and

$$\begin{aligned}G\big(x, x_\nu\big) =& \Big[\Big(1 + x_\nu^2 - x\Big)\Big(1 + 2x + x_\nu^2\Big) - 4x_\nu^2\Big] \\ & \times \sqrt{\lambda\big(1, x, x_\nu^2\big)} \cdot 12\pi \text{Im}\,\hat{\Pi}_{ij,V}^{1+0}(m_\tau^2 x),\end{aligned} \tag{4.49}$$

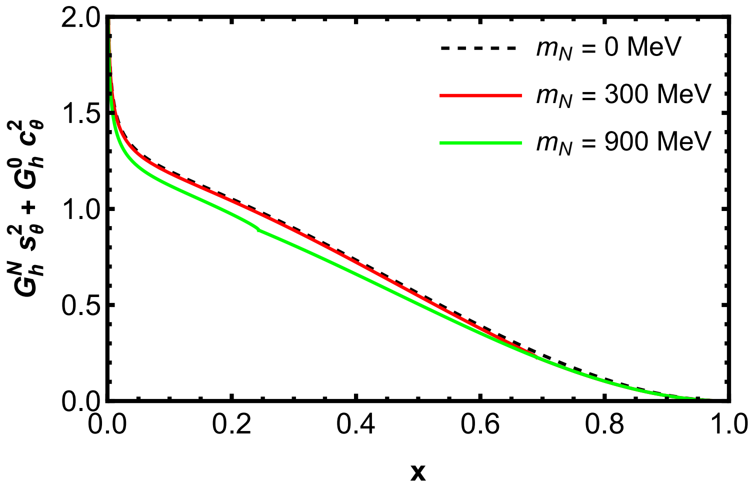

Figure 4.25.: Sum of the G functions $G_h^N s_\theta^2 + G_h^0 c_\theta^2 = G(x, m_N/m_\tau)\sin^2\theta + G(x,0)\cos^2\theta$. We use the mixing angle $\sin\theta = 0.32$. The black dashed line shows the SM case ($m_N = 0$) whereas the coloured lines show the effect of a non-zero sterile neutrino. The green curve is for illustrative purposes.

where we use the correlator given in Eq. (2.54). As for the leptonic energy spectrum the measurable hadronic energy spectrum is the incoherent sum of the SM and the sterile neutrino contribution

$$\begin{aligned}\frac{d\Gamma_{\text{had}}^{\text{exp.}}}{ds} =& \frac{d\Gamma(\tau \to \nu_\tau X)}{ds} + \frac{d\Gamma(\tau \to N X)}{ds}\\ =& N_c \frac{G_F^2 m_\tau^3 V_\nu^2 \cdot 2(|V_{ud}|^2 + |V_{us}|^2)}{192\pi^3} S(m_\tau, m_Z)\\ &\times \left[G(x, x_N)\sin^2\theta + G(x,0)\cos^2\theta\right]. \end{aligned} \tag{4.50}$$

Here we omit strange quark mass corrections. In Fig. 4.25 we show $G(x, m_N/m_\tau)\sin^2\theta + G(x,0)\cos^2\theta$ for different sterile neutrino masses. Qualitatively this is similar to the leptonic energy spectrum. The smaller the mass of the sterile neutrino is the harder it is to discern from the SM. As in the leptonic energy spectrum stronger deviations from the SM case require larger sterile neutrino masses. In the hadronic case, however, masses $m_N > 600$ MeV cannot be reliably calculated using perturbative methods (i.e. the green curve is for illustrative purposes).

4.4. Discussion

We begin the discussion of the previously presented results by comparing our bounds obtained from τ decays to experimental constraints on the mixing angle. To that end we first give an overview of the experimental bounds available and then compare them to our bounds obtained from leptonic and semi-hadronic τ decays. Then we discuss some aspects of our calculation of the branching fractions and explain the impact of them on experimental searches. Parts of the discussion are based on Ref. [126].

Overview of current experimental bounds: All bounds obtained from τ decays probe the mixing angle $V_{N\tau} = \sin\theta$. As mentioned in Sec. 2.4 we do not allow mixing of sterile neutrinos between different lepton flavours i.e. we consider only one mixing angle at a time with all others being zero. This is because as soon as the HSN is allowed to interact with more than one lepton flavour it impacts electroweak precision observables like the Fermi constant (see Ref. [105]). This strongly limits the number of experimental constraints we can compare our bounds to because measuring third generation interactions is difficult and the detection of electrons or muons is usually easier than detecting tauons. From a theory viewpoint BSM interactions with the third lepton generation are therefore very appealing seeing as they are generally the least constrained interactions. The plethora of experimental constraints focusing on the N-ν_e and N-ν_μ couplings are thus not comparable to our constraints on the N-ν_τ coupling. Nevertheless there are experimental constraints on $|V_{N\tau}|$. Both the CMS [142, 160, 161] and ATLAS [162–164] experiments have searched for HSN. The ATLAS experiment constrained HSN interactions with only the electron or muon lepton flavour. In addition, they considered scenarios in which the HSN couples to all lepton flavours simultaneously. These constraints are not comparable to ours. In Ref. [162] the ATLAS experiment presents constraints on the tau mixing angle. These are however weaker than the ones presented by CMS. The CMS experiment presents constraints on the tau mixing angle in the mass range $1.0\,\mathrm{GeV} \leq m_N \leq 1\times10^3\,\mathrm{GeV}$. In the mass range $3.0\,\mathrm{GeV} \leq m_N \leq 10\,\mathrm{GeV}$ they give the constraint [160][2]

$$|V_{N\tau}^{\mathrm{CMS}}| \lesssim 14.1\cdot 10^{-2}. \tag{4.51}$$

For HSN masses $1.0\,\mathrm{GeV} \leq m_N \lesssim 2.2\,\mathrm{GeV}$ the CMS experiment states an interval of excluded values of the mixing angle [142]. Towards larger HSN masses this excluded window becomes smaller and the bounds weaken; at $m_N = 2.0\,\mathrm{GeV}$ the allowed mixing angle is given as the interval

$$|V_{N\tau}|^2 \lesssim 4\cdot 10^{-4} \quad \wedge \quad 2\cdot 10^{-3} \gtrsim |V_{N\tau}|^2. \tag{4.52}$$

The CMS constraints are slightly stronger than the constraints obtained by the DELPHI experiment [165] in the range $1.0\,\mathrm{GeV} \leq m_N \lesssim 1.9\,\mathrm{GeV}$. Smaller HSN masses in the range $0.4\,\mathrm{GeV} \leq m_N \leq 1.6\,\mathrm{GeV}$ are constrained by the ArgoNeuT experiment [166], the BABAR experiment [167], and the Belle experiment [168] with the strongest of these bounds coming from ArgoNeuT and BABAR. The strongest constraint from BABAR is for HSN with a mass of $m_N = 1.2\,\mathrm{GeV}$ with the excluded mixing angle

$$|V_{N\tau}| < 0.2\cdot 10^{-2}. \tag{4.53}$$

These bounds are all weaker than the bounds obtained from the recasts [169, 170] of the CHARM [171, 172] and the WA66 [173] experiments in the mass range $0.4\,\mathrm{GeV} \leq m_N \leq 1.6\,\mathrm{GeV}$. In Fig. 4.26 we compiled all of these exclusion limits in one plot.

[2] This analysis is older than the one in Ref. [161]. We point out that the bound in Ref. [161] is stronger than the one given in Ref. [160] however in the former one they only constrain down to $m_N = 10\,\mathrm{GeV}$.

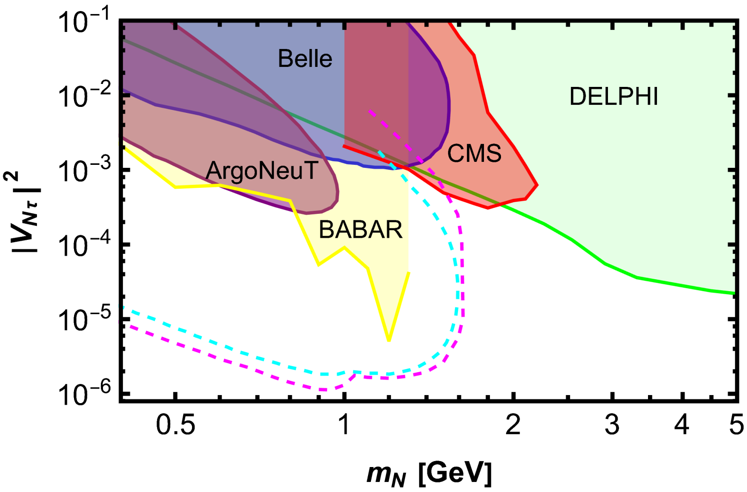

Figure 4.26.: Here we show the current exclusion limits of the experiments DELPHI (green) [165], ArgoNeuT (purple) [166], BABAR (yellow) [167], Belle (blue) [168], and CMS (red) [142]. The exclusion bounds of the DELPHI experiment are weaker for mixing with ν_τ by a factor of four for $m_N \leq 2.0\,\text{GeV}$ and by a factor of 1.5 for $m_N \geq 3\,\text{GeV}$. In between these regions it is stated that the bound loosens with a factor rapidly rising from 1.5 to four [165]. To accommodate this, we linearly increase the factor from 1.5 to four in the mass region $2.0\,\text{GeV} \leq m_N \leq 3.0\,\text{GeV}$. The dashed lines belong to the recasts of the CHARM experiment (cyan) [169] and the WA66 experiment (magenta) [170].

Comparison of our bounds to experimental bounds: Now we may compare our bounds obtained from τ decays to these experimental bounds. We start by discussing the case $m_N < m_\tau$. From the τ lifetime we find $|V_{N\tau}| \lesssim 0.2$ for the sterile neutrino mass $m_N = 600\,\text{GeV}$. This bound is not competitive and excluded by ArgoNeuT, BABAR, and Belle as well as the recasts. For the case $m_N > m_\tau$ we obtain bounds from the τ lifetime in Eq. 4.30 and from leptonic and semi-hadronic τ decays in Eqs. (4.39) to (4.43). Our bound from the τ lifetime is comparable to that of CMS (Eq. (4.51)) but weaker than the DELPHI bounds. Our bounds from the leptonic and semi-hadronic decays are comparable in size to those from the τ lifetime and thus also weaker than the bound from DELPHI (and CMS) in the HSN mass range $m_\tau < m_N < 5.0\,\text{GeV}$. We point out that the bounds from the τ lifetime and the leptonic and semi-hadronic decays only assume that $m_N > m_\tau$ and hence extend over a large parameter space.

Lastly, we can compare our leptonic τ decay bound to the leptonic τ decay bound obtained by Kobach and Dobbs ($m_N > m_\tau$) [146] who updated the bound presented in Ref. [113]. They give the bound $|V_{N\tau}| \lesssim 7.1 \cdot 10^{-2}$ at the 2σ level. Our leptonic bound in Eq. (4.41) is at the 3σ level and therefore stronger. Comparing the leptonic and the semi-hadronic bounds we see that the semi-hadronic bounds in Eq. (4.42) exclude a zero mixing angle at the 1σ level. We did not account for correlations in the uncertainties but these numbers could point towards a possible evidence for $|V_{N\tau}| \neq 0$ with better measurements in the future. In Fig. 4.27 we show a comparison of our bounds to the

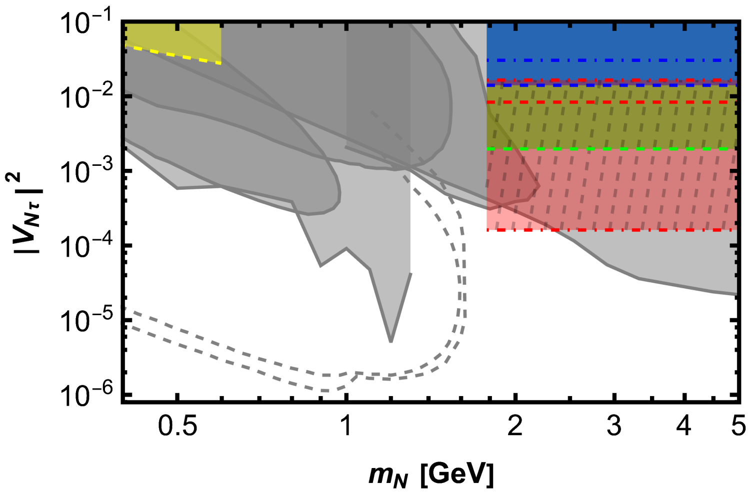

Figure 4.27.: Our bounds obtained from τ decay in comparison to the experimental bounds (grey) shown in Fig. 4.26. The yellow bound comes from the τ lifetime for $m_N < m_\tau$ (see Eq. (4.27) and Fig. 4.22 purple region). For the case $m_N > m_\tau$ the τ lifetime leads to the dashed blue line with the excluded region being the blue region above the line (at the 1σ level, see Eq. (4.30)); the dot-dashed blue line corresponds to the same limit as Eq. (4.30), but evaluated at the 3σ level. The dashed green line with the excluded region being the green region above the line comes from the bound of both leptonic τ decays for $m_N > m_\tau$ (see Eq. (4.41)) at the 3σ level. The dashed red line comes from the semi-hadronic τ decays for $m_N > m_\tau$ (see Eq. (4.42)) and the dot-dashed red lines delimit the ends of the 1σ uncertainty band. This red band, further highlighted by the black mesh, marks the region of parameter space allowed by the weighted average of the semi-hadronic τ decays.

previously discussed experimental bounds shown in Fig. 4.26.

While our bounds are weaker compared to the experimental bounds they are also less model-dependent. Many of these experiments make assumptions on e.g. the size of the branching ratios of the HSN. This makes their bounds model-dependent as it excludes the possibility of the HSN coupling to other BSM particles e.g. the HSN could decay into other BSM particles or lighter sterile neutrinos. This adds an additional decay channel that reduces the branching ratios of HSN into SM particles. By contrast, our study of τ decays only assumes the interaction of the HSN with the SM neutrino ν_τ to be through the mixing angle. There are no further assumptions on additional interactions with other BSM particles. In a similar way the leptonic τ decays could be affected by NP interactions. The leptonic decays produce two SM neutrinos which are not detected, what is actually measured is therefore $\tau \longrightarrow \ell + E_{\text{missing}}$ where the missing mass squared could also be comprised of decays $\tau \longrightarrow \ell X_{\text{dark}}$ with a dark particle X_{dark}. A dark particle coupling to a τ lepton and a SM neutrino ν_τ could be a majoron [174–176]. To that end we can estimate the size of the dark decay width

$$\Gamma(\tau \longrightarrow \ell + E_{\text{miss}}) = \Gamma_{\text{SM}}(\tau \longrightarrow \nu_\tau \ell \bar{\nu}_\ell) + \Gamma_{\text{NP}}, \tag{4.54}$$

by comparing the measured decay rate on the left side of the equation with the calculated decay rate $\Gamma_{\text{SM}}(\tau \to \nu_\tau \ell \bar{\nu}_\ell)$. We find

$$\Gamma_{\text{NP}} = \frac{\mathcal{BR}^{\text{exp.}}(\tau \to \nu_\tau e \bar{\nu}_e)}{\mathcal{BR}^{\text{exp.}}(\tau \to \nu_\tau \pi)} \Gamma_{\text{SM}}(\tau \to \nu_\tau \pi) - \Gamma_{\text{SM}}(\tau \to \nu_\tau e \bar{\nu}_e) = (3.92 \pm 3.81)\,\mu\text{eV} \tag{4.55}$$

$$\Gamma_{\text{NP}} = \frac{\mathcal{BR}^{\text{exp.}}(\tau \to \nu_\tau \mu \bar{\nu}_\mu)}{\mathcal{BR}^{\text{exp.}}(\tau \to \nu_\tau \pi)} \Gamma_{\text{SM}}(\tau \to \nu_\tau \pi) - \Gamma_{\text{SM}}(\tau \to \nu_\tau \mu \bar{\nu}_\mu) = (3.85 \pm 3.69)\,\mu\text{eV}, \tag{4.56}$$

here we set the mixing angle $\cos\theta = 1$ due to the tight experimental constraints discussed above. Thus the measurements of the leptonic τ decays do not exclude a contribution from a dark particle.

The calculation of the total inclusive HSN decay rate: We calculated the inclusive HSN decay rates for both the charged- and neutral-current interaction and inferred the branching fractions from these decay rates. The model-dependence discussed above equally applies to our calculation of the branching fractions (i.e. our calculation of the branching fractions assumes the HSN only interacts through the mixing angle and does not interact with other dark particles). An interesting property of the QCD corrections is that the massless and the massive corrections individually all carry the same sign: the massless corrections are all positive and the massive corrections all negative. This means there is a cancellation between the massless and the massive terms (due to phase space suppression) and as shown in e.g. Fig. 4.11 the massive terms can significantly reduce the size of the decay rate. The omission of the massive contributions would lead to an overestimation of the branching fractions. Furthermore, it is interesting to see how well-behaved the perturbative description is. The quality of the perturbative description determines the HSN mass window in which we can trust the perturbative calculation. In Tab.4.5 we summarise the mass windows permitting a perturbative description. The uncertainties coming from varying the renomalisation scale are usually at the level of $\mathcal{O}(10\%)$. In this sense we could also relax our criteria on the the mass windows that permit a perturbative description e.g. lowering the limit for the $\ell = \tau$ case from $4.6\,\text{GeV} \lesssim m_N$ down to $4.3\,\text{GeV} \lesssim m_N$ increases the uncertainty induced by varying the renormalisation scale between $m_N/2$ and $2m_N$ from 16% and 12% to 27% and 20%. While this is a sizeable increase it would still

Table 4.5.: Summary table of the HSN mass windows allowing a perturbative description. See also Eqs. (4.20) to (4.22)). The charged-current decay rate for HSN masses smaller than the τ lepton mass is zero.

$N \to \mu X$	$1.5\,\text{GeV} \lesssim m_N < m_\mu + m_{D^+} \quad \wedge \quad 3.5\,\text{GeV} \lesssim m_N$	
$N \to \tau X$	$1.5\,\text{GeV} \lesssim m_N < m_\tau$	only NC decay possible
	$3.0\,\text{GeV} \lesssim m_N \lesssim m_\tau + m_{D^+} \quad \wedge \quad 4.6\,\text{GeV} \lesssim m_N$	
$N \to \nu X$	$1.5\,\text{GeV} \lesssim m_N < 2m_{D^0} \quad \wedge \quad 4.6\,\text{GeV} \lesssim m_N$	

be justifiable to instead use $4.3\,\text{GeV} \lesssim m_N$ as the limit of the perturbative mass window (keeping in mind this affects the 50% criterion and the mass corrections are then larger than half of the massless corrections). At $m_N = 4.0\,\text{GeV}$ the uncertainty approaches up to 70% indicating in this mass range the perturbative description is no longer well-defined. At our given value of $4.6\,\text{GeV} \lesssim m_N$ we are rather conservative. Nevertheless we emphasise that it is not possible to derive a hard limit; hard in the sense that we cannot derive a fixed mass beyond which perturbative QCD predictions are possible or impossible. Instead these limits are to be regarded as general orders of magnitude which do allow some slight variations. Our example of the difference of the uncertainty however shows how quickly the quality of the perturbative description can deteriorate. To that extent our presented limits on the HSN mass may be conservative but they certainly fulfill a well-behaved perturbative description.

There is a large conceptual difference between the charged- and neutral-current decay rates. In addition to the same bubble diagram contributions the neutral current allows for the anomalous triangle diagrams. We have found an inconsistency between the standard calculation of the Z decay axial singlet contribution and the same contribution obtained from the calculation of the rare process $K \to \pi\nu\nu$. In principle the two WC obtained via these two calculations should be the same, up to differences in the renormalisation scheme, seeing as they stem from the same diagram. While the logarithmic term agrees the constant term does not agree between the two calculations and it is not possible to go from one WC to the other by means of a scheme transformation. The origin of this issue is unknown to us. Nevertheless, the numerical impact on the decay rate is negligible as can be seen from Eq. (4.13). Even more so, the impact is only present below the charm scale as above the charm scale the axial singlet contribution vanishes anyway.

Impact on colliders and future prospects: Since we calculated the total inclusive HSN decay rate we can immediately state the lifetime or the proper decay length. Predictions of the proper decay length of the HSN are important to gauge which signals to expect at collider experiments. In general e^+e^- colliders and hadron colliders could both produce HSN. At the e^+e^- collider KEKB [177] and SuperKEKB [178] the B factories Belle [179] and Belle II [180] produce τ leptons copiously either directly through the neutral current $e^+e^- \to \tau^+\tau^-$ or indirectly through the decay of e.g. B mesons. At Belle around $912 \cdot 10^6$ $\tau^+\tau^-$ pairs have been produced and for the targeted integrated luminosity of $50\,\text{ab}^{-1}$ at Belle II it is expected to see around $46 \cdot 10^9$ tau pairs [181]. Whenever there is an interaction with a τ lepton possible the same interaction could also happen with an HSN. Therefore, we may roughly estimate the number of HSN produced at these B factories by multiplying the total amount of tau pairs produced with the square of the mixing angle. We assume the mixing angle $|V_{N\tau}|$ to still be unconstrained i.e. $|V_{N\tau}| \approx 10^{-3}$ for HSN around $m_N \approx 2\,\text{GeV}$ to $5\,\text{GeV}$ (see Fig. 4.26). This leads to around 912 HSN at Belle and $46 \cdot 10^3$ HSN at Belle II. At this level of NP particle abundances it is extremely important that the detection efficiencies are high enough in order to be sensitive to these events. The sensitivity depends on several different factors: (1) The production mode can have a large impact on the reconstruction efficiency of the event. If the HSN is produced directly through the neutral current then either two HSN are produced (very unlikely as this would scale with a factor $|V_{N\tau}|^2$ already at the level of the amplitude) or a single HSN is produced accompanied by a SM neutrino. This means that there is no tagging particle and the whole process already contains missing energy at the level of the production. However, the DELPHI experiment did produce constraints on the HSN mixing angle under these conditions that are competitive with current experiments [165]. By contrast, if the HSN is produced indirectly in a B meson decay the size of the mass of the HSN is kinematically limited to be smaller than the B meson mass but now there is another particle to tag. This severely reduces the number of tau leptons and thus HSN. Belle measured around $772 \cdot 10^6$ $B\bar{B}$ pairs [182]; Belle II targets an integrated luminosity 50 times larger subsequently leading to around $39 \cdot 10^9$ $B\bar{B}$ pairs. With a branching ratio of $\mathcal{BR}(B^+ \to \tau^+ \nu_\tau X) = 2.5\%$ [8] we arrive for the mixing angle $|V_{N\tau}| = 10^{-3}$ at the staggeringly small number of potentially produced HSN in B decays at Belle of around 19 HSN and about 950 HSN at Belle II. (2) The HSN decay mode studied plays a large role in the sensitivity of the analysis. The B factories are capable of producing HSN with masses up to $m_N \approx 5\,\text{GeV}$ but only through the neutral current. In Fig. 4.20 we see that HSN with masses around $m_N \approx 4.8\,\text{GeV}$ have a proper decay length of $c\tau \lesssim 80\,\text{cm}$ for a mixing angle of $|V_{N\tau}| \gtrsim 10^{-3}$. This is a typical displaced vertex signature. If the HSN decays via the charged current $N \to \tau X$ the observed signature would be missing energy from the production of the HSN and a displaced vertex into a τ lepton and a hadronic system. Additionally, leptonic decays of the HSN are also possible. They would lead to a displaced vertex producing a τ lepton and an additional charged lepton which is either an electron, a muon, or another tau lepton together with missing energy in the form of the undetected SM neutrino. A decay through the neutral current would be similar to the charged-current decay with the distinct difference that there is more missing energy in the displaced signature. The benefit of the charged-current hadronic decays is that they produce two charged particles at the origin of the displaced vertex and no missing energy. In contrast, the leptonic decays and the neutral-current decays of the HSN produce missing energy at the displaced vertex. Belle II is already capable of reconstructing displaced vertices with the current reconstruction algorithms. Their efficiency is however small at the order of less than 50% for displacements larger than about 50 cm; by contrast, the new graph neural network algorithms yield better efficiencies upward of 80% for displacements larger than 50 cm [143]. Considering the small number of HSN produced the increase in efficiency by the usage of machine learning techniques is crucial for the detection of an HSN and could lead to strong constraints on the mixing angle.

HSN with smaller masses can quickly obtain proper decay lengths in the vicinity of several meters. An HSN produced in a B decay could possess at most a mass $m_{B^+} - m_{D^0} - m_\tau = 1.6\,\text{GeV}$. At this mass only neutral-current decays are possible and in order for the proper decay length to be less than 80 cm (i.e. the decay can still be reconstructed efficiently with the new tracking algorithms) it is required that the mixing angle is larger than $|V_{N\tau}| > 10^{-2}$. Angles this large have already been excluded. An interesting prospect in this regard is to consider the velocity of the HSN. If it is produced in B decays with a mass of around 1.5 GeV or slightly more it is produced almost at rest, so despite a long lifetime (i.e. small mixing angles) its displacement could still be within the detector making it a prime candidate for a displaced vertex study. The difficulty is then the time resolution of the event. A very slow moving HSN will lead to a long time between production and decay making it hard to resolve the decay process. The same applies to the direct production through the neutral current for HSN with masses $m_N \approx 5\,\mathrm{GeV}$.

It is interesting to note that the BABAR bounds [167] are far stronger than the Belle bounds [168] even though both experiments are based at e^+e^- colliders. In the BABAR analysis they considered HSN produced in hadronic τ decays; specifically, they analysed the 3-prong pionic tau decays and studied the impact of a massive HSN on the kinematics of the visible final state SM particles. In their analysis they assume that the HSN does not decay inside the detector leaving it as missing energy. The Belle analysis on the other hand pursued a very different analysis strategy. Similar to the BABAR experiment they consider HSN produced in τ decays (the semi-hadronic tau decay $\tau \to N\pi$). The key difference in comparison to BABAR is that they assume the HSN decays inside the detector and yields a displaced vertex. To that end they considered the neutral-current decay mode $N \to \nu_\tau \mu\mu$. The Belle analysis bounds being weaker than the BABAR bounds aligns with our expectations; if we consider the proper decay lengths we calculated (Fig. 4.20) we see that for HSN masses below the tau mass and with proper decay lengths at the order of up to 80 cm the Belle analysis excludes roughly the mixing angles we would expect. Furthermore, the Belle bounds are model dependent because they have to make assumptions on the branching fractions. Thus the requirement that the HSN decays inside the detector severely limits the sensitivity of the search. Indeed, since BABAR is not limited to HSN with proper lifetimes below $\sim 80\,\mathrm{cm}$ they can probe far smaller mixing angles. Nevertheless it is important to emphasise that the actual sensitivity of any given analysis cannot easily be estimated on grounds of the proper decay length alone before the analysis is done. Many different factors influence the detection efficiency and for macroscopic decay lengths it is a priori not clear whether displaced vertex searches or missing energy searches are better or what the exact effects of certain systematics are; for instance even large efficiencies do not necessarily help if the ratio of signal to background $S/\sqrt{B}$ is small [183]. However, to get an idea of the capabilities of an experiment it is helpful to consider the proper decay length.

In contrast to e^+e^- colliders it is also possible to produce HSN through virtual W boson decays at hadron colliders. Here the significantly larger backgrounds compete with the fact that the charged-current decay $W^* \to \tau N$ grants access to a charged lepton that can be tagged during the production already. Indeed this search has already been performed by CMS [142]. They look for signals detected in the muon detector induced by the decay products of the HSN decaying. This allows the CMS experiment to be sensitive to proper decay lengths up to $c\tau = 10\,\mathrm{m}$ and leads to the bounds presented in Fig. 4.26. Comparing to our predictions of the proper decay length in Fig. 4.20 we see that sensitivity up to proper decay lengths of 10 m would allow to constrain the mixing angles $|V_{N\tau}| < 10^{-3}$ in the mass range $4.6\,\mathrm{GeV} \lesssim m_N \leq 6.5\,\mathrm{GeV}$ which is an exciting prospect for future analyses.

The proposed Future Circular Collider (FCC) [184] in its e^+e^- collision mode would reach unprecedented luminosities and operation on the Z peak is expected to yield around $170 \cdot 10^9$ $\tau^+\tau^-$ pairs which is more than three times the amount produced at Belle II. As before, we can estimate the number of directly produced HSN to be around $170 \cdot 10^3$. Similarly, it is expected to produce several hundreds of billions of B meson pairs which would lead to thousands of HSN being produced. The FCC-ee is designed to surpass the integrated luminosity ($\hat{\mathcal{L}}$) of the LEP collider by a factor of $\hat{\mathcal{L}}_{\mathrm{FCC-ee}}/\hat{\mathcal{L}}_{\mathrm{LEP}} = 2 \cdot 10^5$; naively rescaling the DELPHI bounds $|V_{N\tau}^{\text{DELPHI}}|^2 \sim 5 \cdot 10^{-4}$ by the increased integrated luminosity suggests $|V_{N\tau}^{\text{FCC-ee}}|^2 \sim |V_{N\tau}^{\text{DELPHI}}|^2 \sqrt{\hat{\mathcal{L}}_{\text{LEP}}/\hat{\mathcal{L}}_{\text{FCC-ee}}} \approx 1 \cdot 10^{-6}$ and leads to a significant increase in sensitivity. This assumes the detection is only limited by statistics. However, the study of massive sterile neutrinos is one of the many prospects of the FCC-ee and so we can expect that the detectors used will be optimised to these long-lived particles and therefore we expect the real sensitivity to be better.

To conclude the discussion we point out that both e^+e^- colliders and hadron colliders are capable of producing HSN. The biggest difference between the two is that e^+e^- colliders do not allow the production of HSN through the charged current and as such cannot produce both the HSN and a lepton which they can tag. This is possible at hadron colliders and thus the strongest bounds on HSN coupling to the SM neutrino ν_τ come from CMS in the mass range $1.6\,\text{GeV} \lesssim m_N \lesssim 1.9\,\text{GeV}$. Nevertheless the CMS bounds are only slightly stronger than the DELPHI bounds in this mass range. HSN with masses $m_N \lesssim 1.6\,\text{GeV}$ are strongly constrained by the recasts of the CHARM and WA66 experiments. We can expect interesting future analyses from both types of colliders. Furthermore, the SHiP experiment is expected to be sensitive to HSN in the mass range we studied here [185, 186].

While we focused on the interaction of HSN with a mixing angle in this work this is not the only way HSN interactions can be described. For example it is also possible to describe interactions of HSN with quarks and leptons via dimension 6 operators. In this framework one can then constrain the size of the WC by looking e.g. at the decay $B \to D\ell\nu$ (see e.g. Refs. [187, 188] and references therein).

5. Conclusion

In this work we have calculated the total inclusive hadronic decay rate of HSN with masses in the range $1\,\mathrm{GeV} \lesssim m_N \lesssim 6\,\mathrm{GeV}$ that mix only with one SM neutrino ν_ℓ with the mixing angle $|V_{N\ell}|$. To that end we calculated the decay rate of HSN into quarks including QCD corrections in the strong coupling constant α_s up to $O(\alpha_s^4)$ for the massless part (i.e. with all quark masses being zero) and up to $O(\alpha_s^3)$ for the massive part (i.e. corrections $\propto m_c^2$) of the charged-current decay and $O(\alpha_s^2)$ for the neutral-current decay rate. This is possible because the entire dynamics of the QCD effects are contained in the well-known gauge boson correlators (Eq. (2.45)) which could be taken from the literature. Kinematically, the charged-current HSN decays are similar to hadronic τ decays and we can use the same correlator used for τ decays for the charged-current HSN decay. However, whereas in τ decays the lepton produced in the final state is a SM neutrino, which can be considered massless in these calculations, an HSN decaying through the charged current produces a charged lepton. For both $\ell = e,\ \mu$ the effects of the massive charged lepton are negligible but for $\ell = \tau$ they can be sizeable. To that end we have calculated the decay rate of the charged-current decays including the effects of a massive charged lepton. We find analytical expressions for the massless part of the decay rate up to $O(\alpha_s^3)$ (Eqs. (3.17)-(3.19)). For the calculation of the massless corrections at $O(\alpha_s^4)$ we have derived a series representation of the Källén function (Eq. (3.20)) to obtain a series representation for the $O(\alpha_s^4)$ contribution with analytical expressions for all coefficients. Furthermore, we have calculated analytical expressions for the massive corrections up to $O(\alpha_s^2)$ (Eqs. (3.37)-(3.39), (3.48)-(3.53)) and used the series representation of the Källén function to calculate the $O(\alpha_s^3)$ corrections (Eqs. (3.41)-(3.54)). Similarly, we have calculated fully analytical expressions for the neutral-current decay (Eqs. (3.90)-(3.102)). Both the massless and the massive higher-order QCD corrections are crucial to determine the mass range in which a perturbative description of HSN decays is applicable. To gauge the quality of the perturbative description we impose on the massless corrections that the sensitivity to the renormalisation scale decreases with higher orders. For the massive corrections we require that the size of the massive correction does not exceed 50% (25%) of the massless correction of the charged current (neutral current). In addition, we demand that the uncertainty induced by a variation of the renormalisation scale between $m_N/2$ and $2m_N$ does not exceed $O(20\%)$. This leads to the HSN mass windows permitting a perturbative description given in Tab. 4.5.

The total inclusive hadronic decay rate following from these calculations allows us to calculate branching fractions of HSN decays as well as the lifetime. In Fig. 4.20 we show the HSN proper decay length for different HSN masses and mixing angles. We find that there is unconstrained parameter space with proper decay lengths in reach of the CMS experiment and with interesting prospects for Belle II.

The neutral current contribution involves a new class of diagrams in comparison to the charged current one. These are the anomalous axial vector flavour singlet triangle diagrams which start at $O(\alpha_s^2)$. These diagrams vanish if the complete SU(2) doublet contributes and the doublet is mass-degenerate; in the SM this is not the case for on-shell Z boson decays and also not for HSN decays. In the literature, the anomalous triangle diagrams have been accounted for in Z decays by integrating out the top quark. We compare the Wilson coefficient containing the top quark dynamics obtained from the Z decay calculations with the Wilson coefficient obtained from the calculation of the rare kaon decay $K \to \pi\nu\nu$. We find an inconsistency in the literature between both calculations and both Wilson coefficients and anomalous dimensions cannot be transformed into each other through a renormalisation scheme transformation. The origin of this inconsistency is unknown. Nevertheless the numerical impact on the HSN decay rate is negligible (see Eq. (4.13)).

Our calculation of the effects of a massive lepton in the final state of the HSN decay can also be adapted to study $\tau \to N +$ had. decays. In this case we have studied two different scenarios: the first scenario addresses sterile neutrinos lighter than the τ lepton. In the second scenario the HSN is heavier than the τ lepton and thus cannot be produced in τ decays. In the latter case there is still a modification of the SM decay of the τ lepton through the cosine of the mixing angle. For $m_N < m_\tau$ we find that a perturbative description of τ decays into sterile neutrinos is possible for $m_N \lesssim 600\,\text{MeV}$; the mixing angle for an HSN with a mass of $m_N = 600\,\text{MeV}$ is then constrained by the τ lifetime to be $|V_{N\tau}| = |\sin\theta| \lesssim 0.2$ (see Fig. 4.22). In the case of the HSN being heavier than the τ lepton, $m_N > m_\tau$, we find the mixing angle to be constrained by the τ lifetime as $|\sin\theta| \leq 11.8 \cdot 10^{-2}$.

Complementary to our bounds obtained from the τ lifetime we also studied the effect of an HSN on the branching fractions of the leptonic decays $\tau \to \nu_\tau \ell \bar{\nu}_\ell$ with $\ell = e, \mu$ and the semi-hadronic decays $\tau \to \nu_\ell P$ with $P = \pi, K$. We find that the leptonic decays constrain the mixing angle at the 3σ level to $|\sin\theta| \leq 4.4 \cdot 10^{-2}$. The semi-hadronic decays permit a non-zero mixing angle at the 1σ level leading to $\sin\theta = (9.1^{+3.7}_{-7.8}) \cdot 10^{-2}$ (see Eqs. (4.39)-(4.43)). While in the semi-hadronic decays a single SM neutrino is produced in the leptonic decays two SM neutrinos are produced. Any experiment measuring this decay thus measures the missing energy of the SM neutrinos $\tau \to \ell + E_{\text{miss}}$. Instead of the SM neutrinos the τ lepton could also decay into other dark particles like e.g. majorons. Indeed we find the leptonic decays permit a non-zero dark decay width (Eqs. (4.55) and (4.56)). We also give expressions for the spectra of leptonic and hadronic τ decays.

We have presented an overview of experimental bounds on the mixing angle of HSN with SM neutrinos ν_τ (Fig. 4.26). Our bounds obtained from the τ lifetime and branching fractions are not competitive with the current collider bounds. Both hadron and e^+e^- colliders can probe HSN with both types of experiments yielding strong bounds on the mixing angle for different HSN masses. We can roughly estimate the number of HSN produced directly at Belle to be around 912 and the number of HSN produced indirectly in B decays to be around 19 for a mixing angle of $|V_{N\tau}| = 10^{-3}$. At Belle II with a data set of $50\,\text{ab}^{-1}$ we expect around $46 \cdot 10^3$ directly produced HSN and around 950 HSN produced indirectly in B decays. The FCC-ee would surpass these numbers significantly and a rough estimate of the sensitivity of FCC-ee suggests a significant tightening of the bounds in comparison to the DELPHI bounds.

The biggest difficulty for e^+e^- collider experiments is the fact that HSN are only produced directly through the neutral current and thus there is no charged particle that can be tagged at the level of the production. Furthermore, the HSN produced are generally very long lived. This gives rise to displaced vertex signatures which have small backgrounds but are difficult to reconstruct. With future implementations of graph neural network tracking algorithms it is expected that Belle II can reconstruct displaced vertices with displacements up to around 80 cm. Only considering the proper decay lengths of HSN this suggests that Belle II is sensitive to mixing angles $|V_{N\tau}| \gtrsim 10^{-3}$ for masses $3\,\text{GeV} \leq m_N \leq 5\,\text{GeV}$ and $|V_{N\tau}| > 10^{-2}$ for masses $m_N \lesssim m_\tau$. This part of the parameter space is already constrained by the DELPHI and the CMS experiment. By contrast, the CMS experiment can resolve long lived particles with proper decay lengths of up to around 10 m. This means that CMS is capable of constraining the mixing angle to $|V_{N\tau}| \lesssim 10^{-3}$ for masses in the range $3\,\text{GeV} < m_N \leq 6.5\,\text{GeV}$ and below $|V_{N\tau}| < 10^{-2}$ for masses $m_N \lesssim m_\tau$.

Sterile neutrinos remain interesting from a theoretical perspective as they arise naturally from an extension of the Standard Model by right-handed neutrinos. Furthermore they are experimentally not excluded and there is still large unconstrained parameter space for heavy sterile neutrinos. Considering the already available sensitivity of experiments like DELPHI and CMS, HSN with masses $m_N \gtrsim 2\,\text{GeV}$ could either be excluded for even smaller values of the mixing angle in the near future or, even better, discovered.

A. Integrated Spectrum Integral

The integrals arising in the integrated spectrum Eq. (3.29) are of the form

$$I_k^{\text{cut}} = \int_0^{x_{\max}} dx \left((1 + x_\ell^2 - x)(1 + 2x + x_\ell^2) - 4x_\ell^2 \right) \sqrt{\lambda(1, x, x_\ell^2)} \ln^k(x). \tag{A.1}$$

Using as notation $x_{\max} = \hat{x}$ we calculate for $k < 3$ the following analytical expressions of these integrals

$$\begin{aligned} I_0^{\text{cut}} - I_0 =& \frac{1}{2}\Bigg(- \left(\hat{x}^2 + 7\right) x_\ell^2 - (\hat{x} + 7)x_\ell^4 + x_\ell^6 \\ &+ (\hat{x} - 1)^2(\hat{x} + 1)\Bigg)\left(\hat{x} - (x_\ell + 1)^2\right) X_r - 24x_\ell^4 \text{ArcTanh}(X_r), \end{aligned} \tag{A.2}$$

$$\begin{aligned} I_1^{\text{cut}} - I_1 =& 12x_\ell^4\left(\Delta\text{Li}_2\left(-\frac{X_-}{2x_\ell}\right) - \Delta\text{Li}_2\left(\frac{X_-}{2}\right) + \Delta\text{Li}_2\left(\frac{1 - X_r}{2}\right)\right) \\ &+ \frac{1}{24}X_r\left(\hat{x} - (x_\ell + 1)^2\right) \\ &\times \Bigg(- 3\hat{x}^3 + 12\big(- (\hat{x}^2 + 7)x_\ell^2 - (\hat{x} + 7)x_\ell^4 + x_\ell^6 + (\hat{x} - 1)^2(\hat{x} + 1)\big) \ln(\hat{x}) \\ &+ 5(\hat{x}^2 + \hat{x}) + (\hat{x}(5\hat{x} + 4) + 85)x_\ell^2 + 5(\hat{x} + 17)x_\ell^4 - 19x_\ell^6 - 19\Bigg) \\ &+ \Bigg(- 8x_\ell^2 - 6x_\ell^4\left(4\ln(\hat{x}) + 2\ln\left(1 - X_r^2\right) - 4\ln(2) + 2\right) \\ &- 8x_\ell^6 + x_\ell^8 + 1\Bigg) \text{ArcTanh}(X_r) \\ &- \left(8x_\ell^2 + 24x_\ell^4 \ln(x_\ell) - 8x_\ell^6 + x_\ell^8 - 1\right) \text{ArcTanh}\left(- X_r \frac{1 + x_\ell}{1 - x_\ell}\right), \end{aligned} \tag{A.3}$$

$$\begin{aligned} I_2^{\text{cut}} - I_2 =& X_r\Bigg[\Bigg(\left(\hat{x}^2 + 7\right)x_\ell^3 - (\hat{x} - 1)\left(\hat{x}^2 + 3\right)x_\ell^2 + (\hat{x} + 3)x_\ell^6 + (\hat{x} + 7)x_\ell^5 \\ &+ (7 - 3\hat{x})x_\ell^4 - (\hat{x} - 1)^2(\hat{x} + 1)x_\ell + \frac{1}{2}(\hat{x} - 1)^3(\hat{x} + 1) - \frac{x_\ell^8}{2} - x_\ell^7\Bigg) \ln^2(\hat{x}) \\ &+ \Bigg(\frac{1}{12}\big(- 3\hat{x}^4 + 8\hat{x}^3 - 24\hat{x} + 19\big) + \left(- 2\hat{x} - \frac{11}{2}\right)x_\ell^6 - \frac{5}{6}(\hat{x} + 17)x_\ell^5 \\ &+ \frac{1}{6}(38\hat{x} - 85)x_\ell^4 + \frac{1}{6}(-\hat{x}(5\hat{x} + 4) - 85)x_\ell^3 \end{aligned} \tag{A.4}$$

$$
\begin{aligned}
&+\frac{1}{6}(\hat{x}(\hat{x}(4\hat{x}-3)+38)-33)x_\ell^2+\frac{1}{6}(\hat{x}(\hat{x}(3\hat{x}-5)-5)+19)x_\ell \\
&+\frac{19x_\ell^8}{12}+\frac{19x_\ell^7}{6}\Bigg)\ln(\hat{x})+\frac{1}{144}\Bigg(9\hat{x}^4-32\hat{x}^3+288\hat{x}-265\Bigg) \\
&+\left(2\hat{x}+\frac{113}{24}\right)x_\ell^6+\frac{23}{72}(\hat{x}+41)x_\ell^5+\frac{1}{72}(943-446\hat{x})x_\ell^4 \\
&+\frac{1}{72}(\hat{x}(23\hat{x}+28)+943)x_\ell^3+\frac{1}{72}(\hat{x}((9-16\hat{x})\hat{x}-446)+339)x_\ell^2 \\
&+\frac{1}{72}(\hat{x}((23-9\hat{x})\hat{x}+23)-265)x_\ell-\frac{265x_\ell^8}{144}-\frac{265x_\ell^7}{72}\Bigg] \\
&+x_\ell^4\Bigg[-16\mathcal{P}_{(0,7,5,0)}\mathrm{ArcTanh}^2(X_r) \\
&+24\ln\left(1-X_r^2\right)\left(\mathrm{Li}_2\left(-\frac{X_-x_\ell}{X_+}\right)-\mathrm{Li}_2\left(-\frac{X_-}{X_+x_\ell}\right)\right) \\
&+24\mathrm{Li}_3\left(-\frac{X_-}{X_+x_\ell}\right)-24\mathrm{Li}_3\left(-\frac{X_-x_\ell}{X_+}\right)+48\mathrm{Li}_3\left(-\frac{X_-}{X_r-1}\right) \\
&+48\mathrm{Li}_3\left(\frac{X_r+1}{(X_r-1)x_\ell}+1\right)+24\mathrm{Li}_3\left(-\frac{(X_r+1)x_\ell}{X_r-1}\right) \\
&+24\mathrm{Li}_3\left(\frac{x_\ell-X_rx_\ell}{X_r+1}\right)+30\mathrm{ArcTanh}(X_r)-48\zeta(3)\Bigg] \\
&+\frac{1}{6}x_\ell^8\mathcal{P}_{(0,19,0,-3)}+x_\ell^6\mathcal{P}_{(0,-\frac{46}{3},-2,4)}+x_\ell^2\mathcal{P}_{(0,2,\frac{46}{3},-4)} \\
&+\ln(x_\ell)\Bigg[x_\ell^8\mathcal{P}_{(0,1,3,0)}-8x_\ell^6\mathcal{P}_{(0,1,3,0)}-12x_\ell^4\mathcal{P}_{(\pi^2,0,2,-1)} \\
&+\ln(\hat{x})\left(-12x_\ell^4\left(4\mathrm{ArcTanh}(X_r)+1\right)+2x_\ell^8-16x_\ell^6\right) \\
&-12x_\ell^4\ln^2(\hat{x})+48x_\ell^4\ln(X_-)\mathrm{ArcTanh}(X_r) \\
&+\ln(X_+)\left(-24x_\ell^4\left(2\ln\left(1-X_r^2\right)+2\mathrm{ArcTanh}(X_r)-1\right)-4x_\ell^8+32x_\ell^6\right) \\
&+48x_\ell^4\ln^2(X_+)+96x_\ell^4\mathrm{ArcTanh}(X_r)\ln(1-x_\ell) \\
&-16x_\ell^2\mathrm{ArcTanh}(X_r)+2\mathrm{ArcTanh}(X_r)\Bigg] \\
&+\ln^2(x_\ell)\left(12x_\ell^4(2\ln(X_+)-\mathcal{P}_{(0,2,0,0)})+\frac{p(x_\ell)}{2}\right)-12x_\ell^4\ln^3(x_\ell) \\
&+\ln(\hat{x})\Bigg[x_\ell^8\mathcal{P}_{(\frac{19}{12},-2,0,0)}+x_\ell^6\mathcal{P}_{(-\frac{26}{3},16,0,0)}+x_\ell^2\mathcal{P}_{(\frac{26}{3},0,-16,0)}+\mathcal{P}_{(-\frac{19}{12},0,2,0)} \\
&-24x_\ell^4\Bigg(\mathrm{Li}_2\left(-\frac{X_-}{X_+x_\ell}\right)-\mathrm{Li}_2\left(-\frac{X_-x_\ell}{X_+}\right) \\
&+2\mathrm{ArcTanh}(X_r)^2+\mathrm{ArcTanh}(X_r)\Bigg)-2p(x_\ell)(\ln(X_+)-\ln(x_\ell+1))\Bigg]
\end{aligned}
$$

$$
\begin{aligned}
&+\frac{1}{2}\ln^2(\hat{x})\left(p(x_\ell)-48x_\ell^4\mathrm{ArcTanh}(X_r)\right)+2\ln^2(X_+)p(x_\ell)\\
&+\ln(X_+)\Bigg[\left(x_\ell^8-1\right)\mathcal{P}_{(-\frac{19}{6},2,2,0)}-\left(x_\ell^4-1\right)x_\ell^2\mathcal{P}_{(-\frac{52}{3},16,16,0)}\\
&+48x_\ell^4\left(\mathrm{Li}_2\left(-\frac{X_-}{X_+x_\ell}\right)-\mathrm{Li}_2\left(-\frac{X_-x_\ell}{X_+}\right)\right)\\
&-4p(x_\ell)\ln(x_\ell+1)+144x_\ell^4\mathrm{ArcTanh}^2(X_r)\Bigg]\\
&+48x_\ell^4\mathrm{ArcTanh}^2(X_r)\ln(X_-)\\
&+\ln(1-x_\ell)\Bigg[8x_\ell^4\Bigg(6\Delta\mathrm{Li}_2\left(\frac{X_-}{1-X_r}\right)+6\Delta\mathrm{Li}_2\left(-\frac{X_-}{2x_\ell}\right)\\
&-6\Delta\mathrm{Li}_2\left(-\frac{1}{2}(X_r-1)(x_\ell+1)\right)\\
&-12\mathrm{Li}_2\left(\frac{X_r+1}{2}\right)+6\ln(X_-)\left(\ln(X_r+1)+\ln\left(\frac{x_\ell+1}{2}\right)\right)\\
&-6\ln(X_+)\left(\ln\left(\frac{1-X_r}{2}\right)+\ln(x_\ell+1)\right)+6\ln(2)\ln\left(1-X_r^2\right)\\
&-6\ln^2(X_r+1)+12\mathrm{ArcTanh}^2(X_r)+\pi^2-6\ln^2(2)\Bigg)\\
&+2p(x_\ell)\left(\ln(\hat{x})-2\ln(X_+)+\ln\left(1-X_r^2\right)\right)\Bigg]\\
&+\frac{1}{6}\Bigg(\mathcal{P}_{(0,0,-19,3)}+p(x_\ell)\Bigg(6\mathrm{Li}_2\left(-\frac{X_-}{X_+x_\ell}\right)+6\mathrm{Li}_2\left(-\frac{X_-x_\ell}{X_+}\right)\\
&+12\ln\left(1-X_r^2\right)\ln(x_\ell+1)+\pi^2\Bigg)\Bigg)\\
&+\mathrm{Li}_2\left(\frac{X_-}{1-X_r}\right)q_-(x_\ell)-\mathrm{Li}_2\left(\frac{X_+}{1+X_r}\right)q_+(x_\ell).
\end{aligned}
$$

All integrals here are given in terms of the integrals I_i in Eqs. (3.17-3.19) and $X_r = \sqrt{(\hat{x}-(1-x_\ell)^2)/(\hat{x}-(1+x_\ell)^2)}$. Above we introduced several additional functions. They read

$$X_\pm = (1-x_\ell)\pm X_r(1+x_\ell), \tag{A.5}$$

$$\mathcal{P}_{a,b,c,d} = a+b\ln(1-X_r)+c\ln(1+X_r)+d\ln^2(1-X_r^2), \tag{A.6}$$

$$\Delta\mathrm{Li}_n(f(X_r)) = \mathrm{Li}_n(f(X_r))-\mathrm{Li}_n(f(-X_r)), \tag{A.7}$$

$$p(x_\ell) = 1-8x_\ell^2+8x_\ell^6-x_\ell^8, \tag{A.8}$$

$$
\begin{aligned}
q_\pm(x_\ell) &= 1-8x_\ell^2-12x_\ell^4-8x_\ell^6+x_\ell^8\\
&\qquad -24x_\ell^4\ln(\hat{x})\pm 24x_\ell^4\ln\left(\frac{\hat{x}(1-X_r^2)}{X_+^2}\right),
\end{aligned} \tag{A.9}
$$

here we denote an arbitrary function depending on X_r by $f(X_r)$.

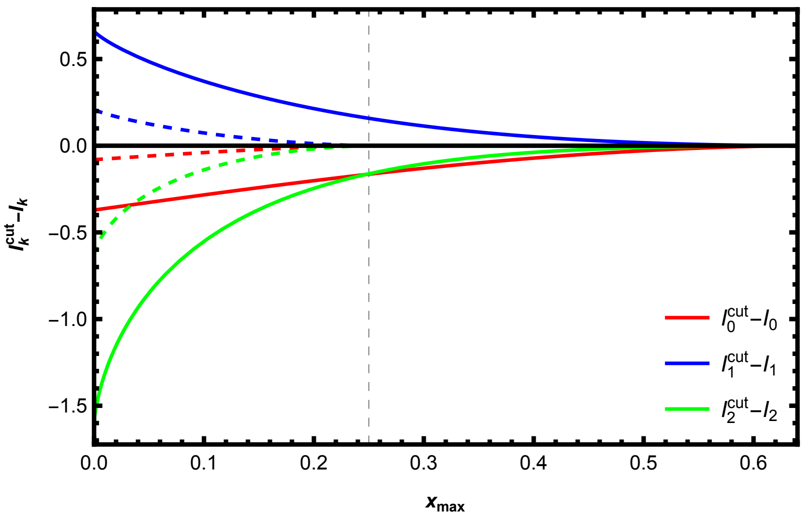

Figure A.1.: Difference of the integrals used for the integrated spectrum and the inclusive HSN decay width $I_k^{\text{cut}} - I_k$. We show the difference for $x_\ell = 0.2$ (closed line) and $x_\ell = 0.5$ (dashed line). The difference goes to zero when the upper limit of the integrated spectrum integral I_k^{cut} approaches $x_{\text{max}} \to (1 - x_\ell)^2$. The dashed line delimits the end of the spectrum $(1 - 0.5)^2 = 0.25$ for $x_\ell = 0.5$.

In Fig. A.1 we show $I_k^{\text{cut}} - I_k$ as a function of $\hat{x} = x_{\text{max}} \leq (1 - x_\ell)^2$ for two different values of x_ℓ.

B. Constants

Here we compile the numerical values of the quantities used in this work (see Tab. B.1).

Table B.1.: Table of numerical values used. The strong coupling constant at the charm and bottom scale was evaluated with the help of `RunDec` [132, 133] using the weighted average of $\alpha_s^{(5)}(M_Z)$ of all measurements included by the PDG except the one using τ decays. The $\overline{\text{MS}}$ mass of the top quark was obtained from the pole mass using the relation given in Ref. [189]. The pion decay constant f_{π^+} was calculated using f_{K^+} and f_{K^+}/f_{π^+}.

G_F	$1.166\,378\,5(6) \times 10^{-5}\,\text{GeV}^{-1}$	PDG Online [8]
$\sin^2\theta_w$	0.23122(6)	PDG Online [8]
$\lvert V_{ud}\rvert$	0.97367(32)	PDG Online [8]
$\lvert V_{us}\rvert$	0.22431(85)	PDG Online [8]
$\lvert V_{cd}\rvert$	0.221(4)	PDG Online [8]
$\lvert V_{cs}\rvert$	0.975(6)	PDG Online [8]
$\alpha_s^{(3)}(\overline{m}_c(\overline{m}_c))$	0.3911	
$\alpha_s^{(3)}(m_\tau)$	0.3160	
$\alpha_s^{(5)}(\overline{m}_b(\overline{m}_b))$	0.2256	
$\alpha_s^{(5)}(M_Z)$	0.1183	PDG Online [8]
$\alpha_s^{(6)}(\overline{m}_t(\overline{m}_t))$	0.1088	[189]
m_e	$0.510\,998\,950\,00(15)$ MeV	PDG Online [8]
m_μ	$105.658\,375\,5(23)$ MeV	PDG Online [8]
m_τ	$1.776\,94(9)$ GeV	HFLAV [144]
$\overline{m}_c(\overline{m}_c)$	1.280(13) GeV	FLAG [138, 190–195]
$\overline{m}_b(\overline{m}_b)$	4.183(7) GeV	PDG Online [8]
M_t^{Pole}	172.56(31) GeV	PDG Online [8]
$\overline{m}_t(\overline{m}_t)$	162.75 GeV	using Ref. [189]
M_Z	91.1880(20) GeV	PDG Online [8]
m_{π^+}	$139.570\,39(18)$ MeV	PDG Online [8]
m_{K^+}	493.677(15) MeV	PDG Online [8]
m_{D^+}	1869.66(5) MeV	PDG Online [8]
$m_{D_s^+}$	1968.35(7) MeV	PDG Online [8]
m_{D^0}	1864.84(5) MeV	PDG Online [8]
f_{π^+}	130.5(3) MeV	
f_{K^+}	155.7(3) MeV	FLAG [134–138]
f_{K^+}/f_{π^+}	1.1934(19)	FLAG [134, 135, 137–140]
f_{D^+}	212.0(7) MeV	FLAG [135, 138, 139]
$f_{D_s^+}$	249.9(5) MeV	FLAG [135, 138, 139]
$\mathcal{BR}^{\text{exp.}}(\tau \to \nu_\tau e \bar{\nu}_e)$	0.1785(4)	HFLAV [144]
$\mathcal{BR}^{\text{exp.}}(\tau \to \nu_\tau \mu \bar{\nu}_\mu)$	0.17366(36)	HFLAV [144]
$\mathcal{BR}^{\text{exp.}}(\tau \to \nu_\tau \pi)$	0.1082(5)	HFLAV [144]
$\mathcal{BR}^{\text{exp.}}(\tau \to \nu_\tau K)$	0.00697(10)	HFLAV [144]
$1/\alpha(m_\tau)$	133.50(2)	[157, 158]
$\tau_\tau^{\text{exp.}}$	290.29(53) fs	HFLAV [144]
τ_τ^{SM}	288.59(231) fs	PDG Print [8] and [145]
$\mathcal{B}_\tau^s$	0.0292(4)	PDG Print [8]
$\delta_{\text{RC}}^{(\pi)}$	0.0194(61)	from [147] and based on [148–151]
$\delta_{\text{RC}}^{(K)}$	0.0204(62)	from [147] and based on [148–151]

Bibliography

[1] Serguei Chatrchyan et al. “Observation of a New Boson at a Mass of 125 GeV with the CMS Experiment at the LHC”. In: *Phys. Lett. B* 716 (2012), pp. 30–61. DOI: 10.1016/j.physletb.2012.08.021. arXiv: 1207.7235 [hep-ex].

[2] Georges Aad et al. “Observation of a new particle in the search for the Standard Model Higgs boson with the ATLAS detector at the LHC”. In: *Phys. Lett. B* 716 (2012), pp. 1–29. DOI: 10.1016/j.physletb.2012.08.020. arXiv: 1207.7214 [hep-ex].

[3] Wolfgang Pauli. “Pauli letter collection”. Typed copy. URL: https://cds.cern.ch/record/83282.

[4] E. Fermi. “An attempt of a theory of beta radiation. 1.” In: *Z. Phys.* 88 (1934), pp. 161–177. DOI: 10.1007/BF01351864.

[5] C. L. Cowan et al. “Detection of the free neutrino: A Confirmation”. In: *Science* 124 (1956), pp. 103–104. DOI: 10.1126/science.124.3212.103.

[6] K. S. Hirata et al. “Observation in the Kamiokande-II Detector of the Neutrino Burst from Supernova SN 1987a”. In: *Phys. Rev. D* 38 (1988), pp. 448–458. DOI: 10.1103/PhysRevD.38.448.

[7] Max Aker et al. “Direct neutrino-mass measurement based on 259 days of KATRIN data”. In: *Science* 388.6743 (2025), adq9592. DOI: 10.1126/science.adq9592. arXiv: 2406.13516 [nucl-ex].

[8] S. Navas et al. “Review of Particle Physics”. In: *Phys. Rev. D* 110 (3 Aug. 2024), p. 030001. DOI: 10.1103/PhysRevD.110.030001. URL: https://link.aps.org/doi/10.1103/PhysRevD.110.030001.

[9] Peter Minkowski. “$\mu \to e\gamma$ at a Rate of One Out of 10^9 Muon Decays?” In: *Phys. Lett. B* 67 (1977), pp. 421–428. DOI: 10.1016/0370-2693(77)90435-X.

[10] Tsutomu Yanagida. “Horizontal gauge symmetry and masses of neutrinos”. In: *Conf. Proc. C* 7902131 (1979). Ed. by Osamu Sawada and Akio Sugamoto, pp. 95–99.

[11] S. L. Glashow. “The Future of Elementary Particle Physics”. In: *NATO Sci. Ser. B* 61 (1980). Ed. by Maurice Lévy et al., p. 687. DOI: 10.1007/978-1-4684-7197-7_15.

[12] Murray Gell-Mann, Pierre Ramond, and Richard Slansky. “Complex Spinors and Unified Theories”. In: *Conf. Proc. C* 790927 (1979), pp. 315–321. arXiv: 1306.4669 [hep-th].

[13] Rabindra N. Mohapatra and Goran Senjanovic. “Neutrino Mass and Spontaneous Parity Nonconservation”. In: *Phys. Rev. Lett.* 44 (1980), p. 912. DOI: 10.1103/PhysRevLett.44.912.

[14] Andrea Giuliani. "The Quest for Neutrinoless Double Beta Decay: Progress and Prospects". In: *Phys. Cosmos* 1.1 (2026), p. 6. DOI: 10.53941/pac.2026.100006. arXiv: 2604.13696 [nucl-ex].

[15] Takehiko Asaka and Mikhail Shaposhnikov. "The νMSM, dark matter and baryon asymmetry of the universe". In: *Physics Letters B* 620.1–2 (July 2005), pp. 17–26. ISSN: 0370-2693. DOI: 10.1016/j.physletb.2005.06.020. URL: http://dx.doi.org/10.1016/j.physletb.2005.06.020.

[16] Takehiko Asaka, Steve Blanchet, and Mikhail Shaposhnikov. "The νMSM, dark matter and neutrino masses". In: *Physics Letters B* 631.4 (Dec. 2005), pp. 151–156. ISSN: 0370-2693. DOI: 10.1016/j.physletb.2005.09.070. URL: http://dx.doi.org/10.1016/j.physletb.2005.09.070.

[17] M. Fukugita and T. Yanagida. "Baryogenesis Without Grand Unification". In: *Phys. Lett. B* 174 (1986), pp. 45–47. DOI: 10.1016/0370-2693(86)91126-3.

[18] Sacha Davidson and Alejandro Ibarra. "A Lower bound on the right-handed neutrino mass from leptogenesis". In: *Phys. Lett. B* 535 (2002), pp. 25–32. DOI: 10.1016/S0370-2693(02)01735-5. arXiv: hep-ph/0202239.

[19] Asli M. Abdullahi et al. "The present and future status of heavy neutral leptons". In: *J. Phys. G* 50.2 (2023), p. 020501. DOI: 10.1088/1361-6471/ac98f9. arXiv: 2203.08039 [hep-ph].

[20] X. Fan et al. "Measurement of the Electron Magnetic Moment". In: *Phys. Rev. Lett.* 130.7 (2023), p. 071801. DOI: 10.1103/PhysRevLett.130.071801. arXiv: 2209.13084 [physics.atom-ph].

[21] Andrzej Buras. *Gauge Theory of Weak Decays*. Cambridge University Press, June 2020. ISBN: 978-1-139-52410-0, 978-1-107-03403-7. DOI: 10.1017/9781139524100.

[22] F. Englert and R. Brout. "Broken Symmetry and the Mass of Gauge Vector Mesons". In: *Phys. Rev. Lett.* 13 (1964). Ed. by J. C. Taylor, pp. 321–323. DOI: 10.1103/PhysRevLett.13.321.

[23] Peter W. Higgs. "Broken symmetries, massless particles and gauge fields". In: *Phys. Lett.* 12 (1964), pp. 132–133. DOI: 10.1016/0031-9163(64)91136-9.

[24] Peter W. Higgs. "Broken Symmetries and the Masses of Gauge Bosons". In: *Phys. Rev. Lett.* 13 (1964). Ed. by J. C. Taylor, pp. 508–509. DOI: 10.1103/PhysRevLett.13.508.

[25] G. S. Guralnik, C. R. Hagen, and T. W. B. Kibble. "Global Conservation Laws and Massless Particles". In: *Phys. Rev. Lett.* 13 (1964). Ed. by J. C. Taylor, pp. 585–587. DOI: 10.1103/PhysRevLett.13.585.

[26] Peter W. Higgs. "Spontaneous Symmetry Breakdown without Massless Bosons". In: *Phys. Rev.* 145 (1966), pp. 1156–1163. DOI: 10.1103/PhysRev.145.1156.

[27] T. W. B. Kibble. "Symmetry breaking in nonAbelian gauge theories". In: *Phys. Rev.* 155 (1967). Ed. by J. C. Taylor, pp. 1554–1561. DOI: 10.1103/PhysRev.155.1554.

[28] Nicola Cabibbo. "Unitary Symmetry and Leptonic Decays". In: *Phys. Rev. Lett.* 10 (1963), pp. 531–533. DOI: 10.1103/PhysRevLett.10.531.

[29] Makoto Kobayashi and Toshihide Maskawa. “CP Violation in the Renormalizable Theory of Weak Interaction”. In: *Prog. Theor. Phys.* 49 (1973), pp. 652–657. DOI: 10.1143/PTP.49.652.

[30] John C. Collins. *Renormalization : An Introduction to Renormalization, the Renormalization Group and the Operator-Product Expansion.* Vol. 26. Cambridge Monographs on Mathematical Physics. Cambridge: Cambridge University Press, 1984. ISBN: 978-0-521-31177-9, 978-0-511-86739-2, 978-1-009-40180-7, 978-1-009-40176-0, 978-1-009-40179-1. DOI: 10.1017/9781009401807.

[31] Michael E. Peskin and Daniel V. Schroeder. *An Introduction to quantum field theory.* Reading, USA: Addison-Wesley, 1995. ISBN: 978-0-201-50397-5, 978-0-429-50355-9, 978-0-429-49417-8. DOI: 10.1201/9780429503559.

[32] Matthew D. Schwartz. *Quantum Field Theory and the Standard Model.* Cambridge University Press, Mar. 2014. ISBN: 978-1-107-03473-0, 978-1-107-03473-0. DOI: 10.1017/9781139540940.

[33] Joshua Ellis. “TikZ-Feynman: Feynman diagrams with TikZ”. In: *Comput. Phys. Commun.* 210 (2017), pp. 103–123. DOI: 10.1016/j.cpc.2016.08.019. arXiv: 1601.05437 [hep-ph].

[34] Gerard ’t Hooft and M. J. G. Veltman. “Regularization and Renormalization of Gauge Fields”. In: *Nucl. Phys. B* 44 (1972), pp. 189–213. DOI: 10.1016/0550-3213(72)90279-9.

[35] S. A. Larin. “The Renormalization of the axial anomaly in dimensional regularization”. In: *Phys. Lett. B* 303 (1993), pp. 113–118. DOI: 10.1016/0370-2693(93)90053-K. arXiv: hep-ph/9302240.

[36] Andrzej J. Buras and Peter H. Weisz. “QCD Nonleading Corrections to Weak Decays in Dimensional Regularization and ’t Hooft-Veltman Schemes”. In: *Nucl. Phys. B* 333 (1990), pp. 66–99. DOI: 10.1016/0550-3213(90)90223-Z.

[37] Andrei I. Davydychev. “A Simple formula for reducing Feynman diagrams to scalar integrals”. In: *Phys. Lett. B* 263 (1991), pp. 107–111. DOI: 10.1016/0370-2693(91)91715-8.

[38] William A. Bardeen et al. “Deep Inelastic Scattering Beyond the Leading Order in Asymptotically Free Gauge Theories”. In: *Phys. Rev. D* 18 (1978), p. 3998. DOI: 10.1103/PhysRevD.18.3998.

[39] David J. Gross and Frank Wilczek. “Ultraviolet Behavior of Non-Abelian Gauge Theories”. In: *Phys. Rev. Lett.* 30 (26 June 1973), pp. 1343–1346. DOI: 10.1103/PhysRevLett.30.1343. URL: https://link.aps.org/doi/10.1103/PhysRevLett.30.1343.

[40] H. David Politzer. “Reliable Perturbative Results for Strong Interactions?” In: *Phys. Rev. Lett.* 30 (26 June 1973), pp. 1346–1349. DOI: 10.1103/PhysRevLett.30.1346. URL: https://link.aps.org/doi/10.1103/PhysRevLett.30.1346.

[41] William E. Caswell. "Asymptotic Behavior of Non-Abelian Gauge Theories to Two-Loop Order". In: *Phys. Rev. Lett.* 33 (4 July 1974), pp. 244–246. DOI: 10.1103/PhysRevLett.33.244. URL: https://link.aps.org/doi/10.1103/PhysRevLett.33.244.

[42] D.R.T. Jones. "Two-loop diagrams in Yang-Mills theory". In: *Nuclear Physics B* 75.3 (1974), pp. 531–538. ISSN: 0550-3213. DOI: https://doi.org/10.1016/0550-3213(74)90093-5. URL: https://www.sciencedirect.com/science/article/pii/0550321374900935.

[43] O. V. Tarasov, A. A. Vladimirov, and A. Yu. Zharkov. "The Gell-Mann-Low Function of QCD in the Three Loop Approximation". In: *Phys. Lett. B* 93 (1980), pp. 429–432. DOI: 10.1016/0370-2693(80)90358-5.

[44] S. A. Larin and J. A. M. Vermaseren. "The Three loop QCD Beta function and anomalous dimensions". In: *Phys. Lett. B* 303 (1993), pp. 334–336. DOI: 10.1016/0370-2693(93)91441-O. arXiv: hep-ph/9302208.

[45] R. Tarrach. "The Pole Mass in Perturbative QCD". In: *Nucl. Phys. B* 183 (1981), pp. 384–396. DOI: 10.1016/0550-3213(81)90140-1.

[46] O. V. Tarasov. "Anomalous dimensions of quark masses in the three-loop approximation". In: *Phys. Part. Nucl. Lett.* 17.2 (2020), pp. 109–115. DOI: 10.1134/S1547477120020223. arXiv: 1910.12231 [hep-ph].

[47] K. G. Chetyrkin, Johann H. Kuhn, and A. A. Pivovarov. "Determining the strange quark mass in Cabibbo suppressed tau lepton decays". In: *Nucl. Phys. B* 533 (1998), pp. 473–493. DOI: 10.1016/S0550-3213(98)00511-2. arXiv: hep-ph/9805335.

[48] C. Becchi et al. "Light Quark Masses in Quantum Chromodynamics and Chiral Symmetry Breaking". In: *Z. Phys. C* 8 (1981), p. 335. DOI: 10.1007/BF01546328.

[49] David J. Broadhurst. "Chiral symmetry breaking and perturbative QCD". In: *Phys. Lett. B* 101 (1981), pp. 423–426. DOI: 10.1016/0370-2693(81)90167-2.

[50] Antonio Pich. "Precision physics with inclusive QCD processes". In: *Prog. Part. Nucl. Phys.* 117 (2021), p. 103846. DOI: 10.1016/j.ppnp.2020.103846. arXiv: 2012.04716 [hep-ph].

[51] Eduardo de Rafael. "An Introduction to sum rules in QCD: Course". In: *Les Houches Summer School in Theoretical Physics, Session 68: Probing the Standard Model of Particle Interactions.* July 1997, pp. 1171–1218. arXiv: hep-ph/9802448.

[52] Antonio Rodríguez-Sánchez. "Hadronic tau decays". In: (Apr. 2025). arXiv: 2504.21732 [hep-ph].

[53] P. A. Baikov, K. G. Chetyrkin, and Johann H. Kuhn. "Order α_s^4 QCD Corrections to Z and τ Decays". In: *Phys. Rev. Lett.* 101 (2008), p. 012002. DOI: 10.1103/PhysRevLett.101.012002. arXiv: 0801.1821 [hep-ph].

[54] P. A. Baikov et al. "Complete $O(\alpha_s^4)$ QCD Corrections to Hadronic Z-Decays". In: *Phys. Rev. Lett.* 108 (2012), p. 222003. DOI: 10.1103/PhysRevLett.108.222003. arXiv: 1201.5804 [hep-ph].

[55] P. A. Baikov et al. “Adler Function, Sum Rules and Crewther Relation of Order $\mathcal{O}(\alpha_s^4)$: the Singlet Case”. In: *Phys. Lett. B* 714 (2012), pp. 62–65. DOI: 10.1016/j.physletb.2012.06.052. arXiv: 1206.1288 [hep-ph].

[56] K. G. Chetyrkin. “Correlator of the quark scalar currents and $\Gamma_{tot}(H \longrightarrow \text{hadrons})$ at $\mathcal{O}(\alpha_s^3)$ in pQCD”. In: *Phys. Lett. B* 390 (1997), pp. 309–317. DOI: 10.1016/S0370-2693(96)01368-8. arXiv: hep-ph/9608318.

[57] K. G. Chetyrkin and Johann H. Kuhn. “Quadratic mass corrections of order $\mathcal{O}(\alpha_s^3 m_q^2/s)$ to the decay rate of Z and W bosons”. In: *Phys. Lett. B* 406 (1997), pp. 102–109. DOI: 10.1016/S0370-2693(97)00631-X. arXiv: hep-ph/9609202.

[58] P. A. Baikov, K. G. Chetyrkin, and Johann H. Kuhn. “Strange quark mass from tau lepton decays with $\mathcal{O}(\alpha_s^3)$ accuracy”. In: *Phys. Rev. Lett.* 95 (2005), p. 012003. DOI: 10.1103/PhysRevLett.95.012003. arXiv: hep-ph/0412350.

[59] P. A. Baikov, Konstantin G. Chetyrkin, and Johann H. Kuhn. “Towards order α_s^4 accuracy in τ-decays”. In: *Phys. Rev. D* 67 (2003), p. 074026. DOI: 10.1103/PhysRevD.67.074026. arXiv: hep-ph/0212299.

[60] Martin Beneke and Matthias Jamin. “α_s and the τ hadronic width: fixed-order, contour- improved and higher-order perturbation theory”. In: *Journal of High Energy Physics* 2008.09 (Sept. 2008), pp. 044–044. ISSN: 1029-8479. DOI: 10.1088/1126-6708/2008/09/044. URL: http://dx.doi.org/10.1088/1126-6708/2008/09/044.

[61] K. G. Chetyrkin, A. L. Kataev, and F. V. Tkachov. “Higher Order Corrections to $\sigma_{\text{tot}}(e^+e^- \longrightarrow \text{Hadrons})$ in Quantum Chromodynamics”. In: *Phys. Lett. B* 85 (1979), pp. 277–279. DOI: 10.1016/0370-2693(79)90596-3.

[62] Michael Dine and Jonathan Sapirstein. “Higher-Order Quantum Chromodynamic Corrections in e^+e^- Annihilation”. In: *Phys. Rev. Lett.* 43 (10 Sept. 1979), pp. 668–671. DOI: 10.1103/PhysRevLett.43.668. URL: https://link.aps.org/doi/10.1103/PhysRevLett.43.668.

[63] William Celmaster and Richard J. Gonsalves. “Analytic Calculation of Higher-Order Quantum-Chromodynamic Corrections in e^+e^- Annihilation”. In: *Phys. Rev. Lett.* 44 (9 Mar. 1980), pp. 560–564. DOI: 10.1103/PhysRevLett.44.560. URL: https://link.aps.org/doi/10.1103/PhysRevLett.44.560.

[64] S. G. Gorishnii, A. L. Kataev, and S. A. Larin. “Next-To-Leading $\mathcal{O}(\alpha_s^3)$ QCD Correction to $\sigma_{\text{tot}}(e^+e^- \longrightarrow \text{Hadrons})$: Analytical Calculation and Estimation of the Parameter Lambda (MS)”. In: *Phys. Lett. B* 212 (1988), pp. 238–244. DOI: 10.1016/0370-2693(88)90532-1.

[65] Levan R. Surguladze and Mark A. Samuel. “Total hadronic cross-section in e^+e^- annihilation at the four-loop level of perturbative QCD”. In: *Phys. Rev. Lett.* 66 (1991). [Erratum: Phys.Rev.Lett. 66, 2416 (1991)], pp. 560–563. DOI: 10.1103/PhysRevLett.66.560.

[66] S. G. Gorishnii, A. L. Kataev, and S. A. Larin. “The $O(\alpha_s^3)$-corrections to $\sigma_{tot}(e^+e^- \to$ hadrons) and $\Gamma(\tau^- \to \nu_\tau +$ hadrons) in QCD”. In: *Phys. Lett. B* 259 (1991), pp. 144–150. DOI: 10.1016/0370-2693(91)90149-K.

[67] Stephen L. Adler. “Some Simple Vacuum Polarization Phenomenology: $e^+e^- \to$ Hadrons: The muonic-atom x-Ray Discrepancy and $g_\mu - 2$”. In: *Phys. Rev. D* 10 (1974), p. 3714. DOI: 10.1103/PhysRevD.10.3714.

[68] Werner Bernreuther and Werner Wetzel. “Order α_s^2 Massive Quark Contribution to the Vacuum Polarization of Massless Quarks”. In: *Z. Phys. C* 11 (1981), p. 113. DOI: 10.1007/BF01573992.

[69] S. G. Gorishnii, A. L. Kataev, and S. A. Larin. “Three Loop Corrections of Order $\mathcal{O}(m^2)$ to the Correlator of Electromagnetic Quark Currents”. In: *Nuovo Cim. A* 92 (1986), pp. 119–131. DOI: 10.1007/BF02727185.

[70] S. C. Generalis. “Improved two loop quark mass corrections”. In: *J. Phys. G* 15 (1989), pp. L225–L229. DOI: 10.1088/0954-3899/15/11/001.

[71] K. G. Chetyrkin and A. Kwiatkowski. “Mass corrections to the tau decay rate”. In: *Z. Phys. C* 59 (1993), pp. 525–532. DOI: 10.1007/BF01498634. arXiv: hep-ph/9805232.

[72] S. G. Gorishnii et al. “Corrected Three Loop QCD Correction to the Correlator of the Quark Scalar Currents and $\Gamma_{\text{tot}}(H^0 \to$ hadrons)”. In: *Mod. Phys. Lett. A* 5 (1990), pp. 2703–2712. DOI: 10.1142/S0217732390003152.

[73] S. G. Gorishnii et al. “Scheme dependence of the next to next-to-leading QCD corrections to $\Gamma_{\text{tot}}(H^0 \to$ hadrons) and the spurious QCD infrared fixed point”. In: *Phys. Rev. D* 43 (1991), pp. 1633–1640. DOI: 10.1103/PhysRevD.43.1633.

[74] K. G. Chetyrkin et al. “Mass singularities in light quark correlators: The Strange quark case”. In: *Phys. Rev. D* 51 (1995), pp. 5090–5100. DOI: 10.1103/PhysRevD.51.5090. arXiv: hep-ph/9409371.

[75] K. G. Chetyrkin, Johann H. Kuhn, and A. Kwiatkowski. “QCD corrections to the e^+e^- cross-section and the Z boson decay rate”. In: *Phys. Rept.* 277 (1996), pp. 189–281. DOI: 10.1016/S0370-1573(96)00012-9. arXiv: hep-ph/9503396.

[76] K. G. Chetyrkin, R. V. Harlander, and Johann H. Kuhn. “Quartic mass corrections to R_{had} at $\mathcal{O}(\alpha_s^3)$”. In: *Nucl. Phys. B* 586 (2000). [Erratum: Nucl.Phys.B 634, 413–414 (2002)], pp. 56–72. DOI: 10.1016/S0550-3213(00)00393-X. arXiv: hep-ph/0005139.

[77] Stephen L. Adler. “Axial-Vector Vertex in Spinor Electrodynamics”. In: *Phys. Rev.* 177 (5 Jan. 1969), pp. 2426–2438. DOI: 10.1103/PhysRev.177.2426. URL: https://link.aps.org/doi/10.1103/PhysRev.177.2426.

[78] J. S. Bell and R. Jackiw. “A PCAC puzzle: $\pi^0 \to \gamma\gamma$ in the σ model”. In: *Nuovo Cim. A* 60 (1969), pp. 47–61. DOI: 10.1007/BF02823296.

[79] J. Collins, F. Wilczek, and A. Zee. “Low-energy manifestations of heavy particles: Application to the neutral current”. In: *Phys. Rev. D* 18 (1 July 1978), pp. 242–247. DOI: 10.1103/PhysRevD.18.242. URL: https://link.aps.org/doi/10.1103/PhysRevD.18.242.

[80] K. G. Chetyrkin and Johann H. Kuhn. “Complete QCD corrections of order α_s^2 to the Z decay rate”. In: *Phys. Lett. B* 308 (1993), pp. 127–136. DOI: 10.1016/0370-2693(93)90613-M.

[81] Jörg Rittinger. “Totale Zerfallsrate des Z-Bosons nach Hadronen zur Ordnung α_s^4”. PhD thesis. KIT, Karlsruhe, 2012. DOI: 10.5445/IR/1000028694.

[82] Bernd A. Kniehl and Johann H. Kuhn. “QCD Corrections to the Axial Part of the Z Decay Rate”. In: *Phys. Lett. B* 224 (1989), pp. 229–232. DOI: 10.1016/0370-2693(89)91079-4.

[83] Bernd A. Kniehl and Johann H. Kuhn. “QCD Corrections to the Z Decay Rate”. In: *Nucl. Phys. B* 329 (1990), pp. 547–573. DOI: 10.1016/0550-3213(90)90070-T.

[84] Jiro Kodaira. “QCD Higher Order Effects in Polarized Electroproduction: Flavor Singlet Coefficient Functions”. In: *Nucl. Phys. B* 165 (1980), pp. 129–140. DOI: 10.1016/0550-3213(80)90310-7.

[85] Raymond Davis Jr., Don S. Harmer, and Kenneth C. Hoffman. “Search for neutrinos from the sun”. In: *Phys. Rev. Lett.* 20 (1968), pp. 1205–1209. DOI: 10.1103/PhysRevLett.20.1205.

[86] John N. Bahcall, Neta A. Bahcall, and Giora Shaviv. “Present Status of the Theoretical Predictions for the ^{37}Cl Solar-Neutrino Experiment”. In: *Phys. Rev. Lett.* 20 (21 May 1968), pp. 1209–1212. DOI: 10.1103/PhysRevLett.20.1209. URL: https://link.aps.org/doi/10.1103/PhysRevLett.20.1209.

[87] K. S. Hirata et al. “Results from one thousand days of real time directional solar neutrino data”. In: *Phys. Rev. Lett.* 65 (1990), pp. 1297–1300. DOI: 10.1103/PhysRevLett.65.1297.

[88] P. Anselmann et al. “Solar neutrinos observed by GALLEX at Gran Sasso.” In: *Phys. Lett. B* 285 (1992), pp. 376–389. DOI: 10.1016/0370-2693(92)91521-A.

[89] P. Anselmann et al. “Implications of the GALLEX determination of the solar neutrino flux.” In: *Phys. Lett. B* 285 (1992), pp. 390–397. DOI: 10.1016/0370-2693(92)91522-B.

[90] A. I. Abazov et al. “Search for neutrinos from the sun using the reaction ^{71}Ga (ν_e, e^-) ^{71}Ge”. In: *Phys. Rev. Lett.* 67 (1991), pp. 3332–3335. DOI: 10.1103/PhysRevLett.67.3332.

[91] V. N. Gavrin et al. “Latest results from the Soviet-American gallium experiment”. In: *AIP Conf. Proc.* 272 (2008). Ed. by J. R. Sanford, pp. 1101–1110. DOI: 10.1063/1.43281.

[92] B. Pontecorvo. “Neutrino Experiments and the Problem of Conservation of Leptonic Charge”. In: *Sov. Phys. JETP* 26 (1968), pp. 984–988.

[93] V. N. Gribov and B. Pontecorvo. “Neutrino astronomy and lepton charge”. In: *Phys. Lett. B* 28 (1969), p. 493. DOI: 10.1016/0370-2693(69)90525-5.

[94] Y. Fukuda et al. “Evidence for oscillation of atmospheric neutrinos”. In: *Phys. Rev. Lett.* 81 (1998), pp. 1562–1567. DOI: 10.1103/PhysRevLett.81.1562. arXiv: hep-ex/9807003.

[95] Q. R. Ahmad et al. "Measurement of the Rate of $\nu_e + d \to p + p + e^-$ Interactions Produced by ^8B Solar Neutrinos at the Sudbury Neutrino Observatory". In: *Phys. Rev. Lett.* 87 (7 July 2001), p. 071301. DOI: 10.1103/PhysRevLett.87.071301. URL: https://link.aps.org/doi/10.1103/PhysRevLett.87.071301.

[96] Q. R. Ahmad et al. "Direct Evidence for Neutrino Flavor Transformation from Neutral-Current Interactions in the Sudbury Neutrino Observatory". In: *Phys. Rev. Lett.* 89 (1 June 2002), p. 011301. DOI: 10.1103/PhysRevLett.89.011301. URL: https://link.aps.org/doi/10.1103/PhysRevLett.89.011301.

[97] Takaaki Kajita. "Nobel Lecture: Discovery of atmospheric neutrino oscillations". In: *Rev. Mod. Phys.* 88.3 (2016), p. 030501. DOI: 10.1103/RevModPhys.88.030501.

[98] Arthur B. McDonald. "Nobel Lecture: The Sudbury Neutrino Observatory: Observation of flavor change for solar neutrinos". In: *Rev. Mod. Phys.* 88.3 (2016), p. 030502. DOI: 10.1103/RevModPhys.88.030502.

[99] Samoil Bilenky. *Introduction to the Physics of Massive and Mixed Neutrinos.* Vol. 947. Springer, 2018. ISBN: 978-3-319-74801-6, 978-3-319-74802-3. DOI: 10.1007/978-3-319-74802-3.

[100] Stephen F. King. "Right-handed neutrinos: seesaw models and signatures". In: Feb. 2025. arXiv: 2502.07877 [hep-ph].

[101] B. Pontecorvo. "Mesonium and Antimesonium". In: *Sov. Phys. JETP* 6 (1958), pp. 429–431.

[102] B. Pontecorvo. "Inverse Beta Processes and Nonconservation of Lepton Charge". In: *Sov. Phys. JETP* 7 (1958), pp. 172–173.

[103] Ziro Maki, Masami Nakagawa, and Shoichi Sakata. "Remarks on the unified model of elementary particles". In: *Prog. Theor. Phys.* 28 (1962), pp. 870–880. DOI: 10.1143/PTP.28.870.

[104] Ettore Majorana. "Teoria simmetrica dell'elettrone e del positrone". In: *Nuovo Cim.* 14 (1937), pp. 171–184. DOI: 10.1007/BF02961314.

[105] H. Lacker and A. Menzel. "Simultaneous Extraction of the Fermi constant and PMNS matrix elements in the presence of a fourth generation". In: *JHEP* 07 (2010), p. 006. DOI: 10.1007/JHEP07(2010)006. arXiv: 1003.4532 [hep-ph].

[106] Carlo Giunti and Chung W. Kim. *Fundamentals of Neutrino Physics and Astrophysics.* 2007. ISBN: 978-0-19-850871-7. DOI: 10.1093/acprof:oso/9780198508717.001.0001.

[107] Kyrylo Bondarenko et al. "Phenomenology of GeV-scale Heavy Neutral Leptons". In: *JHEP* 11 (2018), p. 032. DOI: 10.1007/JHEP11(2018)032. arXiv: 1805.08567 [hep-ph].

[108] Robert E. Shrock. "General Theory of Weak Processes Involving Neutrinos. 2. Pure Leptonic Decays". In: *Phys. Rev. D* 24 (1981), p. 1275. DOI: 10.1103/PhysRevD.24.1275.

[109] Loretta M. Johnson, Douglas W. McKay, and Tim Bolton. "Extending sensitivity for low-mass neutral heavy lepton searches". In: *Physical Review D* 56.5 (Sept. 1997), pp. 2970–2981. ISSN: 1089-4918. DOI: 10.1103/physrevd.56.2970. URL: http://dx.doi.org/10.1103/PhysRevD.56.2970.

[110] Vladimir Gribanov, Sergey Kovalenko, and Ivan Schmidt. "Sterile neutrinos in tau lepton decays". In: *Nuclear Physics B* 607.1–2 (July 2001), pp. 355–368. ISSN: 0550-3213. DOI: 10.1016/s0550-3213(01)00169-9. URL: http://dx.doi.org/10.1016/S0550-3213(01)00169-9.

[111] Dmitry Gorbunov and Mikhail Shaposhnikov. "How to find neutral leptons of the ν MSM?" In: *Journal of High Energy Physics* 2007.10 (Oct. 2007), pp. 015–015. ISSN: 1029-8479. DOI: 10.1088/1126-6708/2007/10/015. URL: http://dx.doi.org/10.1088/1126-6708/2007/10/015.

[112] Anupama Atre et al. "The search for heavy Majorana neutrinos". In: *Journal of High Energy Physics* 2009.05 (May 2009), pp. 030–030. ISSN: 1029-8479. DOI: 10.1088/1126-6708/2009/05/030. URL: http://dx.doi.org/10.1088/1126-6708/2009/05/030.

[113] Juan Carlos Helo, Sergey Kovalenko, and Ivan Schmidt. "Sterile neutrinos in lepton number and lepton flavor violating decays". In: *Nuclear Physics B* 853.1 (Dec. 2011), pp. 80–104. ISSN: 0550-3213. DOI: 10.1016/j.nuclphysb.2011.07.020. URL: http://dx.doi.org/10.1016/j.nuclphysb.2011.07.020.

[114] Gorazd Cvetič and C. S. Kim. "Rare decays of B mesons via on-shell sterile neutrinos". In: *Phys. Rev. D* 94 (5 Sept. 2016), p. 053001. DOI: 10.1103/PhysRevD.94.053001. URL: https://link.aps.org/doi/10.1103/PhysRevD.94.053001.

[115] R. Mertig, M. Bohm, and Ansgar Denner. "FEYN CALC: Computer algebraic calculation of Feynman amplitudes". In: *Comput. Phys. Commun.* 64 (1991), pp. 345–359. DOI: 10.1016/0010-4655(91)90130-D.

[116] Vladyslav Shtabovenko, Rolf Mertig, and Frederik Orellana. "New Developments in FeynCalc 9.0". In: *Comput. Phys. Commun.* 207 (2016), pp. 432–444. DOI: 10.1016/j.cpc.2016.06.008. arXiv: 1601.01167 [hep-ph].

[117] Vladyslav Shtabovenko, Rolf Mertig, and Frederik Orellana. "FeynCalc 9.3: New features and improvements". In: *Comput. Phys. Commun.* 256 (2020), p. 107478. DOI: 10.1016/j.cpc.2020.107478. arXiv: 2001.04407 [hep-ph].

[118] Vladyslav Shtabovenko, Rolf Mertig, and Frederik Orellana. "FeynCalc 10: Do multiloop integrals dream of computer codes?" In: *Comput. Phys. Commun.* 306 (2025), p. 109357. DOI: 10.1016/j.cpc.2024.109357. arXiv: 2312.14089 [hep-ph].

[119] K. Schilcher and Minh D. Tran. "Duality in Semileptonic τ Decay". In: *Phys. Rev. D* 29 (1984), p. 570. DOI: 10.1103/PhysRevD.29.570.

[120] E. Braaten. "QCD Predictions for the Decay of the tau Lepton". In: *Phys. Rev. Lett.* 60 (1988), pp. 1606–1609. DOI: 10.1103/PhysRevLett.60.1606.

[121] Stephan Narison and A. Pich. "QCD Formulation of the tau Decay and Determination of Lambda (MS)". In: *Phys. Lett. B* 211 (1988), pp. 183–188. DOI: 10.1016/0370-2693(88)90830-1.

[122] E. Braaten, Stephan Narison, and A. Pich. "QCD analysis of the tau hadronic width". In: *Nucl. Phys. B* 373 (1992), pp. 581–612. DOI: 10.1016/0550-3213(92)90267-F.

[123] E. C. Poggio, Helen R. Quinn, and Steven Weinberg. "Smearing the Quark Model". In: *Phys. Rev. D* 13 (1976), p. 1958. DOI: 10.1103/PhysRevD.13.1958.

[124] R. Shankar. "Determination of the quark-gluon coupling constant". In: *Phys. Rev. D* 15 (3 Feb. 1977), pp. 755–758. DOI: 10.1103/PhysRevD.15.755. URL: https://link.aps.org/doi/10.1103/PhysRevD.15.755.

[125] C. S. Lam and T. M. Yan. "Decays of a heavy lepton and an intermediate weak boson in quantum chromodynamics". In: *Phys. Rev. D* 16 (3 Aug. 1977), pp. 703–706. DOI: 10.1103/PhysRevD.16.703. URL: https://link.aps.org/doi/10.1103/PhysRevD.16.703.

[126] Tim Kretz and Ulrich Nierste. "QCD corrections to charged-current decays with Heavy Sterile Neutrinos in initial or final state and their impact on τ decays". In: *JHEP* 06 (2026), p. 146. DOI: 10.1007/JHEP06(2026)146. arXiv: 2512.00476 [hep-ph].

[127] Andrzej J. Buras et al. "Charm quark contribution to $K^+ \to \pi^+ \nu\bar{\nu}$ at next-to-next-to-leading order". In: *JHEP* 11 (2006). [Erratum: JHEP 11, 167 (2012)], p. 002. DOI: 10.1007/JHEP11(2012)167. arXiv: hep-ph/0603079.

[128] K. G. Chetyrkin and Johann H. Kuhn. "Neutral current in the heavy top quark limit and the renormalization of the singlet axial current". In: *Z. Phys. C* 60 (1993), pp. 497–502. DOI: 10.1007/BF01560047.

[129] Konstantin G. Chetyrkin. Private communication. 2024.

[130] K. G. Chetyrkin and O. V. Tarasov. "The α_s^3 corrections to the effective neutral current and to the Z decay rate in the heavy top quark limit". In: *Phys. Lett. B* 327 (1994), pp. 114–122. DOI: 10.1016/0370-2693(94)91538-5. arXiv: hep-ph/9312323.

[131] Martin Gorbahn. "QCD and QED anomalous dimension matrix for weak decays at NNLO". PhD thesis. Oct. 2003.

[132] K. G. Chetyrkin, Johann H. Kuhn, and M. Steinhauser. "RunDec: A Mathematica package for running and decoupling of the strong coupling and quark masses". In: *Comput. Phys. Commun.* 133 (2000), pp. 43–65. DOI: 10.1016/S0010-4655(00)00155-7. arXiv: hep-ph/0004189.

[133] Florian Herren and Matthias Steinhauser. "Version 3 of RunDec and CRunDec". In: *Comput. Phys. Commun.* 224 (2018), pp. 333–345. DOI: 10.1016/j.cpc.2017.11.014. arXiv: 1703.03751 [hep-ph].

[134] R. J. Dowdall et al. "V_{us} from π and K decay constants in full lattice QCD with physical u, d, s and c quarks". In: *Phys. Rev. D* 88 (2013), p. 074504. DOI: 10.1103/PhysRevD.88.074504. arXiv: 1303.1670 [hep-lat].

[135] N. Carrasco et al. “Leptonic decay constants f_K, f_D, and f_{D_s} with $N_f = 2 + 1 + 1$ twisted-mass lattice QCD”. In: *Phys. Rev. D* 91.5 (2015), p. 054507. DOI: 10.1103/PhysRevD.91.054507. arXiv: 1411.7908 [hep-lat].

[136] [FNAL/MILC 14A] A. Bazavov et al. “Charmed and light pseudoscalar meson decay constants from four-flavor lattice QCD with physical light quarks”. In: *Phys.Rev.* D90.7 (2014), p. 074509. DOI: 10.1103/PhysRevD.90.074509. arXiv: 1407.3772 [hep-lat].

[137] C. Alexandrou et al. “Ratio of kaon and pion leptonic decay constants with $N_f = 2 + 1 + 1$ Wilson-clover twisted-mass fermions”. In: *Phys. Rev. D* 104.7 (2021), p. 074520. DOI: 10.1103/PhysRevD.104.074520. arXiv: 2104.06747 [hep-lat].

[138] Y. Aoki et al. “FLAG review 2024”. In: *Phys. Rev. D* 113.1 (2026), p. 014508. DOI: 10.1103/nfzp-p5dn. arXiv: 2411.04268 [hep-lat].

[139] A. Bazavov et al. “*B*- and *D*-meson leptonic decay constants from four-flavor lattice QCD”. In: *Phys. Rev. D* 98.7 (2018), p. 074512. DOI: 10.1103/PhysRevD.98.074512. arXiv: 1712.09262 [hep-lat].

[140] Nolan Miller et al. “F_K/F_π from Möbius Domain-Wall fermions solved on gradient-flowed HISQ ensembles”. In: *Phys. Rev. D* 102.3 (2020), p. 034507. DOI: 10.1103/PhysRevD.102.034507. arXiv: 2005.04795 [hep-lat].

[141] Torben Ferber, Camilo Garcia-Cely, and Kai Schmidt-Hoberg. “Belle II sensitivity to long–lived dark photons”. In: *Phys. Lett. B* 833 (2022), p. 137373. DOI: 10.1016/j.physletb.2022.137373. arXiv: 2202.03452 [hep-ph].

[142] Aram Hayrapetyan et al. “Search for long-lived heavy neutral leptons decaying in the CMS muon detectors in proton-proton collisions at s=13 TeV”. In: *Phys. Rev. D* 110 (2024), p. 012004. DOI: 10.1103/PhysRevD.110.012004. arXiv: 2402.18658 [hep-ex].

[143] Lea Reuter et al. “End-to-End Multi-track Reconstruction Using Graph Neural Networks at Belle II”. In: *Comput. Softw. Big Sci.* 9.1 (2025), p. 6. DOI: 10.1007/s41781-025-00135-6. arXiv: 2411.13596 [physics.ins-det].

[144] Sw. Banerjee et al. “Averages of b-hadron, c-hadron, and τ-lepton properties as of 2023”. In: *Phys. Rev. D* 113.1 (2026), p. 012008. DOI: 10.1103/x87q-tld5. arXiv: 2411.18639 [hep-ex].

[145] Jens Erler and Mingxing Luo. “Precision determination of heavy quark masses and the strong coupling constant”. In: *Phys. Lett. B* 558 (2003), pp. 125–131. DOI: 10.1016/S0370-2693(03)00276-4. arXiv: hep-ph/0207114.

[146] Andrew Kobach and Sean Dobbs. “Heavy Neutrinos and the Kinematics of Tau Decays”. In: *Phys. Rev. D* 91.5 (2015), p. 053006. DOI: 10.1103/PhysRevD.91.053006. arXiv: 1412.4785 [hep-ph].

[147] Vincenzo Cirigliano et al. “Semileptonic tau decays beyond the Standard Model”. In: *JHEP* 04 (2022), p. 152. DOI: 10.1007/JHEP04(2022)152. arXiv: 2112.02087 [hep-ph].

[148] Vincenzo Cirigliano and Ignasi Rosell. "The Standard Model prediction for $R_{e/\mu}^{(\pi,K)}$". In: *Phys. Rev. Lett.* 99 (2007), p. 231801. DOI: 10.1103/PhysRevLett.99.231801. arXiv: 0707.3439 [hep-ph].

[149] Jonathan L. Rosner, Sheldon Stone, and Ruth S. Van de Water. "Leptonic Decays of Charged Pseudoscalar Mesons - 2015". In: (Sept. 2015). arXiv: 1509.02220 [hep-ph].

[150] M. A. Arroyo-Ureña et al. "Radiative corrections to $\tau{\to}\pi(\mathrm{K})\nu\tau[\gamma]$: A reliable new physics test". In: *Phys. Rev. D* 104.9 (2021), p. L091502. DOI: 10.1103/PhysRevD.104.L091502. arXiv: 2107.04603 [hep-ph].

[151] M. A. Arroyo-Ureña et al. "One-loop determination of $\tau \to \pi(\mathrm{K})\nu_\tau\ [\gamma]$ branching ratios and new physics tests". In: *JHEP* 02 (2022), p. 173. DOI: 10.1007/JHEP02(2022)173. arXiv: 2112.01859 [hep-ph].

[152] Toichiro Kinoshita and Alberto Sirlin. "Radiative corrections to Fermi interactions". In: *Phys. Rev.* 113 (1959), pp. 1652–1660. DOI: 10.1103/PhysRev.113.1652.

[153] Yosef Nir. "The Mass Ratio m_c/m_b in Semileptonic b Decays". In: *Phys. Lett. B* 221 (1989), pp. 184–190. DOI: 10.1016/0370-2693(89)91495-0.

[154] Timo van Ritbergen and Robin G. Stuart. "On the precise determination of the Fermi coupling constant from the muon lifetime". In: *Nucl. Phys. B* 564 (2000), pp. 343–390. DOI: 10.1016/S0550-3213(99)00572-6. arXiv: hep-ph/9904240.

[155] M. Steinhauser and T. Seidensticker. "Second order corrections to the muon lifetime and the semileptonic B decay". In: *Phys. Lett. B* 467 (1999), pp. 271–278. DOI: 10.1016/S0370-2693(99)01168-5. arXiv: hep-ph/9909436.

[156] Alexey Pak and Andrzej Czarnecki. "Mass effects in muon and semileptonic $b \to c$ decays". In: *Phys. Rev. Lett.* 100 (2008), p. 241807. DOI: 10.1103/PhysRevLett.100.241807. arXiv: 0803.0960 [hep-ph].

[157] Jens Erler. "Calculation of the QED coupling $\hat{\alpha}(M_Z)$ in the modified minimal subtraction scheme". In: *Phys. Rev. D* 59 (1999), p. 054008. DOI: 10.1103/PhysRevD.59.054008. arXiv: hep-ph/9803453.

[158] Jens Erler. "Electroweak radiative corrections to semileptonic tau decays". In: *Rev. Mex. Fis.* 50 (2004), pp. 200–202. arXiv: hep-ph/0211345.

[159] William J. Marciano and A. Sirlin. "Electroweak radiative corrections to τ decay". In: *Phys. Rev. Lett.* 61 (16 Oct. 1988), pp. 1815–1818. DOI: 10.1103/PhysRevLett.61.1815. URL: https://link.aps.org/doi/10.1103/PhysRevLett.61.1815.

[160] Aram Hayrapetyan et al. "Search for Long-Lived Heavy Neutral Leptons with Lepton Flavour Conserving or Violating Decays to a Jet and a Charged Lepton". In: *JHEP* 03 (2024), p. 105. DOI: 10.1007/JHEP03(2024)105. arXiv: 2312.07484 [hep-ex].

[161] Aram Hayrapetyan et al. "Search for heavy neutral leptons in final states with electrons, muons, and hadronically decaying tau leptons in proton-proton collisions at $\sqrt{s}$ = 13 TeV". In: *JHEP* 06 (2024), p. 123. DOI: 10.1007/JHEP06(2024)123. arXiv: 2403.00100 [hep-ex].

[162] Georges Aad et al. “Search for heavy right-handed Majorana neutrinos in the decay of top quarks produced in proton-proton collisions at s=13 TeV with the ATLAS detector”. In: *Phys. Rev. D* 110.11 (2024), p. 112004. DOI: 10.1103/PhysRevD.110.112004. arXiv: 2408.05000 [hep-ex].

[163] Georges Aad et al. “Search for heavy neutral leptons in decays of W bosons using leptonic and semi-leptonic displaced vertices in $\sqrt{s}$ = 13 TeV pp collisions with the ATLAS detector”. In: *JHEP* 07 (2025), p. 196. DOI: 10.1007/JHEP07(2025)196. arXiv: 2503.16213 [hep-ex].

[164] Georges Aad et al. “Search for heavy neutral leptons in decays of W bosons produced in 13 TeV *pp* collisions using prompt signatures in the ATLAS detector”. In: *Eur. Phys. J. C* 86.2 (2026), p. 153. DOI: 10.1140/epjc/s10052-025-15191-w. arXiv: 2508.20929 [hep-ex].

[165] P. Abreu et al. “Search for neutral heavy leptons produced in Z decays”. In: *Z. Phys. C* 74 (1997). [Erratum: Z.Phys.C 75, 580 (1997)], pp. 57–71. DOI: 10.1007/s002880050370.

[166] R. Acciarri et al. “New Constraints on Tau-Coupled Heavy Neutral Leptons with Masses mN=280–970 MeV”. In: *Phys. Rev. Lett.* 127.12 (2021), p. 121801. DOI: 10.1103/PhysRevLett.127.121801. arXiv: 2106.13684 [hep-ex].

[167] J. P. Lees et al. “Search for heavy neutral leptons using tau lepton decays at BaBaR”. In: *Phys. Rev. D* 107.5 (2023), p. 052009. DOI: 10.1103/PhysRevD.107.052009. arXiv: 2207.09575 [hep-ex].

[168] M. Nayak et al. “Search for a heavy neutral lepton that mixes predominantly with the tau neutrino”. In: *Phys. Rev. D* 109.11 (2024), p. L111102. DOI: 10.1103/PhysRevD.109.L111102. arXiv: 2402.02580 [hep-ex].

[169] Iryna Boiarska et al. “Constraints from the CHARM experiment on heavy neutral leptons with tau mixing”. In: *Phys. Rev. D* 104.9 (2021), p. 095019. DOI: 10.1103/PhysRevD.104.095019. arXiv: 2107.14685 [hep-ph].

[170] Ryan Barouki, Giacomo Marocco, and Subir Sarkar. “Blast from the past II: Constraints on heavy neutral leptons from the BEBC WA66 beam dump experiment”. In: *SciPost Phys.* 13 (2022), p. 118. DOI: 10.21468/SciPostPhys.13.5.118. arXiv: 2208.00416 [hep-ph].

[171] F. Bergsma et al. “A Search for Decays of Heavy Neutrinos”. In: *Phys. Lett. B* 128 (1983). Ed. by J. Tran Thanh Van, p. 361. DOI: 10.1016/0370-2693(83)90275-7.

[172] F. Bergsma et al. “A Search for Decays of Heavy Neutrinos in the Mass Range 0.5-GeV to 2.8-GeV”. In: *Phys. Lett. B* 166 (1986), pp. 473–478. DOI: 10.1016/0370-2693(86)91601-1.

[173] Amanda M. Cooper-Sarkar et al. “Search for Heavy Neutrino Decays in the BEBC Beam Dump Experiment”. In: *Phys. Lett. B* 160 (1985), pp. 207–211. DOI: 10.1016/0370-2693(85)91493-5.

[174] Y. Chikashige, Rabindra N. Mohapatra, and R. D. Peccei. "Are There Real Goldstone Bosons Associated with Broken Lepton Number?" In: *Phys. Lett. B* 98 (1981), pp. 265–268. DOI: 10.1016/0370-2693(81)90011-3.

[175] G. B. Gelmini and M. Roncadelli. "Left-Handed Neutrino Mass Scale and Spontaneously Broken Lepton Number". In: *Phys. Lett. B* 99 (1981), pp. 411–415. DOI: 10.1016/0370-2693(81)90559-1.

[176] Gabriela Barenboim and Ulrich Nierste. "Modified majoron model for cosmological anomalies". In: *Phys. Rev. D* 104.2 (2021), p. 023013. DOI: 10.1103/PhysRevD.104.023013. arXiv: 2005.13280 [hep-ph].

[177] S. Kurokawa and Eiji Kikutani. "Overview of the KEKB accelerators". In: *Nucl. Instrum. Meth. A* 499 (2003), pp. 1–7. DOI: 10.1016/S0168-9002(02)01771-0.

[178] Kazunori Akai, Kazuro Furukawa, and Haruyo Koiso. "SuperKEKB Collider". In: *Nucl. Instrum. Meth. A* 907 (2018), pp. 188–199. DOI: 10.1016/j.nima.2018.08.017. arXiv: 1809.01958 [physics.acc-ph].

[179] A. Abashian et al. "The Belle Detector". In: *Nucl. Instrum. Meth. A* 479 (2002), pp. 117–232. DOI: 10.1016/S0168-9002(01)02013-7.

[180] T. Abe et al. "Belle II Technical Design Report". In: (Nov. 2010). arXiv: 1011.0352 [physics.ins-det].

[181] Denis Bodrov. "Tau physics at Belle and Belle II". In: *Int. J. Mod. Phys. A* 39.26n27 (2024), p. 2442006. DOI: 10.1142/S0217751X24420065. arXiv: 2405.16512 [hep-ex].

[182] Francesco Tenchini. "Recent Results from Belle and Belle II". In: *Springer Proc. Phys.* 292 (2023), pp. 1–10. DOI: 10.1007/978-3-031-30459-0_1. arXiv: 2306.17340 [hep-ex].

[183] Torben Ferber. Private communication. 2026.

[184] A. Abada et al. "FCC Physics Opportunities: Future Circular Collider Conceptual Design Report Volume 1". In: *Eur. Phys. J. C* 79.6 (2019), p. 474. DOI: 10.1140/epjc/s10052-019-6904-3.

[185] Sergey Alekhin et al. "A facility to Search for Hidden Particles at the CERN SPS: the SHiP physics case". In: *Rept. Prog. Phys.* 79.12 (2016), p. 124201. DOI: 10.1088/0034-4885/79/12/124201. arXiv: 1504.04855 [hep-ph].

[186] C. Ahdida et al. "Sensitivity of the SHiP experiment to Heavy Neutral Leptons". In: *JHEP* 04 (2019), p. 077. DOI: 10.1007/JHEP04(2019)077. arXiv: 1811.00930 [hep-ph].

[187] Florian U. Bernlochner et al. "Model independent bounds on heavy sterile neutrinos from the angular distribution of $\mathrm{B} \to \mathrm{D}^{*}\ell\nu$ decays". In: *JHEP* 01 (2025), p. 040. DOI: 10.1007/JHEP01(2025)040. arXiv: 2410.11945 [hep-ph].

[188] Motoi Endo et al. "$b \to c$ semileptonic sum rule: exploring a sterile neutrino loophole". In: (Mar. 2026). arXiv: 2603.15029 [hep-ph].

[189] Peter Marquard et al. "Quark Mass Relations to Four-Loop Order in Perturbative QCD". In: *Phys. Rev. Lett.* 114 (14 Apr. 2015), p. 142002. DOI: 10.1103/PhysRevLett.114.142002. URL: https://link.aps.org/doi/10.1103/PhysRevLett.114.142002.

[190] N. Carrasco et al. "Up, down, strange and charm quark masses with N_f = 2+1+1 twisted mass lattice QCD". In: *Nucl. Phys. B* 887 (2014), pp. 19–68. DOI: 10.1016/j.nuclphysb.2014.07.025. arXiv: 1403.4504 [hep-lat].

[191] Bipasha Chakraborty et al. "High-precision quark masses and QCD coupling from $n_f = 4$ lattice QCD". In: *Phys. Rev. D* 91.5 (2015), p. 054508. DOI: 10.1103/PhysRevD.91.054508. arXiv: 1408.4169 [hep-lat].

[192] C. Alexandrou et al. "Baryon spectrum with $N_f = 2 + 1 + 1$ twisted mass fermions". In: *Phys. Rev. D* 90.7 (2014), p. 074501. DOI: 10.1103/PhysRevD.90.074501. arXiv: 1406.4310 [hep-lat].

[193] A. Bazavov et al. "Up-, down-, strange-, charm-, and bottom-quark masses from four-flavor lattice QCD". In: *Phys. Rev. D* 98.5 (2018), p. 054517. DOI: 10.1103/PhysRevD.98.054517. arXiv: 1802.04248 [hep-lat].

[194] D. Hatton et al. "Charmonium properties from lattice QCD+QED : Hyperfine splitting, J/ψ leptonic width, charm quark mass, and a_μ^c". In: *Phys. Rev. D* 102.5 (2020), p. 054511. DOI: 10.1103/PhysRevD.102.054511. arXiv: 2005.01845 [hep-lat].

[195] C. Alexandrou et al. "Quark masses using twisted-mass fermion gauge ensembles". In: *Phys. Rev. D* 104.7 (2021), p. 074515. DOI: 10.1103/PhysRevD.104.074515. arXiv: 2104.13408 [hep-lat].

Acknowledgements - Danksagung

Als Erstes bedanke ich mich bei Prof. Ulrich Nierste, der es mir ermöglicht hat, zu promovieren. Ich erinnere mich noch, wie ich am Anfang meines Studiums bei Dir Theorie B gehört habe und wie sehr mich Deine Vorlesung begeistert hat. Auch später, als ich das Glück hatte, bei Dir Theoretische Teilchenphysik I zu hören, hat mich Deine Vorlesung begeistert und es war eine großartige Ablenkung vom Corona Alltag. Dann konnte ich bei Dir promovieren und durfte selber Teil Deiner Lehrveranstaltungen werden und habe versucht meine Begeisterung, so wie Du, an die Studenten weiterzugeben. Ich habe so viel von Dir gelernt während meiner Promotion und dafür bin ich Dir unglaublich dankbar. Von Anfang an hast Du mir so viel Vertrauen entgegengebracht und ich wusste, wann auch immer ich eine Frage habe, kann ich zu Dir kommen und wir finden eine Lösung. Von ganzem Herzen lieber Uli, danke für Deine Unterstützung und diese besondere Möglichkeit!

Ebenso danke ich Prof. Thomas Schwetz-Mangold, der die Zweitbegutachtung meiner Dissertation übernommen hat. Vielen Dank!

Besonders bedanke ich mich bei Robert Ziegler, der die Betreuung meiner Masterarbeit übernommen hat und mir maßgeblich dabei geholfen hat, meine Promotionsstelle zu bekommen. Lieber Robert, es war immer mein großes Ziel einmal zu promovieren und während meiner Masterarbeit habe ich Dich gefragt, ob es möglich ist, das am KIT zu tun. Du hast mit Uli gesprochen und so bin ich zu meiner Promotionsstelle gekommen. Robert, vielen Dank für Deine Unterstützung.

I wholeheartedly thank Syuhei Iguro. During my PhD time we have worked closely together on the sum rule project. Thank you for this opportunity. Even more so I want to acknowledge that you carefully proofread my thesis and provided valuable feedback, thank you! But above all else I want to thank you for the wonderful friendship with you and also with Kaoru; I greatly enjoyed spending time with you and visiting you in Japan was an amazing journey I will always remember, thank you very much!

In much the same way I wholeheartedly thank Francesco Moretti. I look fondly upon our frequent exchanges and bantering with you about any topic always took away a lot of the stress that I had, especially in the last few months of my PhD. I knew, your door was always open and I could always come and ask you a question. I also acknowledge your proofreading of my thesis. Thank you very much!

A special thank you also goes out to my office mates (office 12/19) Ann Cathrin Wesener, Maksym Riabokon, Nicoline Hemme and Sowmiya Balan. I always felt welcome in the office and I greatly enjoyed our frequent discussions. For your encouragement during writing my thesis I thank you. Thank you to Maksym Riabokon for proofreading parts of the thesis.

I had the great pleasure of meeting many new friends at KIT with whom I have spent wonderful times together: Amir Khan, Benedetta Belfatto, Berkan Demir, Dominik Grau, Giovani Dalla Valle Garcia, Henda Mansour, Jonas Matuszak, Kierthika Chathirathas, Lena Rathmann, Manuel Egner, Marco Fedele, Marco Vitti, Martina Schorn, Martin Lang, Matteo Tresoldi, Monika Blanke, Pascal Reeck, Philipp Goller, Prem Agarwal, Saiyad Ashanujjaman, Surabhi Tiwari and Xiyuan Gao and many more. Thank you everyone!

Finally, this brings my journey at KIT, which I started in 2016, to an end. I want to thank everyone at the TTP and the other institutes that I met. I greatly enjoyed my time at the TTP. Thank you everyone for warmly welcoming me into the institute and for all the interesting discussions we had. Thank you.

Ich danke meinen Freunden, die mich in den drei Jahren meiner Promotion immer wieder unterstützt haben, vielen Dank.

Besonders danke ich meiner Familie. Ihr habt es mir ermöglicht zu studieren und mich immer unterstützt. Ohne Euch hätte ich es nie geschafft diese Arbeit abzuschließen. Immer dann als ich aufgeben wollte, habt Ihr mich wieder aufgebaut und dafür bin ich dankbar. Von ganzem Herzen, danke, für alles was Ihr für mich getan habt und dafür, dass Ihr immer für mich da seid.